Graphene-modified pencil graphite mercury-film electrodes for the determination of trace metals by cathodic adsorptive stripping voltammetry

A thesis submitted in fulfilment of the requirements for the degree of

Magister Scientiae in Nanoscience (Chemistry)

Department of Chemistry: SensorLab

University of the Western Cape

August 2018

By

Ronald Tekenya

Supervisor: Prof. Nazeem Jahed

Co-supervisor: Prof. Emmanuel I. Iwuoha

KEY WORDS

Graphene

Graphene oxide

Thin-mercury film

Pencil graphite electrode

Trace metal analysis

Electrochemically reduced graphene oxide pencil graphite electrode (ERGO-PGE)

Square-wave Adsorptive Cathodic stripping voltammetry

Nioxime

Dimethylglyoxime (DMG)

Raman Spectroscopy

Nanocomposite

ABSTRACT

This project focuses on the simple, fast and highly sensitive adsorptive stripping voltammetry detection of Nickel and Cobalt complexed with DMG and Nioxime respectively at a Reduced Graphene Oxide modified pencil graphite electrode in water samples. This research as well demonstrates a novel electrochemically reduced graphene oxide (ERGO)/mercury film (MF) nanocomposite modified PGE, prepared through successive electrochemical reduction of graphene oxide (GO) sheets and *in-situ* plated mercury film. The GO and graphene were characterized using FT-IR, HR-SEM, HR-TEM, XRD and Raman spectroscopy. The FT-IR results supported by X-ray diffraction analysis confirmed the inclusion of oxygen moieties within the graphitic structure during the chemical oxidation step. Microscopic and spectroscopic analysis was used to confirm the stackings of graphene on the pencil electrode. The ERGO-PG-MFE, in combination with a complexing agents of [dimethylglyoxime (DMG) and Nioxime] and square-wave cathodic stripping voltammetry (SW-CSV), was evaluated towards the individual determination of Ni^{2+} and Co^{2+} respectively and simultaneous determination of both metals from the combination of DMG and Nioxime mixture. A single-step electrode pre-concentration approach was employed for the *in-situ* Hg-film electroplating, metal-chelate complex formation and its non-electrolytic adsorption at – 0.7 V for the individual analysis of Ni^{2+} and Co^{2+}. The current response due to metal-ligand(s) complex reduction were studied as a function of experimental variables; deposition/accumulation potential, deposition/accumulation time, rotation speed, frequency and amplitude and carefully optimized for the individual determination of $Ni^{2+}$and Co^{2+} and simultaneous determination of Ni^{2+} and Co^{2+} at low concentration levels (μg L^{-1}) in 0.1 M NH_3-NH_4Cl buffer solution (pH 9.4) solution. The recorded limit of detection for the individual analysis of $Ni^{2+}$and Co^{2+} was found to be 0.120 μg L^{-1} and 0.220 μg L^{-1} respectively, at an accumulation time of 120 s for both metals. The recorded limit of detection of the simultaneous analysis of Ni^{2+} and Co^{2+} was found to be 6.1 μg L^{-1} and 1.8 μg L^{-1} respectively. The ERGO-PG-MFE further demonstrated a highly selective stripping response toward all trace metal analysis. The testing of the applicability of graphene-based sensor and method in laboratory tap water samples was evaluated. This electrode was found to be sensitive enough to detect metal ions in the tap water samples at the 0.2 μg L^{-1} level for individual analysis and 0.001 μg L^{-1} for simultaneous, well below WHO standards.

DECLARATION

I declare that this work "Graphene**-modified pencil graphite mercury-film electrodes for the determination of trace metals by cathodic adsorptive stripping voltammetry"** is my own work, that has not been submitted for any degree or examination at any universities and that all the sources I have used or quoted have been properly indicated and acknowledged by complete references.

Ronald Tekenya **August 2018**

Signature .....

ACKNOWLEDGEMENTS

Firstly, I would like to thank God the almighty for giving me the strength, endless possibilities and the drive and hunger throughout my life. I pray that you give me the same hunger moving forward.

Secondly, I would like to thank my supervisor Prof Jahed for your guidance, encouragement, support and be there for me as a friend. I thank you for naturing me to a person I am today. Furthermore, I would like to thank Dr Keagan Pokpas for the same reasons as Prof Jahed. The two of you played a crucial role in my academic life.

I am grateful to be under the SensorLab group under the leadership of Prof E.Iwuoha who is my co-supervisor. I thank you for opportunity and continuous support.

To the members of the department of Chemistry, University of the Western Cape, South Africa, I say thank you for the good and the cordial working relationship I enjoyed during my studies.

Lastly, a special thanks to my parents and family for being the pillar of my strength. You have been with me through thick and thin, may God bless you. Without your support I wouldn't be here right now.

LIST OF ABBREVIATIONS

AAS - Atomic absorption spectrometry

AdSV - Adsorptive stripping voltammetry

ASV - Anodic stripping voltammetry

BiFE - Bismuth film electrode

CNS - Central nervous system

CSV - Cathodic stripping voltammetry

CVD - Chemical vapor deposition

DPSV - Differential pulse stripping voltammetry

EDS - Electronic data system

FT-IR - Transformed infrared spectroscopy

GCE - Glassy carbon electrode

GC-Gr-TFE - Graphene modified glassy carbon thin film electrode

MDE - Hanging mercury drop electrode

HRTEM - High resolution transmission electron microscopy

ICP-OES - Coupled plasma optical emission spectrometry

LSSV - Linear sweep stripping voltammetry

MCL - Maximum contamination level

MFE - Mercury film electrode

N.D - Not determined

NPSV - Normal pulse stripping voltammetry

ppb - parts per billion

RDE - Rotating disk electrodes

RGO - Reduced graphene oxide

RSD - Relative standard deviation

SbFE - Antimony film electrode

SCE - Saturated calomel electrode

SEM - Scanning electron microscopy

SiC - Silicon carbide

SV - Stripping voltammetry

SWSV - Square wave stripping voltammetry

TEM - Transmission electron microscopy

TMFE - Thin mercury film electrode

WDS - Windows deployment services

XRD - X-ray diffraction

XRF - X-ray fluorescence

TABLE OF CONTENTS

LIST OF FIGURES

LIST OF TABLES

CHAPTER 1

Introduction

Heavy metals and their effect on human health

Nickel (Ni) is a metallic element which is a member of the transition metal class and is widely applied in industrial settings. Due to its unique physical and chemical properties, it is noted as one of the most important transition metal ions in biological systems [1], exhibiting both vital and toxic effects. Its toxicology has been well documented [2], [3] and Ni^{2+} compounds have been classified as group one human carcinogens [4]. Moreover, it has been linked to serious health problems including respiratory system cancer [5], skin allergies, dermatitis or nickel-eczema [6]. Ni has been widely used in industrial applications as pipes and fittings, electroplating, stainless steel and alloys [5]. Considering its ever-growing consumption, environmental pollution by nickel-containing products remains prevalent. In particular, human exposure to nickel occurs primarily through digestion and inhalation [2]. The maximum allowable level for Ni in drinking water is set at 0.1 mg L^{-1} [7] by the World Health Organisation (WHO).

Cobalt is a major constituent of vitamin B12, is important for humans and other living organisms. Cobalt can be found in trace levels both in water and other biological samples. A radioactive isotope of cobalt is an important use in the treatment of cancer and other related diseases[8]. However, at high concentration cobalt have been linked to a variety of illnesses such as polycythaemia, skin allergies, pulmonary disorders, and other adverse reactions[8]. Blue silica gel has been banned in other countries worldwide as they contain too much cobalt which leads to such illnesses. The environment which is contaminated by cobalt becomes a health hazard not only for humans but for all the animals involved in the food chain, as such system to monitor cobalt level in water is of necessity.

Stripping voltammetry techniques

Contemporary analytical techniques such as flame [9], [10], electrothermal [11] and graphite furnace [12] atomic absorption spectrometry (AAS), neutron activation analysis (NAA) [13], [14], x-ray fluorescence spectrometry, (XRF) [15], inductively coupled plasma optical emission spectrometry (ICP-OES) [16], [17], and electrochemical techniques have been used for heavy

metals determination. These spectroscopic methods, however, are limited by availability, *ex-situ* measurements and, expensive and complicated instrumentation. In contrast, electrochemical approaches have recently gained traction due to their high speed, good selectivity, high sensitivity, and low instrumentation cost [18]. Among these, stripping analysis remains the most common.

Anodic stripping voltammetry has widely been recognized as one of the most effective tools for analysis of metals, with many established works having been performed. Heavy metals, rare earth metals, and platinum group metals, among others, have been investigated to date. While less popular, adsorptive cathodic stripping voltammetry (AdCSV) has been shown to be an extremely effective electroanalytical technique for the trace level determination of metal ions that have an interfacial adsorptive character onto the working electrode surface [19]. The technique relies on an accumulation step in which the electrode surface is pre-concentrated with the analyte by simple non-electrolytic adsorption. Ni^{2+} and Co^{2+}, however, remain the most widely applied application [20], [21], [30]–[32], [22]–[29].

The development and application of carbon-based electrodes have received considerable attention in recent years for the analysis of the redox activity of inorganic and organic substances alike [33]. Graphite [34], carbon-paste [35]–[37], edge-plane pyrolytic graphite [38], pencil graphite [39] and more recently hand-drawn pencil graphite electrodes [40] have all been investigated. Among these, pencil graphite electrodes (PGE) have received particular interest in stripping analysis, owing to their many advantageous properties. Their good electrical conductivity, lack of pre-treatment, low cost, availability and low background current [41] are particularly valuable and make it an attractive alternative to the well-known glassy-carbon and gold electrodes (GCE and GE) [18]. Recently, a number of studies on the use of PGEs for the analytical determination of different heavy metal ions (Zn^{2+}, Cd^{2+} and Pb^{2+}) [18], [39], [42], [43], antioxidants [41], nicotine [44], polycyclic aromatic hydrocarbons (PAHs) [45] and nucleic acids [46], [47] have been reported.

While less toxic working electrode materials, such as antimony (Sb), bismuth (Bi), lead (Pb) and silver (Ag) amalgam films have been suggested, electroanalysis of heavy metals at mercury-film and hanging mercury drop electrodes remain extremely popular due to their ability for amalgam formation in the pre-concentration step. Additionally, the high overpotential of hydrogen evolution

[48] and the possibility of a constantly renewable surface are attractive features for its use. Hereby, the possibility of electrode poisoning by pre-deposited matter may be eliminated. To date, Hg-film electrodes coupled with stripping techniques have been recognized as the most sensitive method for the determination of heavy metals such as nickel. For AdSV detection of metal ions, separate accumulation and deposition potentials have usually been employed.

Graphene

Graphene is a single atomic layer of carbon atoms tightly packed in a two-dimensional honeycomb lattice which makes electricity flow very quickly. This novel material is atomically thin, chemically inert, consists of light atoms, and possesses a highly ordered structure [49]. Graphene is the strongest ever material measured and has a remarkable electrically, mechanical and thermally conductivity. These remarkable properties make graphene the ideal support film for graphite pencil electrodes. Since it was first produced in 2004, graphene has attracted attention and has shown to significantly improve the sensitivity in various applications due to rapid electron transfer [50] and high surface-to-volume ratio. Graphene has been used in a wide range of electrochemical sensing devices to date. To the best of our knowledge, only two studies have been conducted on graphene-modified sensors for application in the AdSV detection of metal ions. Zhan *et al*. first reported a β-cyclodextrin and chemically reduced graphene oxide (β-CD-rGO) nanocomposite in order to investigate its electrochemical response towards Pb^{2+} detection [51]. The study demonstrated the excellent adsorption ability of β-CD and extraordinary electron conductivity of rGO for electrochemical analysis of metal ions by both synergistic and electrolytic electrode pre-concentration. Our research group further exhibited a Nafion graphene, dimethylglyoxime modified glassy carbon electrode (NGr-DMG-GCE) for Ni^{2+} detection by AdCSV. The work performed by Pokpas *et al*. was the first reported signal amplification approach of graphene for Ni^{2+} detection. It further showed a novel method for improved selectivity towards Ni^{2+} in the presence of Co^{2+} and Zn^{2+} [23]. To date, no work has been investigated for graphene modified sensors by AdSV in the presence of metallic-films or alternative electrode materials such as disposable pencil graphite.

Motivation to the study

Contamination by heavy metals in the environment has been on the rise mainly due to the ever increase demand of the use of toxic metals in the industries.

Here we illustrate, an electrochemically reduced graphene oxide pencil graphite electrode (ERGO-PGE) prepared through cyclic voltammetric reduction of graphene oxide in acetate buffer solution in conjunction with an *in-situ* plated mercury film for the improved selectivity and signal amplification towards the trace determination of $Ni^{2+}$and Co^{2+} individually and simultaneously by adsorptive cathodic stripping voltammetry (AdCSV). To the best of our knowledge, this is the first report on the use of graphene-modified electrodes in conjunction with an electroplated metallic-film with dimethylglyoxime, Nioxime and a mixture of both ligands as chelating agents for the AdCSV of Ni^{2+}, Co^{2+} and simultaneously, respectively in tap water samples. Further, a single deposition and accumulation potential is demonstrated in order to simplify the mechanism for electrochemical adsorption and detection.

Objectives

- To investigate and understand the adsorptive square wave stripping voltammetry technique
- To synthesize graphene oxide and characterize it using Fourier Transform-Infrared (FT-IR) spectroscopy, Raman spectroscopy, Transmission Electron Microscopy (TEM), Scanning Electron Microsopy(SEM) and X-ray diffraction (XRD)
- To electrochemically reduce graphene oxide onto pencil graphite electrode followed by *in situ* plating of a mercury film to give the ERGO-PG-MFE
- To investigate the ERGO-PG-MFE responses towards the simultaneous determination of $Co^{2+}$and Ni^{2+} in a mixed ligand electrolyte.
- To investigate the ERGO-PG-MFE responses towards $Co^{2+}$and Ni^{2+}
- To investigate the responds towards different complexing agents
- To optimize instrumental parameters and determine the analytical parameters of the ERGO-PG-MFE for $Co^{2+}$and Ni^{2+}
- To develop an analytical procedure for the determination of heavy metals ions in water samples using the ERGO-PG-MFE

Research Questions

- Would pencil graphite electrodes be suitable for use in trace metal analysis?
- Would the coated pencil graphite electrode with graphene improve the sensitivity of the electrode
- Would the selected ligands offer the selectivity for the trace metals investigated i.e. DMG for Ni^{2+} and Nioxime for Co^{2+}
- Do mercury film electrodes offer comparable results to other thin-metal films electrodes in terms of limits of detection and recoveries for real water samples?
- Would a mixture of DMG and Nioxime be able to give well separated stripping peaks of Ni^{2+} and Co^{2+} at a ERGO-PG-MFE

Thesis Structure

This thesis comprises of five chapters and is structured as follows:

Chapter 1: Introduction

Chapter 1 gives an introduction to a brief introduction of heavy metals with their effect on health, the stripping analysis techniques involved in the determination of those heavy metals as well as graphene. This is followed by the motivation of the current study as well as the target objectives.

Chapter 2: Literature review

Chapters 2 gives a much more detail descriptions of the all the aspects to be looked at in this study. Such aspects include graphene, trace metals, stripping analysis techniques and metal-thin films. A much more detailed background of stripping voltammetry principles will be highlighted. Characterization techniques used for the characterization of graphene will be looked into.

Chapter 3: Methodology

Chapter 3 gives an outline of the specific technique and equipment used in this work. A much detail step by step description of the synthesis, electrode cleaning, sample collections are all provided, as well as the characterization techniques to be used.

Chapter 4: Results & Discussions

The results and discussion compromise of 3 subtopics of which each subtopic represent a different research on specific metal or ligand being investigated. In all part, electrochemically reduced graphene oxide pencil graphite electrode is used.

Part A: focuses on the investigation of individual analysis of Nickel with DMG as the ligand used.

Part B: will focus on the results and discussion of individual analysis of Co^{2+} using Nioxime as the complexing ligand.

Part C: further discussion on the results of the mixed ligand of DMG and Nioxime for simultaneous analysis of Ni and Co.

Chapter 5: Conclusion and future work

Chapter 5 concludes this thesis by summarizing the main points highlights the novelty of the research and, provides conclusions and recommendations as well as future work.

CHAPTER 2

Literature Review

2.1. General basis for voltammetry

2.1.1. Voltammetry

Voltammetry is an electrochemistry techniques based on current (i) measurement as function of voltage (E_{app}) which consist of the working electrode, reference electrode, counter electrode and the supporting electrolyte. The working electrode is usually made of platinum, gold, silver, glassy carbon, nickel, or palladium and is the place where redox occurs of which the surface area is a few mm^2 to limit current flow [52]. Reference electrode is a constant potential reference ,the saturated calomel electrode (SCE) and the silver/silver chloride (Ag/AgCl) electrodes are the most common [53], while the counter electrode is an inert material (e.g. Hg, Pt) which plays no part in redox but rather completes the circuit. The supporting electrolyte is an electrolyte solution which contains chemical species that are not electroactive (within the range of potentials used) and which has an ionic strength and conductivity much larger than those due to the electroactive species added to the electrolyte. In all electrochemical methods, the rate of oxidation & reduction depend on mass transport and electrode kinetics [52]. Below is a schematic representation of a three electrode electrochemical cell system to be used in this experiment.

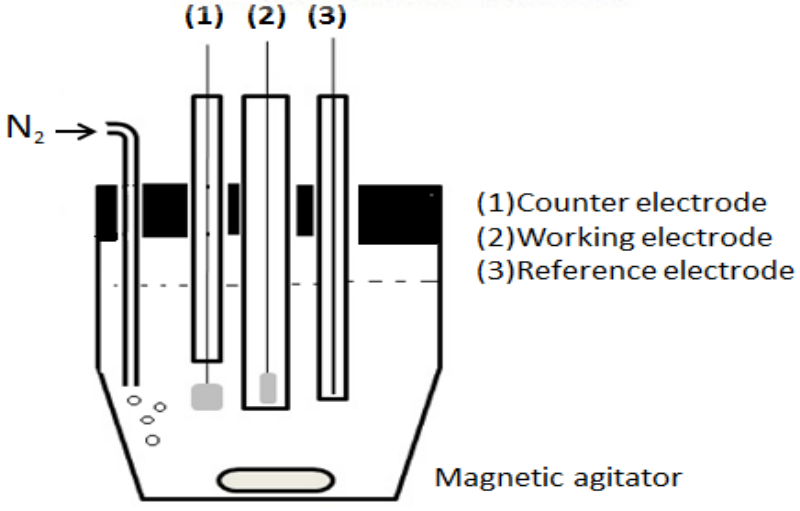

Figure 2.1. A schematic representation of a three electrode electrochemical cell system [54]

2.1.2. Stripping voltammetry

Stripping voltammetry comprises of a group of various techniques including anodic stripping voltammetry (ASV), cathodic stripping voltammetry (CSV) and adsorptive stripping voltammetry (AdSV). Stripping voltammetry is a two-step technique that allows individual to simultaneous detection of various inorganic and organic substances in sub-nanomolar range. The first step consists of the electrolytic deposition of a chemical species onto an inert electrode surface (carbon, gold or chemically modified electrodes) at a constant potential. The pre-concentration step explains the remarkable sensitivity of the technique. It can involve either an anodic or cathodic process [55].

The stripping voltammetry consists of several discrete steps which include the conditioning of electrode, deposition, equilibrium and stripping steps. During the conditioning step, a specific potential is applied to the electrode for a controlled time in order to remove contaminants or materials not removed during the stripping step from the electrode surface. The conditioning of the thin-film mercury electrodes (TFME) is a very crucial step as these will ensure that the surface of the TFME is as reproducible as possible prior to each analysis. The second step is the most crucial part of the stripping experiment which is the deposition step (accumulation step) in which the metal ions in the solution are deposited onto or into a working electrode by applying a reduction potential of the metals being analyzed. Stirring the solution is of necessity as it increases the efficiency of the process i.e. by maximizing the analyte-electrode contact. The choice of the deposition potential can provide some selectivity in the measurement [55]. The length of the deposition time determines the analyte concentration hence determining the detection limit of the technique [56]. In the equilibrium step, stirring is halted allowing for homogeneous dispersal of the analyte to decreasing the convection currents to a negligible level. The final step is the stripping step which involves the metals stripping out of metals back into the solution after applying an excitation waveform. The materials deposited in or on the working electrode will be stripped at potentials very close to their half-wave potentials.

Stripping voltammetry comprises of a group of various techniques including anodic stripping voltammetry (ASV), cathodic stripping voltammetry (CSV) and adsorptive stripping voltammetry (AdSV). The figure below shows the metals that can be determined by stripping analysis.

The metals in italics (in *Figure 2.2*) are the species that are normally determined only after electrolytic accumulation, the underlined species are the ones which are normally determined after

non-electrolytic accumulation and the ones in bold are the species that can be determined after electrolytic or non- electrolytic accumulation

											Al					
		Sc	Ti	V	Cr	Mn	Fe	Co	Ni	**Cu**	**Zn**	Ga	Ge	**As**	*Se*		
		Y	Zr		Mo	Tc			Pd	**Ag**	**Cd**	**In**	**Sn**	**Sb**			
		La	Hf						Pt	**Au**	**Hg**	*Tl*	**Pb**	*Bi*			

Ce	Pr				Eu			Dy	Ho			Yb	Lu
Th		U											

Figure 2.2. A periodic table which shows metals which can be determined by stripping analysis [57].

2.2. Various types of stripping analysis technique

2.2.1. Anodic Stripping Voltammetry (ASV)

Anodic stripping voltammetry (ASV) is the most common stripping technique which is used to determine trace metal cations. ASV is well known for its pre-concentration (deposition) of analyte on the electrode surface in order to lower the detection limit of the analyte by applying a deposition potential which is more negative than half-wave potential of the electroactive metal to be determined [55] followed by an anodic scan to oxidize the reduced electroactive metal back into solution. The preconcentration step involves the reduction of M^{n+} cations to the metallic state at the mercury electrode, which leads to the formation of M/Hg amalgam. The mechanism can be described as follows:

$$Mn^+ + ne^- \rightarrow M(Hg)$$

The accumulated (deposited) metals are then stripped off by applying a positive (anodic) potential scan which results in the observation of the current peaks when the potential scan reaches the oxidation potentials of the desired metals. The mechanism can be described below as follows:

$$M(Hg) \rightarrow Mn^+ + ne^-$$

The resulting voltammogram will provide the analytical information of interest. The peak potential corresponds to analyte investigated while the peak current is proportional to the analyte in sample of the reproducible deposition conditions is assumed [58]. The figure below is the summary of the anodic stripping voltammetry technique.

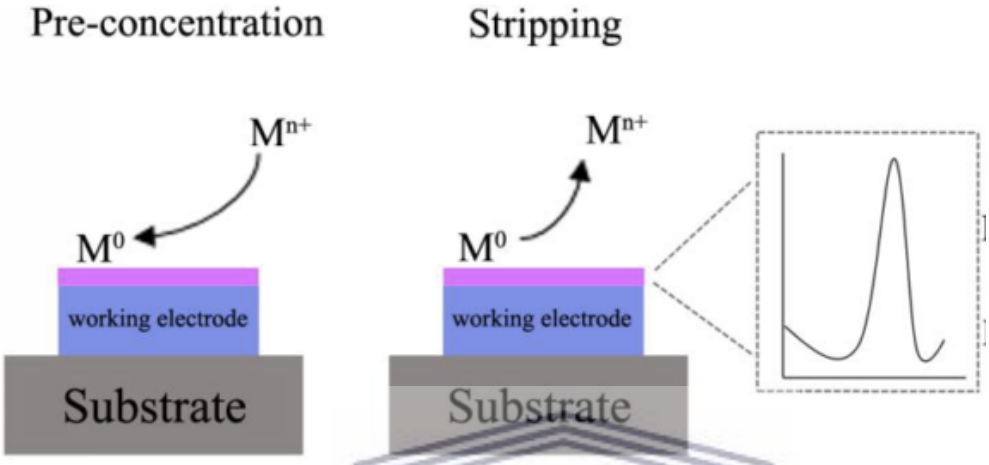

Figure 2.3. Summary of the anodic stripping voltammetry technique [59]

2.2.2. Cathodic Stripping Voltammetry (CSV)

Cathodic stripping voltammetry is the method of which the pre-concentration for the technique is the formation of an insoluble film on the surface of the mercury electrode. The method is used to determine those organic and inorganic compounds which forms insoluble salts with the electrode [58]. An insoluble film is formed on the surface of the working electrode by applying a positive (anodic) potential followed by stripping in a negative-going potential scan. The working electrode is not inert hence taking an active role in the formation of the deposit as follows:

$$Hg \rightarrow Hg^{+} + e^{-}$$

$$2Hg^{+} + 2M^{-} \rightarrow Hg_2M_2(insoluble\ film)$$

Where M is the analyte. Following the deposition step, the deposited analyte salt is stripped back into the solution from the working electrode by applying a cathodic potential scan (negative going). The observed peak current is proportional to the concentration of the analyte (M):

$$Hg_2M_2 + 2e^{-1} \rightarrow 2Hg + 2M^{-1}$$

The difference between CSV and ASV is CSV involves the formation of a film on the surface of an electrode as compared to ASV which a homogeneous amalgam is formed hence making the linearity of CSV at high concentration unusual but still reproducible as compared to the ASV.

2.2.3. Adsorptive Stripping Voltammetry (AdSV)

In ASV and CSV techniques, the preconcentration was achieved by oxidation or reduction, however for AdSV a non-electrolytic nature of preconcentration of the analyte onto the electrode surface is achieved by adsorption. The organic species or inorganic complexed species are accumulated on the active electrode surface by adsorption. A greater sensitivity and selectivity is achieved by an application of either a cathodic or anodic potential which electrolyze the adsorbed species on the active surface back into the solution [60]. The preconcentration step in the AdSV plays a crucial role as it widens the linear dynamic range and low detection limit, as such sampling handling are risk of sample contamination are all decreased in the process. The other advantage which AdSV brings is the enabling of multi element analysis [61].

The combination of simplicity of the instrumentation, expensiveness, portable size for both lab and field study makes the AdSV the obvious choice for metal analysis.

When thinking of increasing the sensitivity and detection limits of the AdSV, modification to the working electrode needs to be done. The mostly commonly used method for the incorporation of a chemical modifier onto an electrode surface is by a polymer film or nanomaterials [58]. In recent years, chemically modified electrodes has gain a popularity due to its vast advantages which ranges from low cost and easy manufacturing, renewability, fast response, high selectivity, low detection limit and environmental friendly. As such a vast majority of chemically modified electrodes has been introduced for the determination of heavy metals. For the determination of nickel and cobalt chemically modified electrodes such as: chloropalladium(II) complex-modified MWCNTs paste electrode [24], electrochemically deposited graphene/bismuth nanocomposite film-modified glassy carbon electrode [49], tin–bismuth alloy electrode [62], carbon paste electrode modified with montmorillonite clay [63] etc. has been used.

Among all the chemically modified electrodes use, graphene modified electrodes has gain considerably popularity due to the properties graphene possess. Graphene is still considered a

wonder material as not much of it is known yet. Electrochemically modified graphene oxide electrodes have been reported but very few on pencil graphite electrodes.

2.3. Why use stripping voltammetry

Stripping analysis is capable of measuring four to six trace metals simultaneously in the sub- parts per billion ranges. Contemporary analytical techniques such as flame [9], [10], electrothermal [11] and graphite furnace [12] atomic absorption spectrometry (AAS), neutron activation analysis (NAA) [13], [14], x-ray fluorescence spectrometry, (XRF) [15], inductively coupled plasma optical emission spectrometry (ICP-OES) [16], [17], and electrochemical techniques have been used for metal determination. These spectroscopic methods as mentioned in chapter 1, however, are limited by availability, *ex-situ* measurements and, are expensive and have complicated instrumentation. In contrast, electrochemical approaches have recently gained traction due to their high speed, good selectivity, high sensitivity, and low instrumentation cost [18]. Among these, stripping analysis remains the most common.

2.4. Principles of stripping voltammetry

2.4.1. Deposition step

In stripping voltammetry, the deposition of the analyte onto or into the active surface of the working electrode contributes to the very low detection limit of the stripping analyses. A fixed deposition potential is applied for a certain period of time to allow the cause the analyte of interest to be deposited onto/into the surface of the working electrode. The deposition of heavy metals onto/into mercury electrodes usually forms amalgams. Finally, alloys are formed when bismuth, tin or antimony electrodes are used for electrolytic accumulation of alloy-forming metals [57].A constant stirring of the solution is a necessity to maximize the contact of the analyte onto/into the electrode [55]. Enhanced mass transportation is achieved when stirring the solution during preconcentration step. The choice of the deposition/accumulation potential contributes to the selectivity of the method; however, this is carried out either by anodic or cathodic deposition or by accumulation method depending on weather the analyte of interest is to be oxidized or reduced.

The amount of species deposited on the working electrode correspond to the resulting i_p, hence i_p is propositional to the time taken to deposit the analyte onto the electrode.

2.4.2. Equilibration time

After the preconcentration step, the solution is equilibrated for about 10 to 30 s which allows the uniform distribution of metal concentration onto or into the electrode active surface or metal-film. The equilibration time also ensures that the next step (stripping step) occurs in quiet solution.

2.4.3. Stripping step

During the stripping step, the pre-concentrated analyte onto/into the working electrode is either oxidized or reduced back into the solution at specific potential. This process is done by applying the potential towards the cathodic or anodic direction which electrolyzes the deposited material back into the solution. The deposited target metals will be stripped off when the standard potential is reached which results in electron transfer causing a current flow. The equation below describes the process explained above:

$$M(Hg) \rightarrow Mn^{+} + ne^{-}$$

The resulting voltammetry from the process above will provide information on the peak current and peak potential. The potential waveforms which can be used for the stripping step are differential pulse, square wave, linear sweep, or staircase. Of all the above potential waveforms, square wave has advantages of faster scan rate and increased sensitivity [64]. Common working electrodes can be made of inert materials such as Au, Ag, Pt, glassy carbon (GC) and Hg drop and film electrodes. Mercury film electrodes are most commonly used and more useful because they display a wide negative potential range. The species of interest can be either reduced into/onto the mercury, forming amalgams as in anodic stripping voltammetry, or adsorbed to form an insoluble mercury salt layer, as in cathodic stripping voltammetry [64].

2.4.4. Excitation signals or waveforms

2.4.4.1. Linear sweep stripping voltammetry

Linear sweep mode is the technique in which the current flowing through the electrochemical cell is measured while applying a linear potential ramp simultaneously recording the current-applied potential data [60]. The scanning starts before the discharging potential and stops afterwards.

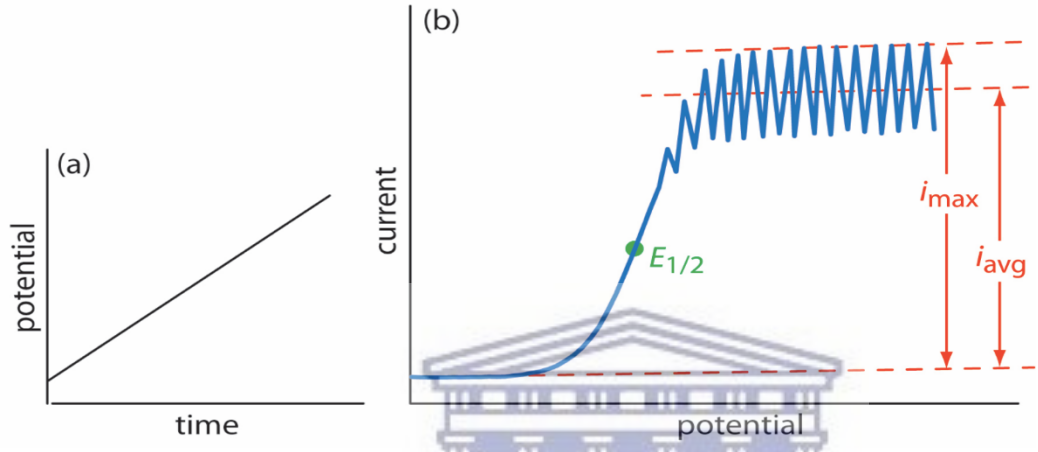

Figure 2.4. (a) The linear potential-excitation signal, and (b) the resulting voltammogram [65]

2.4.4.2. Normal pulse stripping voltammetry

Normal pulse voltammetry is a technique which uses of potential pulses of increasing amplitude and is known to increase sensitivity due to the faradic-to-charging current ratio. In this technique potential pulses of gradual increasing amplitude are applied from a fixed potential of which no reaction at the electrode occurs. Each current measurement is made is made near the end of each pulse hence giving sufficient time for the charging current to decay [64]. The duration of the potential pulse is generally less than 100 ms and the interval between pulses are typically 0.1 to 5 sec. The output voltammetry for each pulse is usually the current vs the potential measured towards the end of each pulse resulting in sigmoidal-shaped voltammogram. The technique is usually carried out at unstirred solution at an electrode.

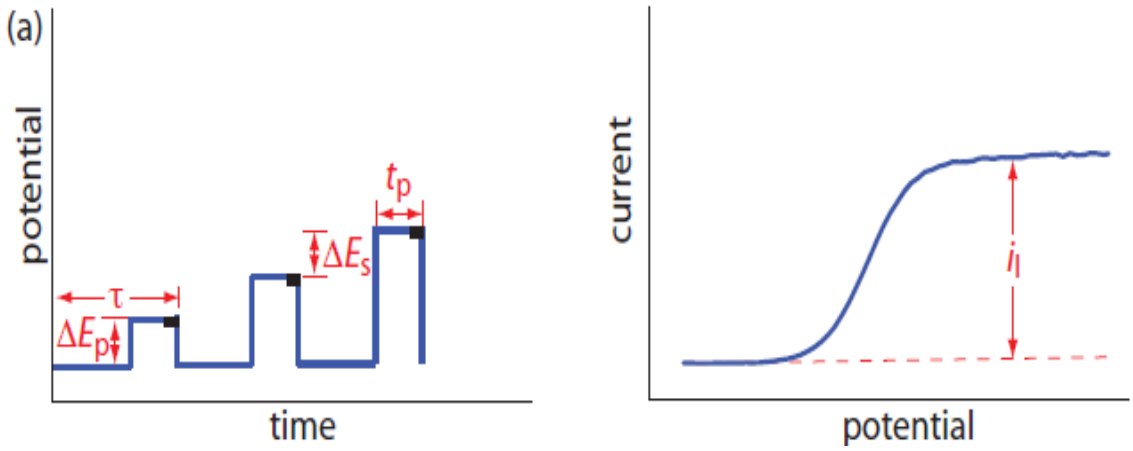

Figure 2.5. Potential-excitation signal and voltammogram of normal pulse voltammogram[65]

2.4.4.3. Differential pulse stripping voltammetry

The differential pulse stripping voltammetry technique is probably the most used stripping technique is comparable to the normal pulse technique since the potential is scanned with a series of pulses. The difference comes from the fixed potential pulses of amplitudes smaller than 100mV. In this technique the pulses of the fixed amplitude are superimposed on a slowly changing base potential [58]. Each pulse is generally about 50ms at most with repetition in every 5s. The current is measured just before the application of pulse and at the end of the pulse resulting in a peak-shaped voltammogram. The output current measured is the difference between the two differences and plotted against the base potential. The highest of the produced peak current is proportional to the concentration of analyte

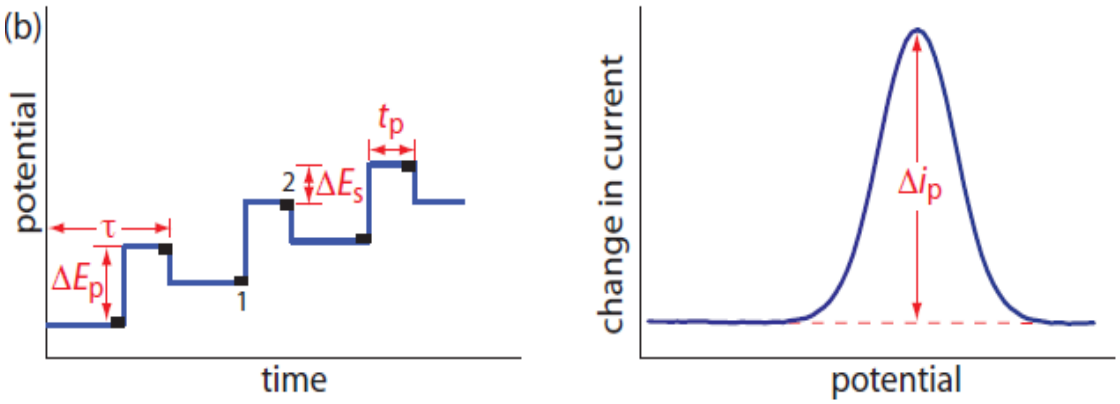

Figure 2.6. Potential-excitation signal and voltammogram of differential voltammogram[65]

2.4.4.4. Square wave stripping voltammetry (SWSV)

The square wave stripping voltammetry technique consist of a symmetrical square-wave pulse of amplitude superimposed on a staircase waveform of step height and is applied to the working electrode. At each square wave cycle, the current is doubled both at the end of the forward pulse and at the end of the reverse pulse, and taking the difference between the two, obtaining the net current, i_{net}. The net current is centered on the redox potential. The resulting difference is plotted versus the base potential. The obtained peak height is directly proportional to the concentration of the electroactive species and direct detection limits [64].

SWSV possess many advantages compared to other stripping modes. SWSV is fast, extremely sensitive as well as, its excellence in rejection of background currents. The SWSV currents are known to be more than 3 times higher than those of differential pulse voltammetry for both revisable and irreversible currents.

The SWSV has been selected for its speed, sensitivity and its ability to determine electroactive species at ultra-trace level

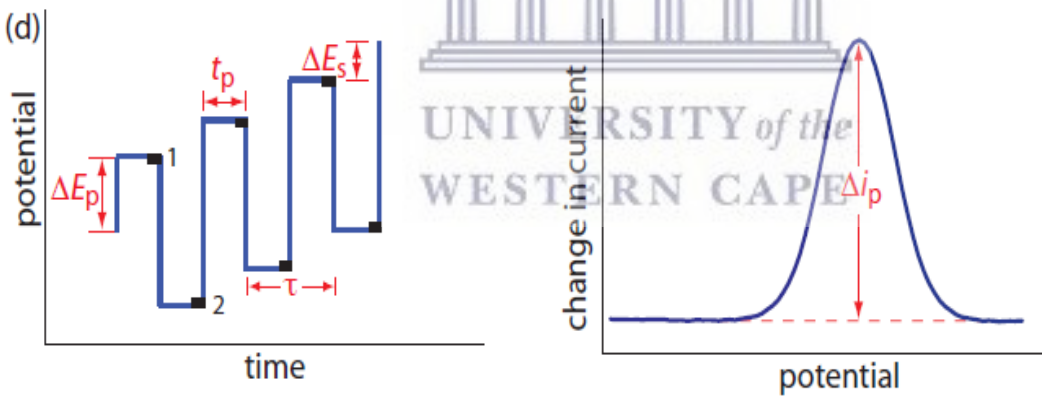

Figure 2.7. Potential-excitation signal and voltammogram of square-wave voltammogram[65]

2.4.4.5. Cyclic Voltammetry (CV)

2.5. Electrodes for stripping voltammetry

The working electrode is the electrode in an electrochemical system where the reaction of interest occurs. They are usually of various geometries and materials. The electrode is usually small hence making it easily polarized [60]. Working electrodes are made of inert materials such as Au, Ag,

Pt, glassy carbon and mercury film and mercury drop etc.; it is at this electrode where the potentials are applied for the electrochemical reaction to occur. The performance of the stripping voltammetry analysis is hugely influenced by the material of the working electrode.

2.5.1. The hanging mercury electrode (HMDE)

The hanging mercury electrode has been the mostly used electrode for stripping analysis traditionally mainly due to the fact that a clean electrode surface is easily regenerated with a new mercury electrode making it extremely reproducible. An entire stripping voltammetry analysis on the working electrode is done by a single mercury drop. Moreover, metals with a very high electronegative can be detected due to the fact that the potential window where mercury stays electro-inactive is very large [59]. The drops generated by modern Hg drop electrodes are very small (e.g. VA Stand 663 from Metrohm (Switzerland) produces drops with an area of 0.52 mm^2, and safe storage and recycling of the used Hg ensures minimal environmental risks. After the stripping analysis experiment, the mercury drop is discarded and replaced with a new drop for the next experiment. The amounts of mercury to operate these electrodes are still far below the loads typical for industrial use or the production of consumer goods (e.g., saving lamps). The measured current in an electrochemical experiment is proportional to the electrode area. The HMGE is still being upgraded and used to this day for the determination of Nickel, Cobalt, Zinc and other heavy metals, for example in the literature cobalt was detected by HMDE [66][67][68], using a combination of different complexing agents. However, HMDE suffers from drawbacks such as the toxicity from the mercury being used, also in maintaining the drop on the end of the capillary. If the mercury drop falls off, the experiment will have to be aborted. Other drawback is that metallic ions such as Hg, Au and Ag cannot be measured. Thin film mercury electrode has been used as an alternative as less mercury is used.

2.5.2. Thin film mercury electrode (TFME)

The introduction and later intensive propagation of the mercury film electrodes (MFEs,) represents, so far, the most successful attempt to replace the hanging mercury film electrode (HMFE). Thin film mercury electrodes are made by depositing a thin mercury film onto the

working electrode surface. TFME is mostly used for anodic stripping voltammetry, however, it has been used successfully in cathodic and adsorptive stripping voltammetry. Mercury displays a wide negative potential range because it is difficult to reduce hydrogen ion or water at the mercury surface, moreover its surface is readily regenerated by producing a new film, and many metal ions can be reversibly reduced into it. Mercury thin film electrodes are very sensitive electrodes because a very small amount of mercury is amalgamated into the film, and upon applying deposition potential, a concentrated amalgam gets formed [55]. However, because of the toxicity of mercury researchers have switched focus to alternative electrodes of less toxicity with similar performance to that of mercury. The alternative and less toxic electrodes used are antimony [69], bismuth [62], tin and lead [20], however, the performances of these electrodes has not reached that of mercury film. Most of the mercury free electrodes have been found to offer low background contribution, poor precision and resolution. Even though mercury is more toxic, the use of very low concentration for the formation of thin film layer in the micro or nanometer thicknesses for analysis is enough for the modification of electrode, hence reducing their danger and disposal. The concentration of mercury used is negligible when comparing to that of mass industrial use.

The TFMEs can be prepared ex situ by placing the working electrode in a solution containing reagent grade $Hg(NO_3)_2$ and once the TFME is formed it is then transferred into the sample solution, or they can be prepared by in situ in which the mercury ions are added directly to the sample solution to be analyzed. The ex situ prepared TFME has to be protected from the external oxygen to prevent any oxidation of the film [55]. During the preparation of TFMEs, very low concentration of mercury has to be used as the film is extremely thin.

2.5.3. Bismuth film electrode (BiFE)

The toxicity of the mercury based electrodes has made researchers change focus to more environmental friendly electrodes. Recently introduced bismuth electrodes offer a very attractive alternative to commonly used mercury electrodes. Thin-film bismuth electrodes show similar performances to that of mercury film electrodes since they have the ability of forming fused multicomponent alloys with heavy metals [70]. The other attractive qualities of thin-film bismuth electrodes are the ability to display well-defined, undistorted and highly reproducible response,

favorable resolution of neighboring peaks. To increase the performance of the bismuth thin film electrodes, polymeric materials such as nafion can be used hence improving the sensitivity and selectivity. Carbon-based nanomaterials have also been used and incorporated with bismuth film electrodes to increase the performance of the electrodes.

The major drawback for the thin-film bismuth electrodes is the narrowing of the cathodic potential range and its suffering from the instability in air due to its natural oxidation [71].

Bismuth film has been fabricated onto many conductive substrates such as the glassy carbon electrode, pencil graphite electrodes, ad noble metals etc.

2.5.4. Antimony film electrode (SbFE)

Antimony film electrodes like bismuth film electrodes offers alternative to commonly used mercury electrodes due to their environmentally friendliness. Introduced in 2007, seven years after the first introduction of the bismuth film electrodes, antimony has been found to exhibit excellent performance in more acidic media [57]. Antimony is usually fabricated on the conductive substrate by electroplating and microfabrication [57]. The SbFE features some interesting characteristics such as, favorable negative over-voltage of hydrogen evolution, wide operational potential window and interestingly low stripping signal for antimony itself, however, like BiFE the SbFE suffers from the same drawback such as their limited anodic range since these metals are oxidized at a more negative potential than mercury.

2.6. Complexing Agents (Ligands)

The selection of the suitable complexing agent is very important in achieving high sensitivity and selectivity. The complexing agents are chosen specifically due to their specificity of the ligand towards the metal of interest, absorbability of the ligand on the electrode surface, the pH and buffer being used and mostly for the resulting measurement sensitivity.

The definition of a ligand is the molecules or ions that are attached to the metal in a complex ion.

2.6.1. Dimethylglyoxime (DMG)

DMG has been one of the most commonly used ligands for the complexing of Ni and Co ions for the stripping analysis, which forms Ni/Co-DMG complex due to characteristic sensitivity and stability. DMG is a chemical compound described by the formula $CH_3C(NOH)C(NOH)CH_3$. DMG has the ability to be adsorbed on the electrode surface and significantly enhance the electrochemical response to Ni or Co metal ions [72]. Due to this property, DMG has been successfully used to detect Ni ions in natural water. A wide range of complexing agents have been employed in stripping analysis Ni^{2+} and are highly dependent on the application. The popularity use of DMG as a complexing agent hasn't stopped researchers to come up with other suitable complexing agents such as Pyrogallol Red [67], nitroso-R salt etc.

Using the adsorptive stripping voltammetry technique which is based on the accumulation of analyte species, the presence of DMG on an electroplated metal film helps to improve the detection of Ni which is often complicated and associated with low electrochemical signals. Hence improving/enhancing the sensitivity and selectivity of electrochemical sensors for Ni^{2+} determination.

Other metals such as Pb(II), Mn(II), Bi(III), Co(II), Cd(II), Zn(II), and Fe(II) at high enough concentration have been found to interfere with the determination of Ni^{2+}, however the introduction of chemically modified electrodes has come in handy in eliminating most of these intermetallic interferers. Below is the structure of Ni^{2+} and DMG complex.

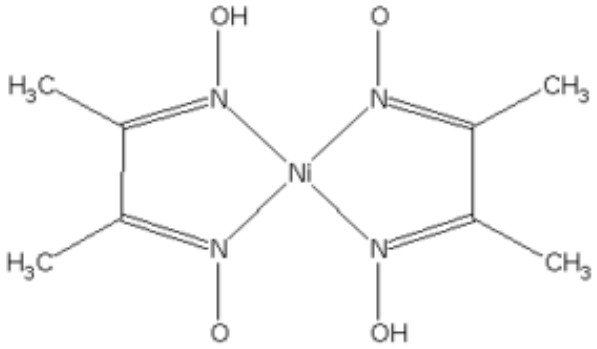

Figure 2.8. Structure of Ni – DMG complex

2.6.2. 1,2-Cyclohexanedione dioxime (Nioxime)

Nioxime is one of the most commonly used ligand used for the adsorptive stripping voltammetry of Co^{2+}. Nioxime fall under the family of dioxide. Various complexing agents has been used for the adsorptive stripping voltammetry of Co^{2+} including DMG [73], nitroso-S, calcon carboxylic acid, quercetin, 1–nitroso–2–naphthol, furyldioxime, and 4–(2– pyridylazo)resorcinol [67]. Among them, DMG and Nioxime are the most popular complex agents because they offer the higher selectivity, the better shape of voltammetric signal, and the more excellent sensitivity. Nioxime offers high selectivity for the stripping of Co in water samples than most complexing agents [8].

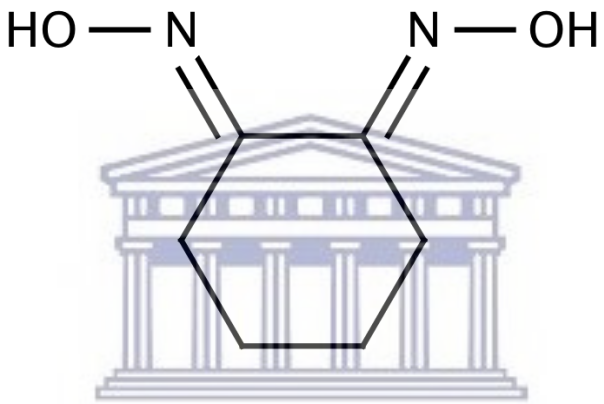

Figure 2.9. Structure of Nioxime

2.7. Application of stripping analysis

Stripping voltammetry techniques has been widely used in the analysis of a variety of numerous trace metals in environmental and surface active non-electroactive and electroactive organic substances in industrial and clinical samples, as well as for assays of foodstuffs, beverages, gunshot residues. Its merit lies in its ability to measure at trace level, hence possessing the ability to determine analytical species at extremely low concentration. The other advantage of using stripping analysis is its simultaneous determination of several analyte, the ability to determine kinetic and mechanistic parameters, a well-developed theory and thus the ability to reasonably estimate the values of unknown parameters [64]. Electroanalytical techniques can easily solve many problems of pharmaceutical and environmental interest with a high degree of accuracy, precision, sensitivity, and selectivity.

2.7.1. Environmental Analysis

Heavy metal pollution is one of the most serious environmental problems as so regulations are becoming stricter. Stripping analysis provides easy and fast analysis of metals as compared to other traditional methods of analysis such as atomic absorption or emission spectroscopies (AAS, AES, Inductively coupled plasma mass spectrometry (ICP-MS), cold vapor atomic fluorescence spectrometry (CVAFS) etc. these traditional methods are however expensive and require laborious pre-treatment processes. Many efforts have been made to develop sensors for monitoring heavy metals in the environment. Heavy metals (HMs) are persistent in the environment (waters and soils), which means that they cannot be degraded [59]. The growing demand for clean water has led to the increased attention surrounding water purification and monitoring and as a result the need for determination and characterization of these contaminants. Determination of heavy metals has traditionally been carried out in laboratories, where time-consuming sampling, transportation, preparation and storage steps are employed.

Heavy metals enter the environment mainly through mining, smelting, or different kinds of wastes. Once the environment has been pullulated, it is a necessity to monitor these toxic metals especially in the drinking water as it's the main consumptions of the population of such toxic metals. The consumptions of heavy metals above the required dosage can cause damage mainly to the nervous system, contribute to kidney diseases, causes damage to skin, eyes, and liver [59].

Although anodic stripping voltammetry has been a widely used technique for water analysis because of its low detection limit and specific sensitivity for different chemical forms of dissolved metals [55] and it requires no chemical pre-concentration by other chemical reagents, however, some metals like nickel, cobalt, zinc etc. are more suitable for the adsorptive stripping voltammetry as the complexing agent has the ability to be adsorbed on the electrode surface and significantly enhance the electrochemical response to Ni or Co metal ions.

2.7.2. Clinical Analysis

Electrochemical stripping voltammetry techniques have cemented their importance in the clinical analysis over the years. Electrochemical techniques are mostly used in the determination of pharmaceutical compounds in dosage forms such as tablets, capsules, injections and suspension. Electrochemical determination of biological samples such as real and spiked urine samples, blood and serum has also been reported [58].

Stripping analysis with the aid of chemically modified electrodes has enabled the improvement in the sensitivity and selectivity in the analysis of biological and pharmaceutical samples.

2.8. Nanoscience

Nanoscience is the study of structures and materials in the nanoscale range and can be used in science fields such as chemistry, physics, materials science, and engineering. Nanomaterials or nanoparticles whose size ranges from 1- 100nm are called nano-material/particles.

Nanomaterial/particles can be synthesized by top-down and bottom-up approaches. The top-down approach is whereby the nanoparticles are reproduced by breaking larger materials into smaller particles [74]. Typical examples top-down approach includes etching through the mask, ball milling, and application of severe plastic deformation. In top-down approach the bulk is machined down to the nanometer length scale by lithographic or laser ablation-condensation techniques. However, top-down methods are expensive, slow and not suitable for large scale production. In bottom-up, nanomaterial/particles are synthesized from atoms or molecules. During self-assembly the physical forces operating at nanoscale are used to combine basic units into larger stable structures. Examples are quantum dots and formation of nanoparticles from colloidal dispersion

Nanomaterials can be implemented in paint, coating, energy, cosmetics, medicine and drugs and clothing. One of the outstanding nanotechnology devices are nanosensors which are providing new solutions in chemical and biological sensing improving the detection sensitivity, specificity, and multiplexing capability in portable devices for a wide variety of health, safety, and environmental assessments.

2.9. Graphene

Carbon is a unique element with unique electronic structure and properties which allows hybridization to form more stable and strong allotropes than any other elements. Of those carbon allotropes, graphite and diamond are the most common ones. Both graphite and diamond are abundant natural minerals. Fullerenes and nanotubes are some of the carbon allotropes which were recently discovered, about 10-20 years ago and are currently a focus of attention for many physicists and chemists. The capability of carbon atoms to form complicated networks is fundamental to organic chemistry and the basis for the existence of life [75]. The diamond and graphite which are three-dimensional, nanotubes which are one-dimensional and fullerenes which are zero-dimensional were previously known, however the missing of the two-dimensional carbon allotrope was unknown until recently due to difficulties in experimental observation.

Graphite is made by hexagonally arranged carbon–carbon bonds which are rich in electrons, making it conduct well along the layers. Graphene, however, consist of single layers of carbon atoms tightly packed into a two-dimensional (2D) honeycomb crystal lattice. Graphene has unique properties, which makes it interesting for both fundamental studies and future applications. Graphene is viewed as the building block for other carbon allotropes such as the: 2D graphite by stalking individual graphene sheets on top of each other [76], rolling of graphene sheets forming 1D nanotubes and by rolling of graphene sheets by forming a 0D fullerenes as shown in *figure 2.11.* .

Graphene is very strong, ultra-thin, transparency and versatile [76] which makes it one of the most sort after studied materials in the recent years. Graphene has shown to significantly improve the sensitivity in various applications [71]. Due to these interesting properties of graphene, several applications of graphene are being successfully investigated, which include lightweight but durable electronic equipment, versatile processes for medical and other industries, solar cells, electrical circuits and many more. At normal temperatures the electrical charge carriers in graphene moves at speed 10-100 faster than modern silicon chips [77].

Graphene has found many usefulness in electrochemistry by successfully modifying sensor/electrodes for stripping analysis of heavy metals [18] and organic species [78].

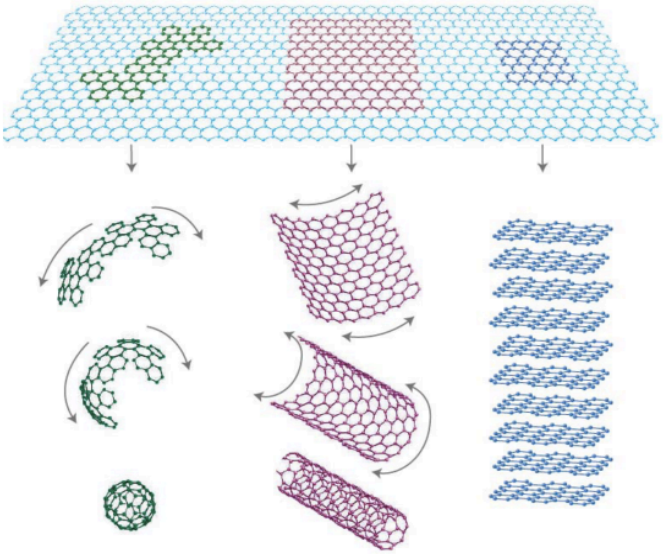

Fullerenes **carbon nanotubes** **graphite**

Figure 2.11. Formation of C60 fullerene molecules (0D), carbon nanotubes (1D) and graphite (3D) formed from the graphene layers (2D) [79]

The structure of graphene in *Figure 2.12.* represents a one atom thick graphene. Graphene is a single layer of graphite and a two-dimensional form of carbon which is one atom thick. Graphene is a honeycomb lattice of carbon atoms. The crystal structure of graphene is viewed from the electronic structure of an isolated C atom is $(1s)^2(2s)^2(2p)^4$; in a solid-state environment the 1s electrons remain more or less inert, but the 2s and 2p electrons hybridize. There is more than one stable configuration to the flat one-atom-thick membrane of graphene, therefore, by stacking sheets of graphene on top of each other we get graphite. The π orbitals between the different graphene layers only interact weakly, so the layers are only held together by a weak van der Waals attraction. This weak inter-layer coupling is what makes the graphite in pencils write so effectively [80].

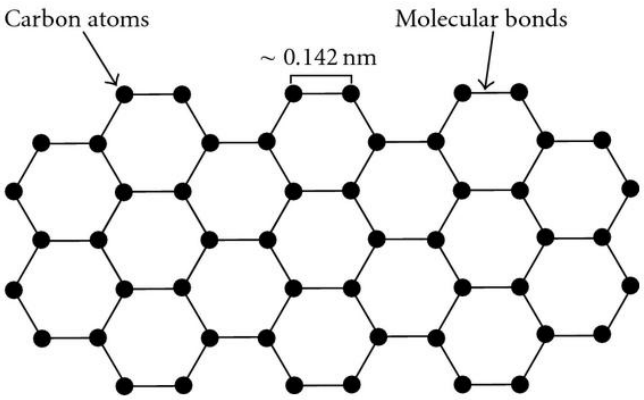

Figure 2.12. Structure of graphene

2.9.1. Discovery of graphene

Graphene was discovered by two working physicist Andre Geim and Konstantin Novoselov, working at the University of Manchester in the early 2000s. The two scientists were motivated by the study of carbon nanotubes; however, they found a way to lift off the flakes of material from a graphite surface using sticky tape obtaining graphene layers of few atoms thick. This was first technique to yield graphene layers [77]. The pair went on to win the noble price for physics in 2010.

2.9.3. Properties of graphene

2.9.3.1. Electronic and Electrical properties

Most of the current interest in graphene is in understanding and utilizing its unusual electrical properties. Electrical conductive is a measure of how easily charge carriers can move in the system. The electrical conductivity of a 2D graphene sheet is given by:

$$\sigma = en\mu$$ [79].

The electrical conductivity of graphene depends on two material parameters which are the carrier density (n) and the mobility (μ), however, the carrier density depends on the band structure of the graphene material and the Fermi Energy of the system [81]. The mobility is theoretically limited to $\mu = 200\ 000\ cm^2V^{-1}s^{-1}$ by acoustic phonons at a carrier density of $n = 1012\ cm^{-2}$. Graphene has resistivity of $\rho = 31$. The conductivity of bulk graphene is $0.96 \times 106\ \Omega^{-1}cm^{-1}$.

2.9.3.2. Mechanical properties

Among all the novelty of the wonder graphene material, its mechanical strength stood out as the outstanding of them all. Its outstanding properties include graphene been harder than diamond and is also known to be 300 times harder than steel of the same thickness [76]. Graphene has a breaking strength of 42 Nm^{-1}. Graphene mechanical properties depends on its quality, defect and structure. Graphene has been reported to stretch up until 20% of its original length. Graphene is very light with the weight of 0.77 mgm^{-2} and is nearly 100 times lighter than that of 1 m^2 of paper.

2.9.3.3. Optical properties

Graphene is a 2D atom thick gapless semiconductors where else graphite of many single graphene sheets piled on top of each other is a semimetal. Graphene has a very simple electron band structure. Graphene's high carrier mobility enables ultrafast extraction of photo-generated carriers, which leads to high-bandwidth operation. Graphene also has a wide spectral range from the ultraviolet to the infrared. Graphene band structure affects how it interacts with light and in optical absorption (A) of graphene is given by the equation below:

$$A = \pi\alpha = 2.3\%$$

Where, α = 1/137 is the fine structure constant. Graphene is almost transparent [82], owing to its unique electronic properties which absorb as high as 2.3% of light passing through it [76]. As such electronics companies are desperately looking for a cheap and plentiful material as a transparent electrode replacement for expensive and brittle indium tin oxide, employed, for example, in liquid crystal displays (LCDs).

2.9.3.4. Thermal properties

Graphene and its derivatives possess unique thermal properties due to their strong anisotropic bonding and the low mass of the carbon atoms. The thermal property of graphene arises due to the presence of elastic wave propagating through the graphene lattice called phonon. Graphene has a much higher thermal conductivity with an estimate of 5 000 $Wm^{-1}K^{-1}$ which is dominated

by photon and is known to be higher than copper (400 $Wm^{-1}K^{-1}$) and other carbon structures such as carbon nanotubes, graphite and diamond [76]. The substrate of which the graphene is onto can influence the thermal conductivity of graphene since there is a loss of photons at the interface of graphene-substrate and scattering at the interface [76].

2.9.4. Synthesis of graphene

The first laboratory method which was used to make graphene sheets involved a much harder and more laborious method of isolating monolayer graphene sheet from graphite by peeling of graphite. Ever since the first historical discovery of making graphene large-scale synthetic approaches for the making of graphene has become a necessity. Further research and methods has been introduced in order to improve the quality of graphene as well as to increase the cost-efficiency of it synthesis. The methodology for the synthesis of graphene is based on the exfoliation of pristine graphite into single layers of graphene sheets by two pathways, physical and chemical techniques [76]. The physical method for the synthesis of graphene include mechanical cleavage of graphite by Scotch tape protocol, epitaxial growth on silicon carbide substrate/wafer, chemical vapor deposition (CVD) of graphene on metal, growth of graphene from metal-carbon melts, exfoliation of graphite by ultrasonication, etc. The major factor in such techniques is there draw backs in large scale production, however, researchers has been able to synthesis high-quality graphene regardless the draw-backs. The CVD is the most effective method for the mass production of graphene while limiting the number of defects [83]. Mechanical exfoliation method is known to have a poor reproducibility and is not amenable to large-scale fabrication, however it produces graphene of less defects. Epitaxial based method has little or no defects for every single graphene island, however, the graphene produced is discontinuous.

The alternative to the physical method is the chemical based method which includes oxidation of graphite followed by reduction, unzipping of carbon nanotube by control oxidation, and total organic synthesis of graphene [76]. The synthesis of GO was first introduced by Brodie [76] and years that followed Staudenmaier [80] was able to modify the method which resulted in the production of highly oxidized GO in a one-step reaction process. In the 1950s Hummers reported a more popular method and ever since researchers have been modifying the Hummers method for

the synthesis of GO. The figure below shows the schematic chemical methods for the synthesis of GO from 3 different methods.

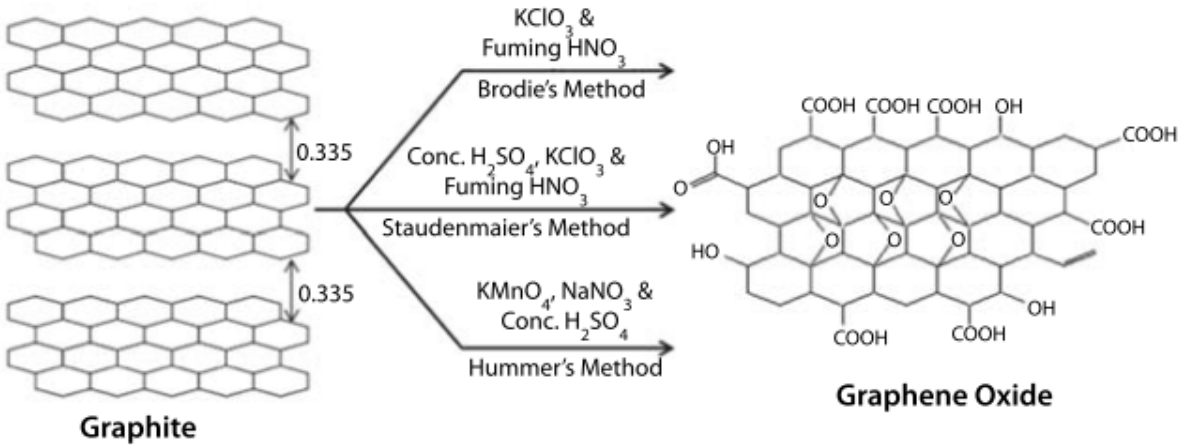

Figure 2.13. Schematic illustration of Brodie's method, Staudenmaier's method and Hummers' method for the synthesis of graphene oxide by chemical oxidation techniques[76]

In conclusion the oxidation of graphite followed by reduction based method is a better fit for the mass production of small graphene sheets, while the CVD method is more efficient for the mass production of high-quality graphene. The oxidation of graphite followed by reduction based method is of low cost and suitable for mass production and the majority of the defects can be removed in the process.

2.9.5. Application of graphene

The discovery of graphene special and unique properties has spiked a lot of researches around the world exploiting a wide range of applications. Graphene is a very light and strong material with a combination of its ability to conduct heat and electricity better than anything else makes it a very favourable material for many applications. Such unique properties of graphene can also be applied to existing materials to improve their performance and efficiency. Other application of graphene ranges from energy storage, photovoltaic cells, composite materials, high performance sensors, optical electronics and biological engineering.

Graphene-modified electrodes possess higher surface area, improved electron transfer rate, increased mass-transport rate, lower solution resistance, and higher signal-to-noise ratio [71].

Graphene and reduced graphene oxide have been incorporated in many carbon based electrodes for the detection of metals and other biological samples. Graphene-based electrodes have attracted many researchers in the analysis of heavy metals in water samples. It has been found that graphene-based electrodes have the ability to eliminate the memory effect and interferences of other ions from intermetallic compounds. Sohee Lee a and Seung-Keun Park reported voltammetric determination of trace heavy metals using an electrochemically deposited graphene/bismuth nanocomposite film-modified glassy carbon electrode [49]. Their work showed improved enhanced sensing platform as well as exhibiting high, sharp peaks for heavy metal ions, showing improved detection limits compared to unmodified carbon-based electrodes. In other work the graphene-based electrode was found to shows superior detection capabilities as a result of the improved surface-area-to-volume ratio and enhanced electron transfer kinetics following the incorporation of single layer graphene [84].

2.10. Pencil graphite electrodes

The development of portable sensors which are of low cost, easily prepared and widely available has been a priority for researchers. Pencil graphite electrodes (PGEs) have gained a large applicability to the analysis of various types of inorganic and organic compounds due to their electrochemical and economical characteristics.

2.11. Characterization technique for the characterization of Graphene and graphene oxide

The characterization techniques are a very inessential tool in understanding the quality and properties of the graphene and graphene oxide being synthesized. Each technique provides complementary information, from the number of defects in graphene to the purity of the synthesized graphene. The techniques used in this study includes Fourier transformed infrared spectroscopy (FT-IR), x-ray diffraction (XRD), Raman spectroscopy, Transmission electron microscopy (TEM) and scanning electron microscopy (SEM). A brief discussion of all the techniques will be carried out below.

2.11.1. Fourier transformed infrared spectroscopy (FT-IR)

FT-IR is one of the most preferred infrared spectroscopy. The electro-magnetic radiation of FT-IR

falls in the region from 0.7 mm to 1000 mm. However, the region between 2.5 mm and 25 mm (4000 to 400 cm^{-1}) is the most attractive for chemical analysis. The sample to be analyzed is radiated by the Infrared (IR) resulting in either absorption or transition. The absorption and transition of radiation by the sample gives rise to the spectrum of sample hence creating a molecular fingerprint.

FT-IR is used to identify unknown materials, to determine the quality or consistency of a sample and the peak size of the spectrum can be used to determine the amount of components in a mixture.

2.11.2. Raman

Raman spectroscopy is a spectroscopic technique used in condensed matter to study vibrational, rotational, bending of sample molecules (for the bulk sample, as well as adsorbed surface species) and other low- frequency modes in a system [85]. It relies on inelastic scattering of monochromatic light, usually from a laser in the visible, near infrared, or near ultraviolet. In Raman spectroscopy, the photons from the laser beam light are absorbed and re-emitted after laser light impinges onto the molecule of interest [86]. The shift in energy gives information about the phonon modes in the system. The energies of these transitions are plotted as a spectrum, i.e. identifying the molecule.

Raman spectroscopy finds its use mostly in chemistry since vibrational information is very specific for the chemical bonds in molecules. Raman offers high information content and one of its main advantages is the lack of sample preparation and it is compatible with aqueous systems.

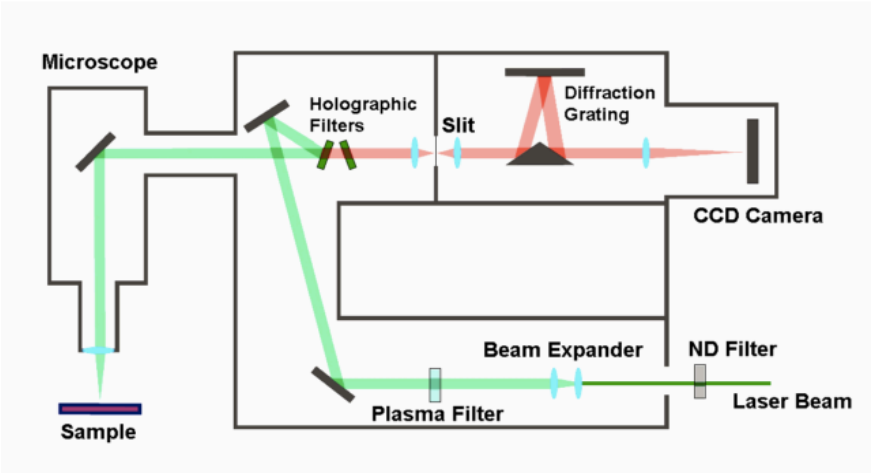

Figure 2.14. Schematic diagram of a Raman spectrometer

2.11.3. X-ray diffraction (XRD)

XRD provides information about crystallinity, crystallite size, orientation of the crystallites and phase composition. In XRD general scattering occurs when an X-ray beam encounters a crystalline lattice structure. X-rays are diffracted by crystals, as such when scattering in a certain direction is in phase with scattered rays from other atomic planes. Diffraction occurs when there is interference between X-ray scattered by the electrons in the various atoms at different locations in the unit cell. The interaction between the X-rays with atoms in two lattice planes, and the path length difference between rays equals a whole multiple of the wavelength of the radiation, constructive interference occurs [87]. Using the Bragg's law, the spacing between the planes and unit cells can be determined considering that the X-ray wavelength and diffraction are all know. The technique uniquely provides phase identification (e.g. graphite or diamond), along with phase quantification, crystallinity, crystallite size and unit cell size.

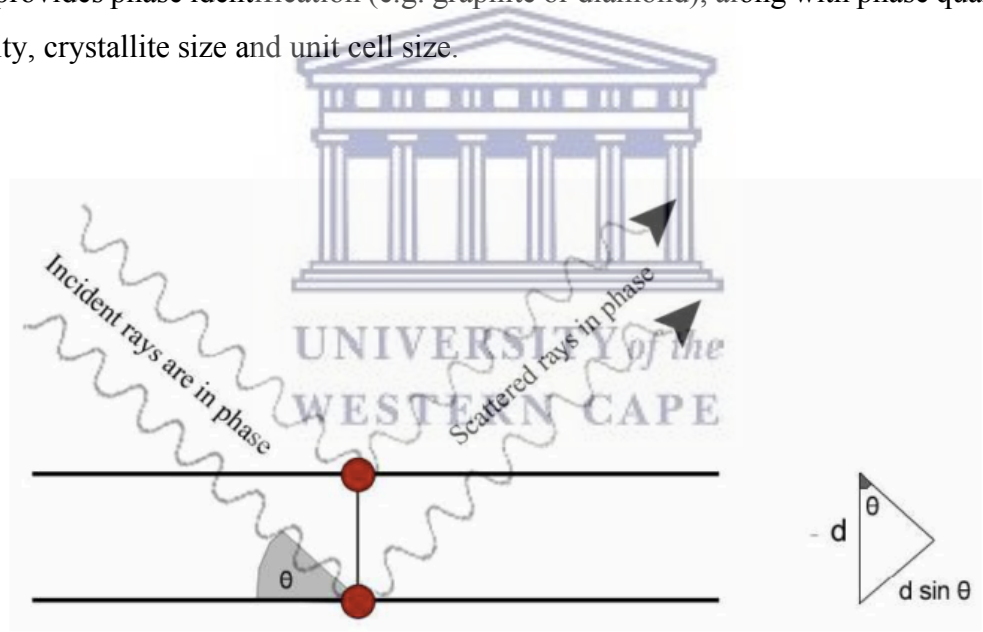

Figure 2.15. A schematic diagram of XRD[85]

2.11.4. High Resolution Transmission Electron Microscopy (HRTEM)

HRTEM allows the imaging of the crystallographic structure of a sample at an atomic scale hence considered as one of the most powerful technique material science. TEM allows lattice defects, atoms and even their movements to be seen. Compared to optical microscopy, Tem using a beam

of electrons instead of light. An electron gum emits electrons which travel through the vacuum chamber and interacts with the sample and the objective lenses produces an intermediate magnified image. The visualized image can be seen and the morphology of the sample is determined.

2.11.5. High Resolution Scanning Electron Microscopy (HRSEM)

HRSEM was first developed in the early 1900 s to overcome the challenges which were faced by the optical microscopy as it can observe and characterize organic and inorganic materials external morphology at increased magnification and resolution. In HRSEM the incident electron beam and the solid specimen interact and the resulting signal provides the information of the surface morphology and particle size

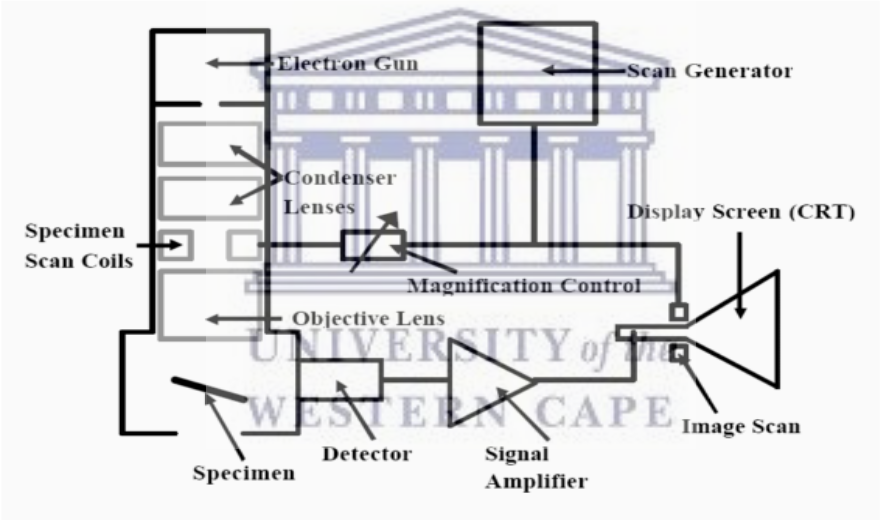

Figure 2.16. Schematic representation of HRSEM

CHAPTER 3

Methodology

3.1. Apparatus

Square-wave cathodic stripping voltammetric measurements were performed using a (a) 797 VA COMPUTRACE instrument (Metrohm, Switzerland) controlled by a (b) personal computer. A three electrode electrochemical system consisting of an electrochemically reduced graphene oxide pencil-graphite mercury-film electrode (ERGO-PG-MFE) served as the working electrode. An Ag/AgCl (saturated KCl) and platinum wire served as the reference and counter electrodes, respectively. All experiments were performed in a one compartment (c) 20 mL voltammetric cell at room temperature.

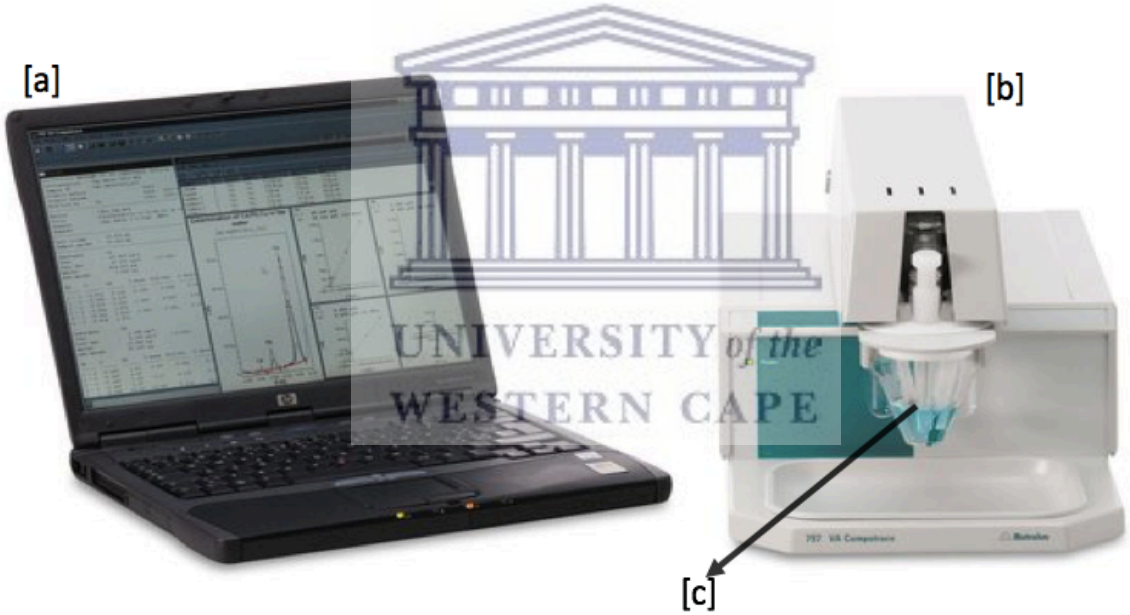

Figure 3.1. 797 VA COMPUTRACE

3.2. Chemicals and Reagents

All chemicals used in this study were analytical reagent grade and used without further purification. Standard stock solutions (1 000 mg L^{-1}, atomic absorption standard solution) were obtained from Sigma-Aldrich and diluted as required.

Ammonia-ammonium chloride solution buffer (0.1 M, pH 9.4) was used as supporting electrolyte and prepared by mixing ammonium chloride and ammonium hydroxide followed by diluting the solution with ultra-pure distilled water (Millipore). A pH meter (Metrohm 827 pH lab.) was calibrated using pH 4, pH 7 and pH 9 calibration buffer solutions and, then used to verify the pH of the ammonia-ammonium chloride buffer solution (supporting electrolyte) solution.

Chemical	**Source**
Nickel (1000mg/L)	Fluke
Cobalt (1000mg/L)	Fluka
Zinc (1000mg/L)	Fluka
Copper (1000mg/L)	Fluka
Mercury (1000mg/L)	Fluka
99% Ethanol	Saarchem
Hydrochloric acid	Saarchem
55% Nitric acid	KIMIX
Sodium acetate	Sigma
Dimethylglioxime (DMG)	Sigma-Aldrich
Nioxime	Sigma-Aldrich
Morin	Sigma-Aldrich

3.3. Standard solutions

3.3.1. Acetate buffer solution (pH 4.6)

Ultrapure water was mixed with 4.102 g of sodium acetate and 2.9 mL of acetic acid to make 0.1 M of acetate buffer solution (ABS) which was used for preparation of graphene oxide solution.

3.3.2. Ammonia-Ammonium chloride buffer solution (pH 9.4)

Ultrapure water was mixed with appropriate amount of ammonium hydroxide and ammonium chloride to make a solution of 0.1 M ammonia-ammonium chloride buffer solution of pH in the range of 9.2 – 9.4 which was used as the electrolyte for all electrochemical experiments.

3.3.3. Metal ions solution

Standard solutions were prepared in polyethylene vials in order to limit absorption onto the inner walls of the vial. Target metal ion solutions were prepared by diluting 1000 ppm, atomic adsorption standard solutions of Co and Ni with 0.01 M HCl. New and fresh metal ions were prepared every third week.

3.3.4. Nitric acid solution (6M)

6 M of Nitric acid solution was prepared by diluting Nitric acid (65 %) with ultrapure water on a volume to volume basis. The solution was used for cleaning and removing metal ions from electrode and glassware

3.4. Synthesis of Graphene Oxide

Graphite oxide was synthesized from graphite powder according to the Hummers method with some modification [88]. Graphite powder (2 g) and sodium nitrite (1 g) was mixed with sulfuric acid (50 mL) in a clean dry conical flask and stirred at room temperature for 30 minutes, followed by subsequent mixing in an ice bath for 20 min. Potassium permanganate (7 g) was added gradually over a 30-minute period with constant stirring. The resulting solution will help to reach room temperature prior to being placed in a water bath set at 35 ˚C and, left to stir for 2 hours. The flask was returned to the ice bath with constant stirring. Ultra-pure water, 150 mL, was added before the addition of approximately 5 mL hydrogen peroxide until effervescence ceases. The flask was removed from the ice bath and allowed to stir at room temperature overnight and centrifuged for 20 minutes. Three successive acid washes were performed followed by one with ultra-pure water.

The resulting product was dried for 48 hours in a vacuum oven. Below is the schematic representation of GO synthesis from graphite powder.

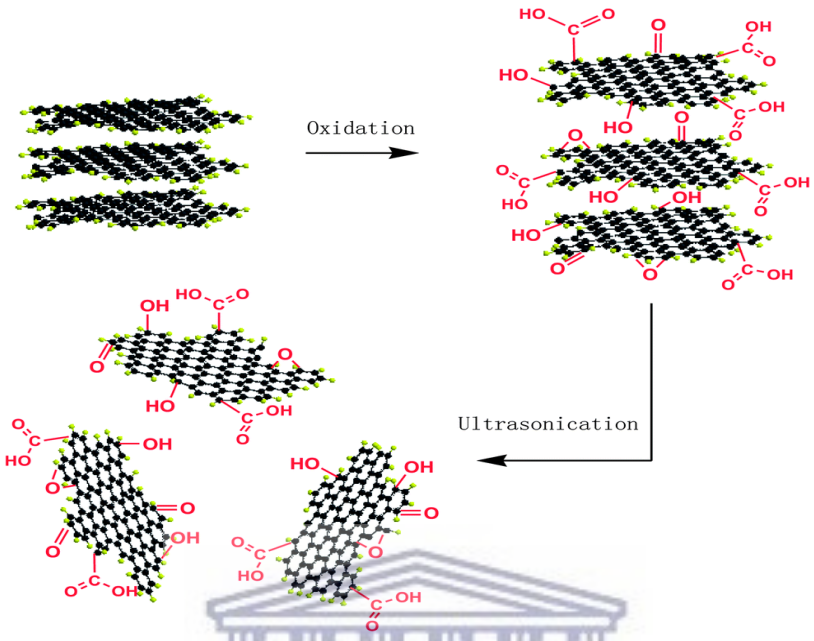

Figure 3.2. Schematic representation of GO synthesis from graphite powder[89]

3.5. Preparation of electrochemically reduced graphene oxide pencil graphite electrode (ERGO-PGE)

The pencil-graphite rods (Pentel, HB of 0.5 mm in diameter and 6 cm in length) was purchased from the local book store. A plastic syringe serves as a holder into which the pencil rod is inserted exposing 1 cm of the rod tip at one end of the syringe. In order to establish electrical connection with the potentiostat a copper wire was attached to the other end of the pencil rod and passed through the top of the syringe.

To make 100 mL of 0.5 mg mL^{-1} of Graphene Oxide solution, 50 mg of Graphene oxide was exfoliated in 100 mL of 0.1 M acetate buffer solution (pH 4.6) by ultrasonication for 2.0 hours to give 0.5 mg mL^{-1} GO solution. A thoroughly cleaned 1 cm of the pencil rod tip was immersed in 20 mL of GO dispersion (0.5 mg mL^{-1}) and cyclic voltammetric reduction of GO will be performed in the potential range between -1.5 and + 0.3 V for five successive cycles. The instrumental parameters that will be used for the electrodeposition procedure are as follows; deposition time (120 s), deposition potential (-0.7 V), cleaning time (30 s), sweep rate (0.1 V) and voltage step (0.005 V).

3.6. Electrode Cleaning

To achieve accurate and reproducible results in quantitative analysis impeccable electrode hygiene was applied. The pencil-graphite electrodes were thoroughly cleaned before their use and this was done by dipping a pencil graphite electrode in a small amount of ethanol for at least 60 secs and the surface of the electrode was gently wiped using a tissue paper followed by thorough rinsing with ultra-pure water. The electrodes were then left to dry in air for at least 5 minutes before using.

3.7. Procedure For Square Wave Adsorptive Cathodic Stripping Voltammetry (SWAdCSV) Analysis

Firstly, the cell, Teflon stirrer, counter electrode and reference electrode were cleaned with 6 M nitric acid and rinsed thoroughly with distilled water. 20 mL of NH_3-NH_4Cl (0.1 M, pH 9.4) buffer solution was pipetted into a volumetric cell. Subsequently, 100 µL Hg (1000 ppm), 100 µL Dimethylglyoxime (0.1 M in ethanol) and 10 µL of 10 mgL^{-1} each of heavy metals individually were added to the solution and purged with Nitrogen gas for 300 s to force out the dissolved oxygen while the solution was stirred and 30 s after each run thereafter. The stirring was stopped and the solution allowed equilibrating for 10 s. A deposition potential of -0.7 V was applied for 120 s using a voltage step of 5 mV, a frequency of 50 Hz and with constant stirring at 800 rpm for the individual analysis of Ni^{2+} and Co^{2+}, while for simultaneous analysis a deposition potential of - 0,3 V was used. After an equilibration time of 10 seconds a square wave waveform was applied from -0.7 V to -1.4 V followed by electrochemically cleaning of any target metals residues by applying a potential of +3 V for 120 s.

Once development of the electrode and an understanding of this technique has been achieved, tap water was collected and analyzed for the determination of $Co^{2+}$and Ni^{2+} using the new sensor developed above. Below is the schematic summary of the theory behind stripping analysis of heavy metals on an ERGO-PG-MFE.

3.8. Quantitation

The method of standard addition was used to determine the concentration of the analytes. For reproducibility purposes, each analysis was repeated for a minimum of three times. The concentrations of the analytes were calculated using the standard addition formula.

3.9. Sample Preparation

For the preparation of the water sample which was analyzed, tap water was collected in our research lab after being allowed to run for 1 minute. 18 mL of tap water and 2 mL of 1 M ammonia-ammonium chloride buffer solution was added to the compartment cell and the analysis of Ni and Co was carried out as describe in **Section 3.7** above.

3.10. Characterization Techniques

3.10.1. Fourier Transform Infrared (FT-IR) spectra

Fourier Transform Infrared (FT-IR) spectra were recorded using a (Perkin Elmer Spectrum 100) coupled to an Attenuated Total Reflectance (ATR) sample holder. FT-IR was used to obtain information and confirmation on graphene oxide.

3.10.2. High Resolution Scanning Electron Microscopy (HR-SEM)

The High Resolution Scanning Electron Microscopy (HR-SEM) images and information were obtained using a LEO 1450 SEM 30 kV instrument equipped with Electronic Data System (EDS) and Windows Deployment Services (WDS).

3.10.3. High Resolution Transmission Electron Microscopy (HRTEM)

High Resolution Transmission Electron Microscopy (HRTEM) measurements were carried out with a Tecnai G2 F20X-Twin MAT Field Emission Transmission Electron Microscope from FEI (Eindhoven, Netherlands) under an acceleration voltage of 200 kV.

3.10.4. Raman Spectroscopy

Raman spectroscopy was obtained using a Dilor XY Raman spectrometer with a Coherent Innova 300 Argon laser with a 514.5 nm laser excitation.

CHAPTER 4

Results & Discussions

Morphology and structural characterization of graphene oxide and reduced graphene oxide

4.1.1. Fourier Transformed Infrared Spectroscopy (FT-IR)

FT-IR spectroscopic analysis was used to investigate the chemical functionality of graphitic samples upon the subsequent chemical oxidation of pristine graphite by $KMnO_4$ and H_2SO_4. The FT-IR spectra of graphite and GO are shown in *Figure 4.1*. As expected, the FT-IR spectra of graphite exhibited little characteristic IR features between 400 and 4000 cm^{-1}. Low transmittance (%T) bands corresponding to O-H stretching vibration at 3595 cm^{-1}, C=O stretching vibration at 1817 cm^{-1} and graphitic domain at 1560 cm^{-1} are observed for commercial pristine graphite. All samples demonstrated a strong and broad peak at approximately 3375 cm^{-1}, attributed to the O-H stretching vibrations of adsorbed water molecules and absorption of crystal water by KBr during the sample preparation for FT-IR analysis [90], [91]. The presence of a variety of oxygen-containing moieties in GO was confirmed at 3375 cm^{-1} (O-H stretching vibrations), 1713 cm^{-1} (stretching vibrations from C=O), 1622 cm^{-1} (skeletal vibrations from un-oxidized graphitic domains), 1204 cm^{-1} (C-OH stretching vibrations), and 1060 cm^{-1} (C-O stretching vibrations). It was further confirmed, from the FT-IR spectra of GO, that both oxidation-approaches demonstrated the inclusion of similar oxygen-containing functional groups within the graphitic structure. The GO however, showed considerably stronger %T bands indicating a more effective oxidation.

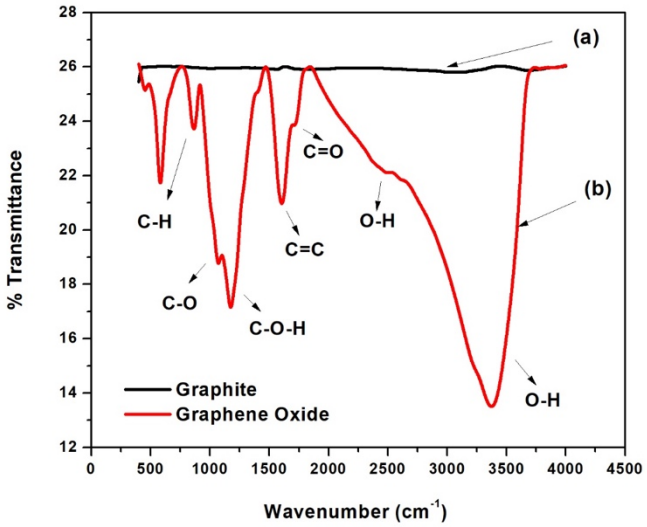

Figure 4.1. FT-IR spectra of (a) graphite and (b) GO by KBr pellets.

4.1.2. Raman Spectroscopy

The exfoliation behavior, structural changes and quality of the as produced graphene oxide, prepared by a modified Hummer's method (GO) from commercial pristine graphite, was analyzed by Raman spectroscopy at a 514 nm laser excitation and recorded in *Figure 4.2*. Defect-activated peaks allow for the interrogation of the graphitic structure "disorder", yielding an accurate technique to differentiate the graphite precursor from prepared graphene oxide [92]. The main Raman features include the D band at ~ 1350 cm^{-1}, as well as G mode at ~ 1600 cm^{-1} and the 2D band (or G' mode) at ~ 2600 – 3200 cm^{-1} which both always satisfies the Raman selection rules. The recorded Raman spectrum of graphite illustrates a significantly weak D bad located at 1350 cm^{-1}, a strong G band at 1575 cm^{-1} and a moderate 2D band at 2720 cm^{-1}. The G band corresponds to optical E_{2g} phonons at the Brillouin zone center and is due to the bond stretching of all pairs of sp^2 atoms in both rings and chains. The D peak is due to the breathing modes of sp^2 atoms in rings, while its intensity serves as a measure of the degree of "disorder" [93]. The relative intensities of the D and G bands (I_D/I_G), used as a measure of "disorder" or defects within the structure [42] was calculated as 0.09 for graphite, demonstrating the highly ordered structure. Furthermore, GO exposed a noteworthy increased intensity for the D band at 1360 cm^{-1}. This occurs as result of the oxygen-containing functional groups present between the individual graphite layers. A significant

decrease, broadening and Raman shift to 1600 cm^{-1} for the G band is also noted. A relative intensity, I_D/I_G ratio of 1.19 was observed depicting an increase in structural "disorder".

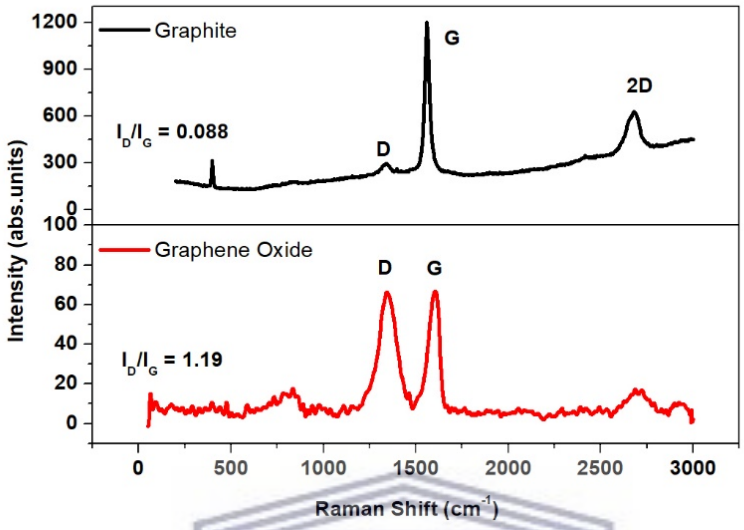

Figure 4.2. A comparison of recorded Raman spectra of graphite and GO at 514 nm.

Raman spectroscopic analysis was further used, for the first time to interrogate the deviation of pristine sp^2 graphitic components of pencil graphite substrates before and after modification with ERGO. The Raman spectra of both the (a) bare and (b) ERGO-PGEs were recorded between 0 – 4 000 cm^{-1} at 514 nm laser excitation and are illustrated in *Figure 4.3*. A typical Raman profile of neatly-ordered, crystalline graphite is seen for the unmodified PGE. D, G and 2D bands at 1345, 1587 and 2435 cm^{-1} respectively (as seen in **Section 4.12**.) correspond to the wavelength dependent and independent D and G bands, attributed to the measure of disorder and order in the graphitic structure as well as the wavelength-dependent sharp 2D band as a result of stacked graphite. Navratil *et al.* reported similar findings at varying pencil graphite substrates [94]. In addition to these, broadening of the 2D band due to stacking in multilayer graphite as well as an increase in disorder results in a $2D_1$ overtone (2713 cm^{-1}) and D+G band (2941 cm^{-1}). All remaining spurious peaks may occur as a result of ordered polymer-graphite features obtained during the graphite rod manufacturing process. The integrated ratios of the D and G band intensities (I_D/I_G) further provide important insight into the PGE's graphitic character. Hence, a highly ordered structure of the unmodified PGE may be inferred from the I_D/I_G of 0.31. Due to its ability for only bulk analysis rather than surface characterization, the Raman spectrum of the

ERGO-PGE is dominated largely by the graphite substrate. As such, deviation in the intensities of the corresponding D, G, 2D, $2D_1$ and D+G bands are observed from the unmodified PGE. A distinct lowering of Raman intensities and an overall increase in D band intensity demonstrates the destruction of the crystalline nature of the PGE and an increase in disorder due to surface modification of the PGE with ERGO sheets. A calculated I_D/I_G of 0.92 is observed. The $I_D/I_G \approx 1$ corresponds to reduced graphene oxide and confirms the deposition of graphene layers at the PGE surface. A study of the effect of the number of deposition cycles on the I_D/I_G at 0, 5, 7 and 35 electrochemical reduction cycles were performed on the PGE surface (*Figure 4.3&4.4)*. An overall increase in I_D/I_G with increasing ERGO layers is demonstrated with I_D/I_G of 0.31, 0.92, 0.91 and 1.12 for the 0, 5, 7 and 35 ERGO cycles. Similar ratios are obtained for both 5 and 7 cycles. The result thus confirms the deposition of more ERGO sheets at the PGE surface with increasing deposition cycles. The similar results for both 5 and 7 deposition cycles is further confirmed by electrochemical characterization in *Figure 4.12* of **Section 4.2.2**.

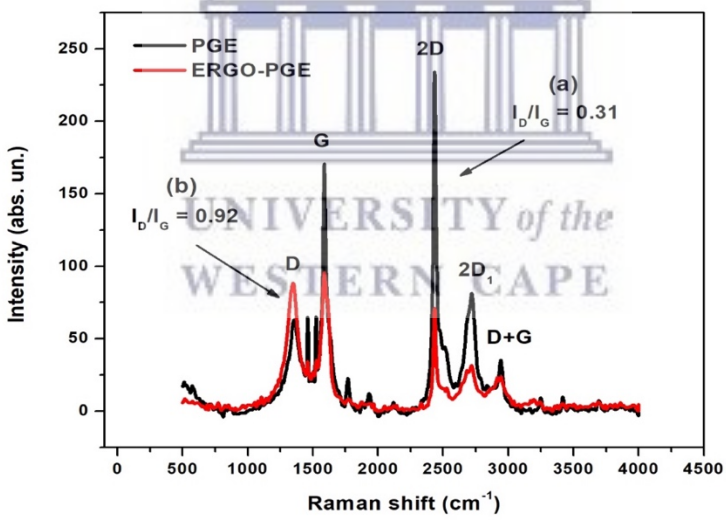

Figure 4.3. A comparison of recorded Raman spectra of (a) bare-PGE and (b) ERGO-PGE at 514nm wavelength

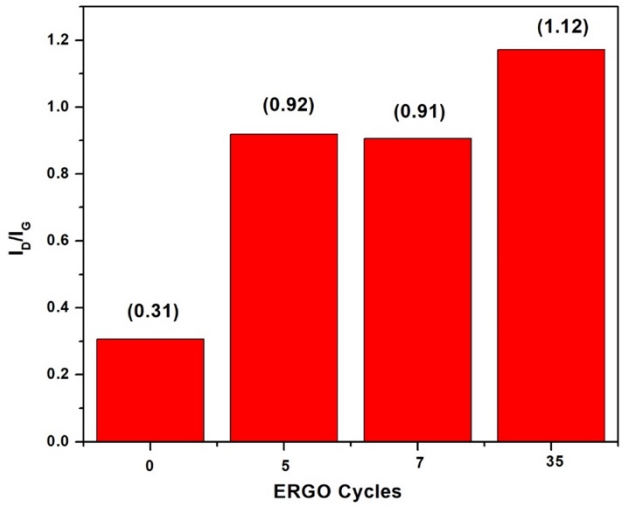

Figure 4.4. A study of the effect of ERGO cycles on the Raman I_D/I_G at PGE substrates.

4.1.3. X-ray Diffraction (XRD

The overall oxidation process was supported by the X-ray diffraction (XRD) analysis. *Figure 4.5* represents the XRD spectra of (a) graphite and (b) GO, respectively. The peaks indexed at 44.6º (004) and 54.7º (110) demonstrate a highly crystalline structure for graphite. The strong, sharp peak at 26,56° signifies a basal reflection of the 002 plane, with an inter-planar distance of 0.34 nm and implies a highly ordered carbon structure [95]. GO exhibited a shift in the basal reflection to 10° attributed to reflection in the 001 plane corresponding to the presence of oxygen-containing functional groups formed during oxidation [18]. An increase in d-spacing or interlayer spacing to approximately 0.7 nm is thus achieved as a result of oxygen intercalation of the basal graphite [96]. These functional groups cause the GO sheets to stack more loosely and, the broad peak at 25° may be due to the appearance of exfoliated GO sheets. Effective oxidation of pristine graphite was thus achieved. Similar results are reported by Yang *et al.* [97].

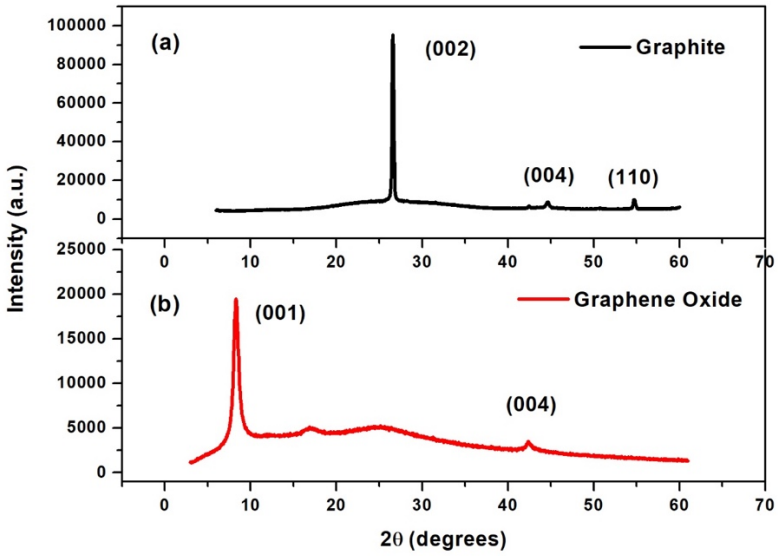

Figure 4.5. X-Ray diffraction spectra of (a) graphite and (b) GO

4.1.4. High Resolution Transmission Electron Microscopy (HRTEM)

The HRTEM images of graphite (a, b) and graphene oxide (c, d), at varying magnifications, are illustrated in *Figure 4.6*. Holey-mesh Cu grids, prepared by drop casting of highly exfoliated samples were used for HRTEM analysis. It may be disclosed, from the HRTEM image of graphite (*Figure 4.6a and 4.6b*), that a highly ordered crystalline orientation exists, as indicated by the dark flake with no distinct shape and straight edges [42]. In contrast, HRTEM images of GO (*Figure 4.6c and 4.6d*), signify that the sample is a layered (indicated by arrows), consisting of stacked GO sheets as a result of intercalation. Further, the larger and increasingly transparent sheets resemble wavy silk veils entangled with one another. Monolayer GO sheets can be seen in *Figure 6d* at higher magnification

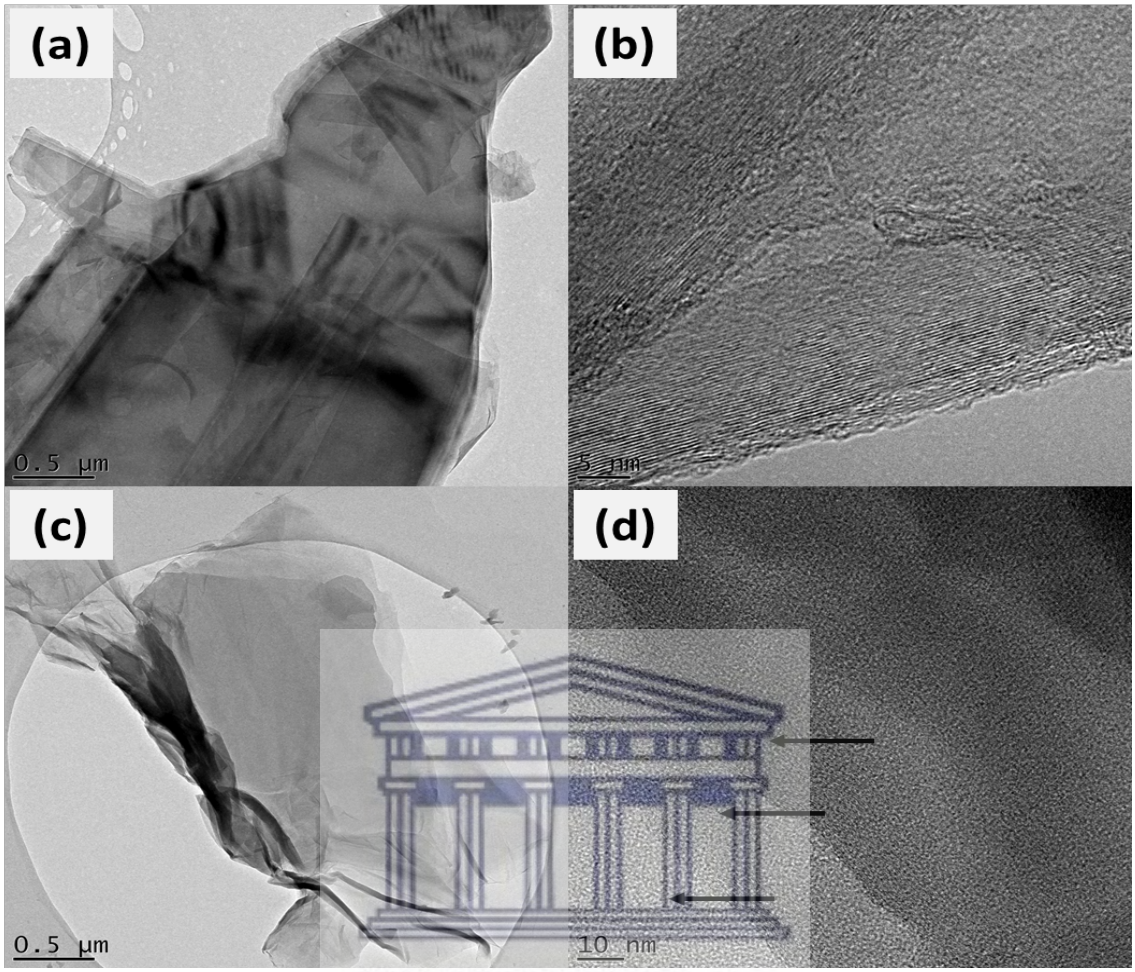

Figure 4.6. HRTEM images of [(a) and (b)] graphite and [(c) and (d)] GO

4.1.5. High Resolution Scanning Electron Microscopy (HRSEM)

Microscopic characterization of electrochemically reduced graphene oxide modified pencil-graphite electrode (ERGO-PGE)

The high-resolution scanning electron microscope (HRSEM) images of the bare PGE and ERGO-PGE surfaces are shown in *Figure 4.7*. Surface roughness with grooves on the surface along the direction of machining can be observed at the bare PGE surface. Following the electrochemical reduction of graphene oxide flakes of graphene sheets are observed at the ERGO-PGE surface confirming adequate electrode coverage.

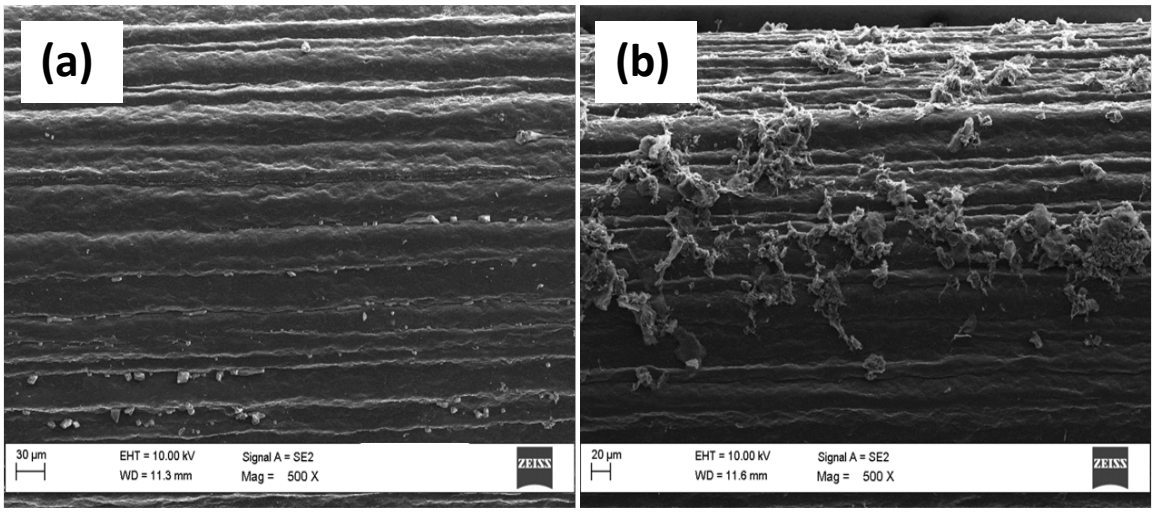

Figure 4.7. HRSEM images of (a) bare-PGE and (b) ERGO-PGE with 5 deposition cycles at 500 times magnification.

HRSEM has the advantages in detecting impurities, ruptures, folds, voids, and discontinuities of synthesized or transferred graphene sheets on a variety of substrates. The SEM images of graphite, GO are shown in *Figure 4.8 (a and b),* respectively**.** A HRSEM image of feathery GO powder *Figure 4.8(b)*, shows an agglomeration of the exfoliated platelets. It is noticed that the GO shows an uneven surface which may be attributed to the oxidation of sheets**.** Furthermore, the SEM images for GO reveals that the GO material consists of thin, haphazardly aggregated, wrinkly sheets closely linked with each other forming a shapeless solid.

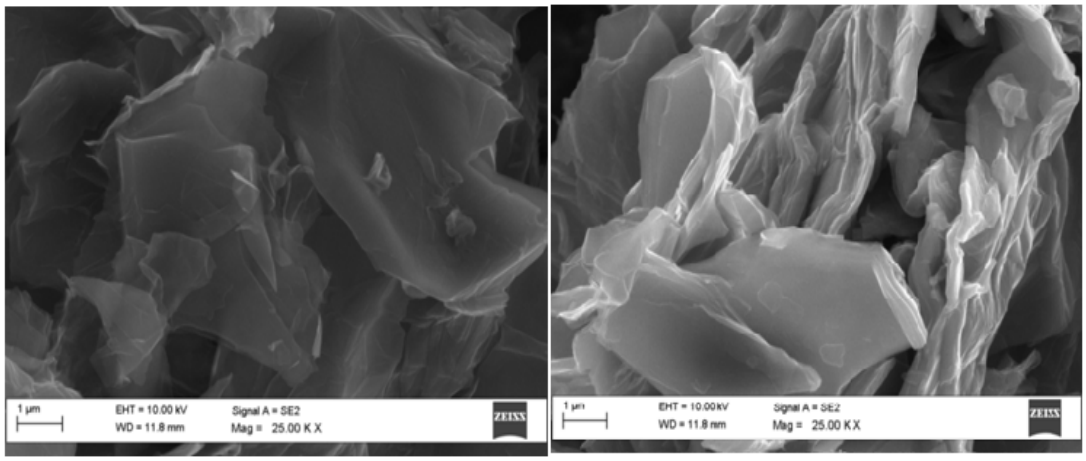

Figure 4.8. HRSEM images of graphite (left) and graphene oxide(right).

Electrochemical Characterization of the ERGO-PGE

4.1.6. Electrochemical Reduction Of Graphene Oxide (GO)

Deoxygenation treatment of GO, to restore the π-network and electrical conductivity of the graphene structure, was accomplished via a one-step electrochemical reduction approach. Here, ERGO thin films were produced on the PGE surface by a direct electrochemical reduction of GO sheets from an aqueous colloidal suspension in the presence of acetate buffer electrolyte [98]. *Figure 4.9*, shows a typical cyclic voltammetric reduction of GO, 0.5 mg mL^{-1}, where a PGE served as the working electrode. The cyclic voltammogram shows two anodic (I and II) and one cathodic (III) wave between – 1.5 and + 0.3 V. A decrease in oxidation peak (II), at ~ 0.2 V with increasing scan number signifies the irreversible deposition of ERGO sheets directly onto the WE surface. The cathodic peak (III) decreases with increasing number of scans can be ascribed to the reduction of electrochemically active oxygen-containing groups on the surface of GO [99]. Five successive deposition cycles were selected for all further experiments. The reduced graphene sheets on a pencil electrode compliments the results shown in Raman spectrum in **Section 4.1.2**.

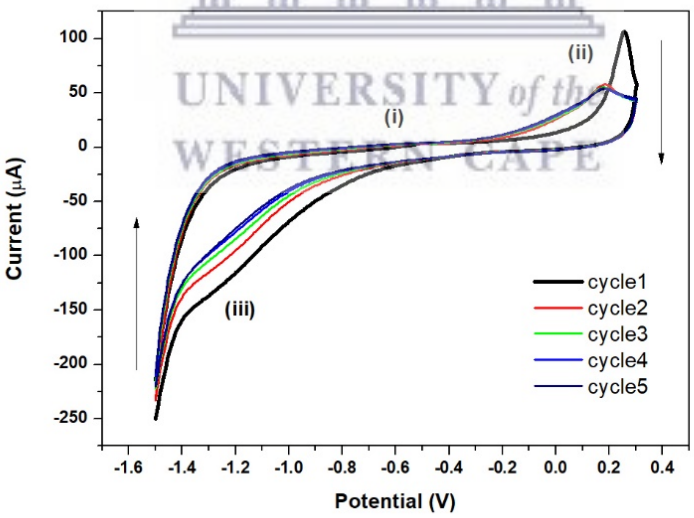

Figure 4.9. Cyclic voltammograms depicting the electrochemical reduction of 0.5 mg mL^{-1} GO in acetate buffer solution (0.1 M, pH 4.6) at the PGE from potential of -1.5 and +0.3 V using the following instrumental parameters: scan rate (10 mV s^{-1}), deposition time (120 s); amplitude (0.05 V) and voltage step (0.005 V).

4.1.7. Electrochemical characterization of the modified pencil graphite electrode

Recorded cyclic voltammograms of 0.1 M ammonia-ammonium chloride buffer solution at the bare PGE and ERGO-PGE are shown in *Figure 4.10*. A significant increase in capacitive current is observed for the ERGO-PGE in comparison with the PGE as a result of enhanced electron transfer rates and electronic conductivity of reduced graphene oxide immobilized at the electrode surface.

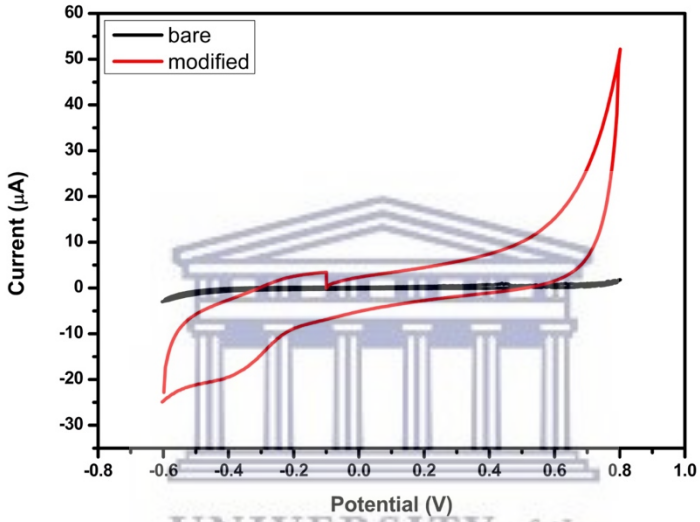

Figure 4.10. Cyclic voltammograms of bare PGE and an ERGO-PGE in NH_3-NH_4Cl buffer solution (0.1 M, pH 9.4) at the following instrumental parameters: scan rate (10 mV s^{-1}), deposition time (120 s), amplitude (0.04 V) and voltage step (0.004 V).

The heterogeneous electron-transfer kinetics between electrochemically reduced graphene oxide (ERGO) thin films immobilized on a PGE surface and a ferri/ferrocyanide ($Fe(CN)_6^{3-/4}$) redox probe was studied by cyclic voltammetry experiments in order to assess its electrochemical response. Typical cyclic voltammograms of 5 mM $Fe(CN)_6^{3-/4}$ in the presence of 0.1 M KCl electrolyte solution at a bare PGE and ERGO-PGE with the corresponding reduction and oxidation of mediator species is shown in *Figure 4.11*. A typical near ideal quasi-reversible system is demonstrated at both modified and unmodified PGEs. It is evident to see that the ERGO deposited on a PG surface increases both the anodic and cathodic redox peaks currents when compared with

the unmodified electrodes. Further, a distinct narrowing in peak separation, ΔE_p ($\Delta E_{p,a}$ - $\Delta E_{p,c}$), of the anodic and cathodic peak potentials recorded at the ERGO-PGE (0.106 V) is observed over the unmodified PGE (0.529 V). A higher electroactive graphene interface was thus formed, moreover owing to its high conductivity and improved active surface area.

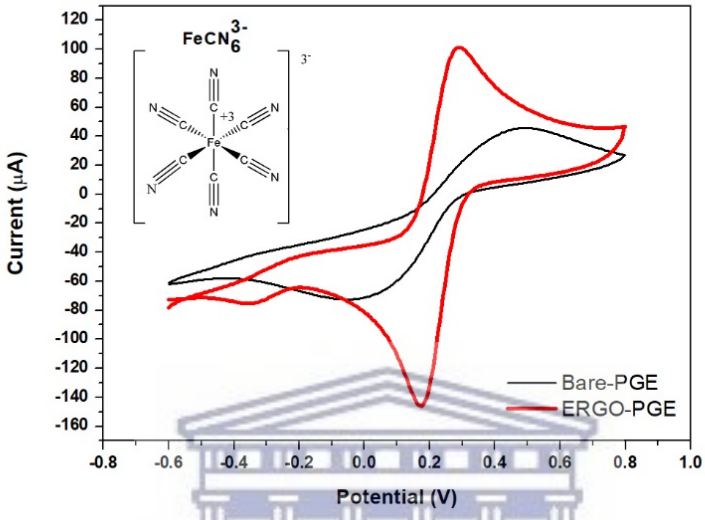

Figure 4.11. Cyclic voltammogram of a bare-PGE and ERGO-PGE in 0.1 mM $K_3Fe(CN)_6$ solution containing 0.1 M KCl. The inset is the $Fe(CN)_6^{3-}$ mediator species structure.

The heterogeneous electron-transfer kinetics between electrochemically reduced graphene oxide (ERGO) thin films immobilized on a PGE surface and a ferri/ferrocyanide ($Fe(CN)_6^{3-/4}$) redox probe was studied by cyclic voltammetry experiments to assess its electrochemical response. Typical cyclic voltammograms of 5 mM $Fe(CN)_6^{3-/4}$ mediator species in the presence of 1 M KCl electrolyte solution at (a) a bare PGE and ERGO-PGE with (b) 5, (c) 7 and (d) 14 reduction cycles are shown in *Figure 4.12*. A typical near ideal reversible one-electron transfer system is demonstrated at the modified and unmodified PGEs. It is evident that the ERGO deposited on a PG surface increases both the anodic and cathodic redox peak currents when compared with the unmodified electrode. Furthermore, a distinct narrowing of peak separation, $\Delta E_p = (E_{pa} - E_{pc})$, of the anodic and cathodic peak potentials recorded at the ERGO-PGE is observed over the unmodified PGE (0.259 V). The ΔE_p values of the ERGO-PGEs with 5, 7 and 14 reduction cycles are 0.063 V, 0.076 V, and 0.077 V respectively. A higher electroactive graphene interface was thus formed, moreover owing to its high conductivity and improved active surface area. The

appearance of the second reduction peak at -0.3 V shows that a higher electroactive graphene interface was thus form, moreover, indicating the thickness of the graphene layer. Five electrochemical reduction cycles provided the ERGO-PGE with the best electrochemical response and was chosen for all further experiments.

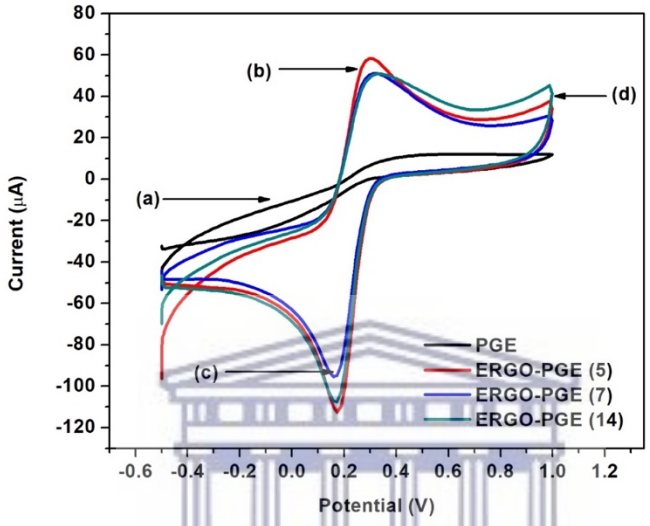

Figure 4.12. Cyclic voltammogram of (a) bare PGE, ERGO-PGE (b) 5 cycles, (c) 7 cycles and (d) 14 cycles in 5 mM $K_3Fe(CN)_6$ solution containing 0.1 M KCl.

The ERGO-PGE was further used in the 0.1 mM $K_3Fe(CN)_6$ solution containing 0.1 M KCl and subjected to potential scan rates from 10mV/s to 100mV/s *Figure 4.13*. For a more positive scan (forward scan) which is sufficiently positive to oxidize $Fe(CN)6^{-4}$, the anodic current on the electrode surface process is as follows:

$$Fe(CN)_6^{-4} \rightarrow Fe(CN)_6^{-3} + e^-$$

In the forward scan $Fe(CN)_6^{-3}$ is electrochemically generated from $Fe(CN)_6^{-4}$ hence the anodic process and for the cathodic process the $Fe(CN)_6^{-3}$ is reduced back to the $Fe(CN)_6^{-4}$ following a reverse scan. The linear dependence of both the reduction and oxidation peak current on the scan rate shows that the ERGO-PGE is diffusion controlled [100]. Oxidation and reduction currents of the Fe(III)/Fe(II) couple was observed to increase with scan rate due to heterogeneous kinetics and

IR effects as shown in *Figure 4.13*. The valuable information concerning the electrode reaction mechanism (rate-determining step) was acquired from the relationship between the peak current and scan rate (v). It is observed that the magnitude of anodic and cathodic peak currents increase with increasing scan rate and an increase in peak separation of the reversible redox couple demonstrate an increase in electro-catalytic activity as well as improve the surface area-to-volume ratio.

The Randle-Sevcik equation (*Equation 1*), at room temperature, was used to estimate the diffusion coefficient (D) and rate of diffusion of ferri/ferrocyanide ions between the aqueous media and modified and unmodified PGE surfaces.

$$i_p = (2.69 \times 10^5)\, n^{\frac{3}{2}} A D^{\frac{1}{2}} C v^{\frac{1}{2}} \qquad (1)$$

Where i_p is the current (amps), n is the number of electrons transferred in the redox event, A is the electrode area (cm^2), D is the diffusion coefficient ($cm^2\ s^{-1}$), C is the concentration ($mol\ cm^{-3}$) and v is the scan rate ($V\ s^{-1}$). A linear plot of peak current vs the square root of scan rate (*Figure 12, inset*) was used. The diffusion coefficients (D) of the anodic and cathodic peaks were calculated as 7.89×10^{-7} and 7.32×10^{-7} $cm^2\ s^{-1}$ respectively. The similar values indicate no permanent electronic changes in the ERGO—film upon cycling. In comparison, the unmodified PGE demonstrated lower estimated D values of 5.66×10^{-7} and 5.39×10^{-7} $cm^2\ s^{-1}$ for the anodic and cathodic peaks. The improved diffusion coefficients as a direct result of electrode modification with ERGO sheets show faster rates of diffusion of $Fe(CN)_6^{3-/4}$ ions due to an enhanced electroactive surface area. Comparable results were reported for diffusion coefficients of 5 mM $Fe(CN)_6^{3-/4}$ ions in 0.1 M KCl electrolyte at PGEs [101], [102]. The active electrode surface area could further be approximated using a literature value for $Fe(CN)_6^{3-/4}$ ions from *Equation 1*. The active electrode surface area was calculated to be 0.043 and 0.051 cm^2 for the bare and ERGO-PGEs respectively. This result further demonstrates the increase in electroactive surface area due to modification with graphene.

The electroactive surface coverage of five-cycle electrochemically reduced graphene oxide (ERGO) thin-films at the PGE surface were then estimated by the Brown-Anson model, as given by *Equation 2*.

$$i_p = n^2 F^2 \Gamma^*_{ERGO-PGE} \left(\frac{Av}{4RT}\right) \qquad (2)$$

Where i_p n, υ and A are the same as described in *Equation 1* above, while F, R and T denote the Faraday constant (96 485 C mol^{-1}), molar gas constant (J K^{-1} mol^{-1}) and temperature (298 K) respectively and Γ^* is the electrode surface concentration. CV plots of potential vs current were used to determine approximate active surface concentrations. The value for Γ^* of the ERGO-PGE (1.25 x 10^{-9} mol cm^{-2}) is greater than that of the unmodified PGE (1.06 x 10^{-9} mol cm^{-2}). The increase in Γ^* indicates enhanced active surface area of the ERGO-PGE over the unmodified PGE due to increased adsorption of the redox mediator species at the ERGO-PGE surface.

Electron transfer between the modified electrode and the electrolyte solution was approximated using the heterogeneous electron transfer rate constant (K_s) according to the Laviron model [103].

$$K_s = mnF\upsilon/RT \qquad (3)$$

F, R, T, n and υ are the same as previously described while m is a constant based on the anodic and cathodic peak separation (ΔE_p). The electron transfers rate (K_s) of 1.2 s^{-1} and 0.5 s^{-1} was estimated for the ERGO-PGE and PGE, respectively. The faster rate confirms the improved electron exchange through the ERGO modified surface.

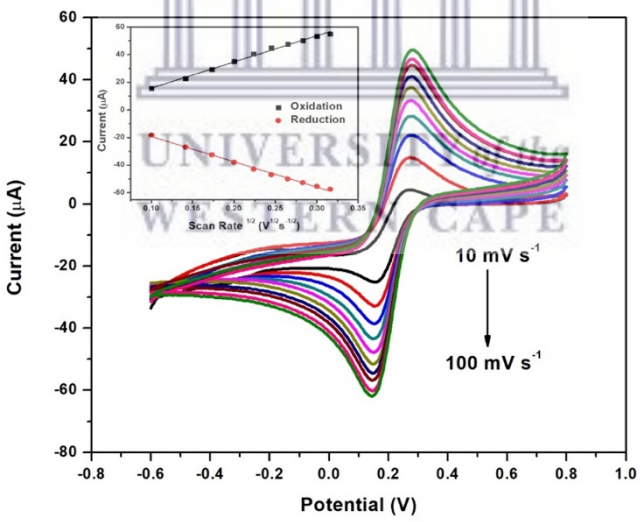

Figure 4.13. Effect of scan rate variation Cyclic voltammogram of a ERGO-PGE in 0.1mM $K_3Fe(CN)_6$ solution containing 0.1 M KCl. from 10mV/s to 100mV/s. The inset is the linear plots of peak current vs. $(\text{scan rate})^{1/2}$ for the anodic and cathodic scans

Electrochemical impedance spectroscopy (EIS) was used to study the electronic changes associated with the electrochemical reduction of graphene oxide sheets at the PGE surface. The impedimetric spectra of (a) bare PGE and (b) ERGO-PGE were studied in the presence of a 5 mM $Fe(CN)_6^{3-/4}$ mediator species in 0.1 M KCl electrolyte solution. *Figure 4.14* shows the Nyquist plot of the unmodified PGE (curve a) and the ERGO-PGE (curve b). Here, semicircle regions at high frequencies demonstrate charge transfer resistance (R_{ct}) and double layer capacitive (C_{dl}) behaviour while low frequencies indicate linear diffusion parameters. EIS fitting was performed by means of a Randles equivalent circuit comprising of solution resistance (R_s), charge transfer resistance (R_{ct}), double layer capacitance (C_{dl}) and Warburg impedance (Z_w) components [104]. The bare PGE shows a large depressed semicircle (R_{ct} = 24 221 Ω) while the ERGO-PGE in contrast is illustrated by a significantly smaller well resolved semicircle (R_{ct} = 2047 Ω). The lower R_{ct} values demonstrate improved electron transfer kinetics associated with highly conductive reduced graphene oxide at the PGE surface [105]. The results confirm the findings of electrochemical characterization above.

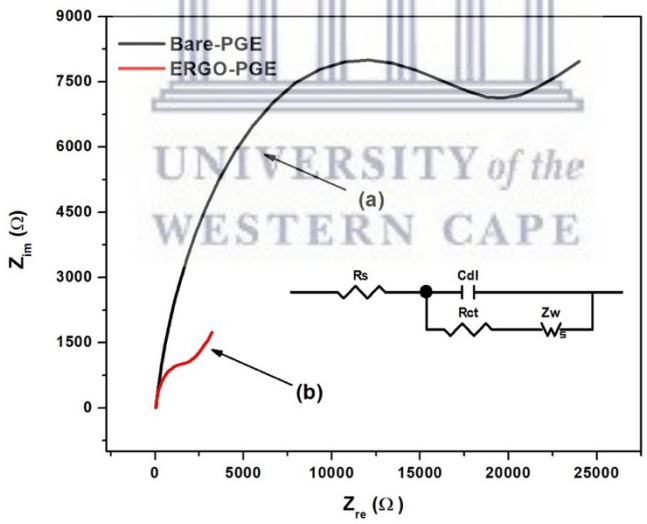

Figure 4.14. Nyquist EIS plot of (a) Bare-PGE and (b) ERGO-PGE in the presence of 5 mM $Fe(CN)_6^{3-/4}$ (1 M KCl).

CHAPTER 4: Part A

The determination of Ni^{2+} with DMG complexes on ERGO-PG-MFE

In this section the stripping voltammetric responses of the Ni ions, were used to obtain the various optimized instrumental parameters and to determine the analytical parameters for the ERGO-PG-HgE. The optimized DMG concentration of 58 mgL^{-1} was used as the complexing agent for the individual analysis of Ni ions. The specificity and selectivity of ERGO-PG-MFE in conjunction with DMG as a complexing agent for the determination of Ni was carried out and the interference by Co, Zn and other interferers was investigated.

4.3.1. Characteristic reduction potential of Ni(II)-$(DMG)_2$ complex

Figure 4.15 illustrates the characteristic reduction potential of the nickel-dimethylglyoxime (Ni(II)DMG_2) complex at the ERGO-MF-PGE between – 0.7 and – 1.5 V by SW-AdCSV. A typical well-resolved and symmetrical stripping peak is exemplified at – 1.087 V, corresponding to a reduction of 20 μg L^{-1} of Ni^{2+} at the ERGO-MF-PGE in 0.1 M NH_3-NH_4Cl buffer solution (pH 9.4). A five-step electrochemical reduction mechanism describing the detection of Ni^{2+} in the presence of dimethylglyoxime chelating agent and *in-situ* plated mercury film is illustrated below (Ma, Jagner, and Renman 1997; Baxter et al.*1998)*:

$$Ni + 2\,DMG \rightarrow Ni(II)DMG_{2(sol)} \quad (1)$$

$$Hg^{2+} + 2\,e^- \rightarrow Hg^o \quad (in\ situ) \quad (2)$$

$$Ni(II)DMG_{2(sol)} + Hg^0 \rightarrow Ni(II)DMG_{2(ads)}Hg \quad (3)$$

$$Ni(II)DMG_{2(ads)}Hg + 2\,e^- \rightarrow Ni^0 + 2\,DMG^{-1}Hg \quad (4)$$

$$2\,DMG^{-1}Hg + 8\,e^- + 5\,H^+ \rightarrow 2\,DHAB + Hg^0 \quad (5)$$

During the mechanism, a complex is formed between Ni ions and DMG (eq.1) followed by the adsorption of the complex on the metal film (eq. 2&3). The adsorbed metal complex will then be reduced by applying a specific potential (eq. 4) stripping out Ni^0 ions and lastly the HgDMG

groups are also irreversibly reduced to 2,3-bishydroxy-laminebutane (DHAB).

Metal-chelate complex formation of Ni^{2+} with DMG occurs spontaneously in solutions buffered at pH values greater than 7. A 1:2 stoichiometric Ni(II)-$(DMG)_2$ complex is formed prior to its non-electrolytic adsorption onto an electroplated Hg-film in a two-step electrode pre-concentration process under a fixed constant applied potential. Following adsorption, the cathodic potential scan results in the reduction of the nickel-dimethylglyoxime complex in a potentiometric stripping step. Both central metal ion and chelating agent are reduced and stripped from the electrode surface. A reduction peak current corresponding to analyte concentration is produced.

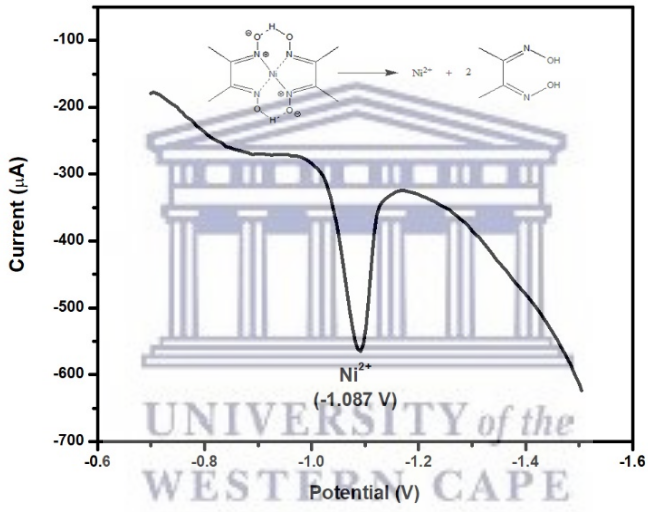

Figure 4.15. Square-wave adsorptive cathodic stripping voltammogram (SW-AdCSV) representing the characteristic reduction stripping potential of 20 μg L^{-1} Ni^{2+} in 0.1 M NH_3-NH_4Cl buffer solution (pH 9.4), 58 mgL^{-1} DMG at the ERGO-MF-PGE under the optimized parameters.

4.3.2. Effects of electrochemically reduced graphene oxide on the stripping peaks currents

The peak current responses of the bare-PG-MFE, ERGO-PGE, and ERGO-PG-MFE platforms towards Ni^{2+} detection in 0.1 M NH_3-NH_4Cl buffer solution (pH 9.4) are compared in *Figure 4.16*. The SW-AdCSV illustrates the effect of electrode modification with ERGO and metallic Hg-films. A considerable increase of ~ 38 times in peak current is observed at the ERGO-PGE in comparison to the bare-PG-MFE. The higher surface area-to-volume ratio, enhanced electron-transfer rates

and conductivity owing to quantum confinement of ERGO in the nanometre range (1-100 nm) all contribute towards the improvement in stripping peak current. The inclusion of electroplated Hg-films further shows to enhance the stripping peak current and peak symmetry when compared to the ERGO-PGE. A single, well-resolved stripping peak is exhibited at – 1.083 V. A further 9-fold enhancement in electrode peak current for the ERGO-PG-MFE over the ERGO-PGE is recorded. An overall improvement in electrode sensitivity is therefore confirmed.

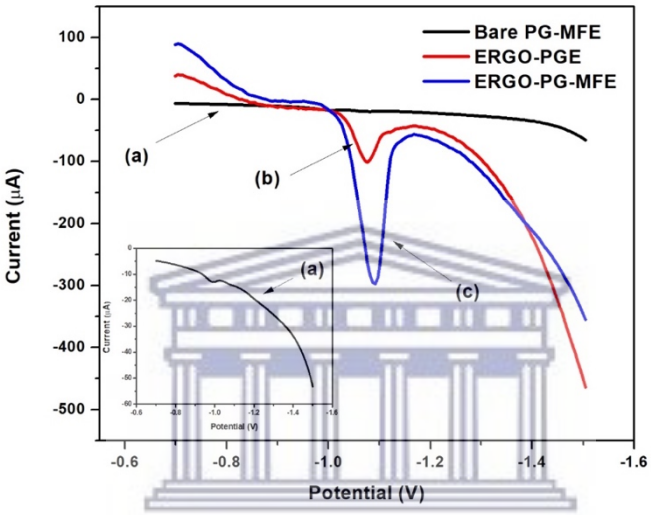

Figure 4.16. SWASV of 20 μgL^{-1} at (a) bare-PG-MFE, (b) ERGO-PGE and (c) ERGO- PG-MFE. The inset is a magnified image of the bare-PG-MFE. Supporting electrolyte (0.1 M NH_3-NH_4Cl buffer solution, pH 9.4), deposition potential (- 0.7 V), deposition time (120 s), frequency (50 Hz), amplitude (0.05 V) and voltage step (0.005 V). 58 mgL^{-1} DMG.

4.3.3. Film stability and reproducibility

Performance metrics including stability and reproducibility of the ERGO-PG-MFEs were crucially investigated. Good relative standard deviation (RSD %) < 5 % were obtained when measuring 10 consecutive replicas (n = 10) of 20 μg L^{-1} Ni^{2+} cations at the ERGO-PG-MFE in 0.1 M NH_4OH-NH_4C buffer (pH 9.4), at optimum conditions. The low standard deviation provides evidence as to the good reproducibility in preparing the ERGO-PG-MFEs. Moreover, the mechanical stability of the mercury film on the pencil graphite substrate was satisfactory since reproducible and well-defined peaks were obtained even at much higher rotation speeds.

4.3.4. Optimization of instrumental parameters

Ni^{2+} stripping peak currents were investigated as a function of square-wave experimental variables; deposition time, deposition potential, cleaning time, frequency, amplitude, and rotation speed at the ERGO-PG-MFE. The performance parameters and analytical response were measured in triplicate (n = 3).

Figure 4,17a demonstrates the influence of deposition/accumulation time on the peak current response of Ni^{2+} between 0 and 300 s. The Ni^{2+} stripping peak current increased with increasing accumulation time up to 200 s. Here, more time is allowed for $Ni(DMG)_2$ to adsorb onto the ERGO-PG-MFE surface during the pre-concentration step. At accumulation times greater than 210 s, the peak height plateaued as electrode saturation was achieved. For all subsequent experiments, a deposition/accumulation time of 120 s was selected in order to enhance the peak current of Ni^{2+}, while avoiding possible saturation of the electrode surface.

The effect of the rotational speed on the peak current of Ni^{2+} was investigated between 200 and 2,000 rpm (*Figure 4.17b*). The peak height of the detected target metal was found to increase linearly, to a maximum, between 200 and 800 rpm. Similar to the trend in accumulation time, a steady and flat peak current is observed above 1000 rpm. A rotational speed of 800 rpm was found to deliver adequate amounts of dissolved material to the electrode surface for electrolytic and non-electrolytic accumulation.

Amplitude control of the square-wave waveform was varied from 10 to 100 mV and shown in *Figure 4.17c*. An increase in stripping peak current of Ni^{2+} with increasing amplitude was found. A 50 mV amplitude of was selected for subsequent experiments.

The influence of deposition/accumulation potential on the peak currents of Ni^{2+} at the ERGO-PG-MFE is demonstrated in *Figure 4.17d*. The accumulation potential range from – 0.4 to – 1.2 V was investigated. At potentials more negative than the reduction potential of the Ni^{2+} cation (- 1.08 V), no/inadequate adsorption of the $Ni(DMG)_2$ complex onto the electrode surface occurred. This resulted in low stripping peak currents being generated. A sharp increase in stripping peak currents between – 1.1 and – 0.7 V can be observed owing to the non-electrolytic accumulation of $Ni(DMG)_2$ in the pre-concentration step. A sharp decrease from - 0.7 to more positive potentials can then be seen as demonstrating a dependence on accumulation potential to facilitate the adsorption process. A deposition potential of – 0.7 V was chosen for further experiments.

Figure 4.17e shows the variation of Ni^{2+} peak height with electrode cleaning time between 0 and 210 s. The peak current of Ni^{2+} increased with increasing cleaning time over the range. Complete removal of un-reduced metal cations was achieved at a cleaning time of 120 s. Thereafter, no influence was experienced on the stripping peak current. A cleaning time of 120 s was chosen for the rest of the experiments.

In *Figure 4.17f* the change in frequency and its influence on the peak current of the target metal over the range from 0 to 100 Hz was investigated. The peak current of Ni^{2+} increased as the frequency was increased. After a frequency of 50 Hz was applied the peak current of Ni^{2+} tapered off. An increase in the frequency results in an increase of the scan rate. A frequency of 50 Hz was chosen as the optimum frequency for this experiment.

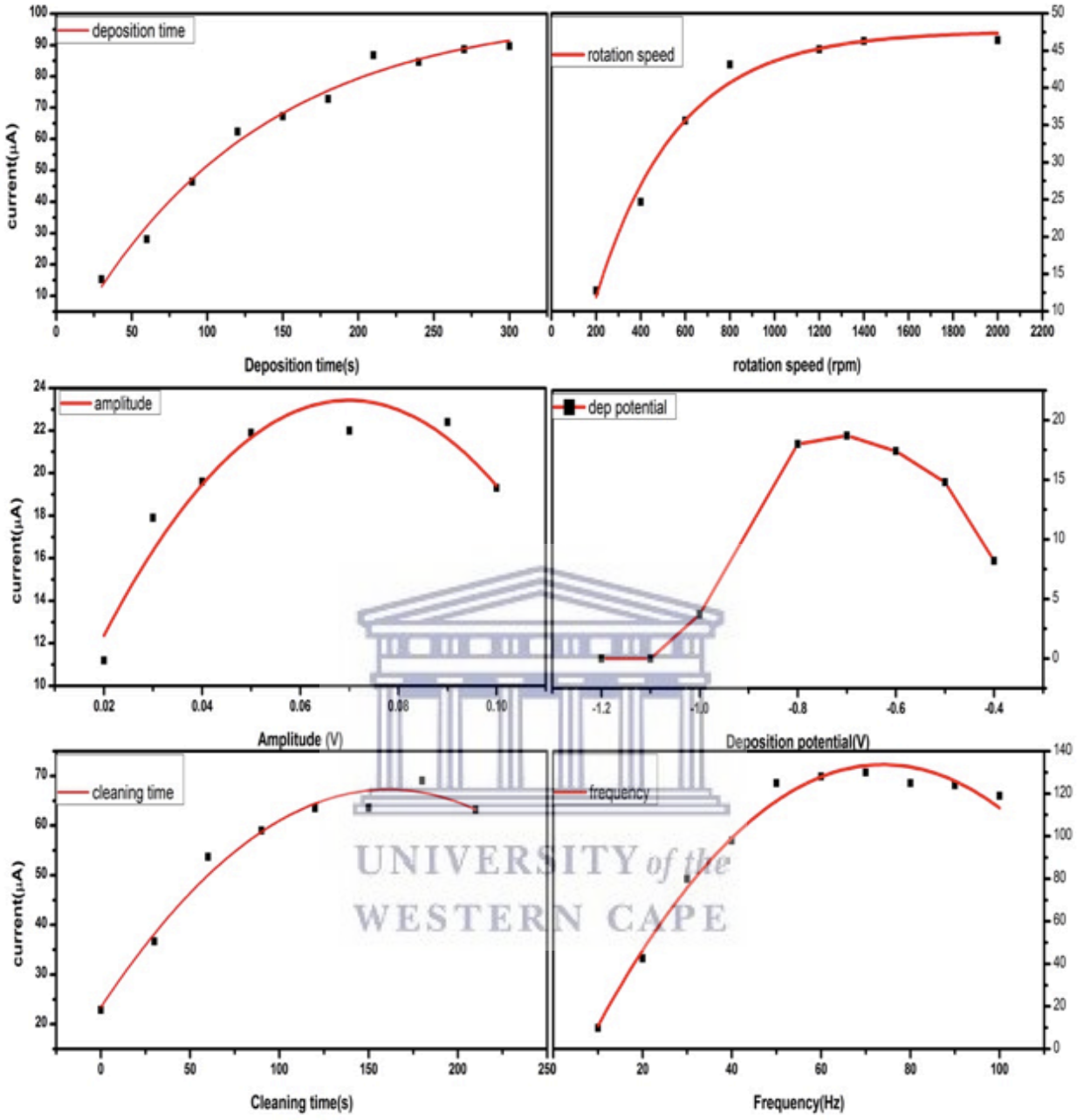

Figure 4.17. The effect of (a) deposition time, (b) rotation speed, (c) amplitude, (d) deposition potential, (e) cleaning time and (f) frequency on the stripping peak of Ni^{2+} at electrochemically reduced graphene oxide pencil graphite mercury film electrode (ERGO-PG-MFE) in 0.1M ammonium hydroxide ammonium chloride buffer solution (pH 9.4) containing 5 μg L^{-1} of Ni^{2+} and 5 mg L^{-1} of Hg^{2+}.

4.3.5. Analytical performances of the electrochemically reduced graphene oxide modified pencil graphite mercury film electrode

The analytical performance/calibration of the ERGO-PG-MFE was investigated under optimized conditions by individual analysis of standard Ni^{2+} solutions with concentrations that ranged between 2 and 16 µg L^{-1}. Three replicate SW-AdCSV measurements were performed for each calibration range. The square wave cathodic stripping voltammograms and its corresponding calibration curve for the analysis of Ni^{2+} in 0.1 M NH_3-NH_4Cl electrolyte (pH 9.4), at the ERGO-PG-MFE, is shown in *Figure 4.18,* below. The calibration data was evaluated by linear regression analysis. The limit of detection (LOD) was determined by the $3\sigma_{blank}$/ slope method, where it is 3 times the standard deviation of the blank divided by the slope (sensitivity) of the calibration plot. The limit of quantification (LOQ), described as the lowest concentration at which the performance of a measurement system is acceptable, was calculated as 3.3 times the LOD. The recorded LOD and LOQ are presented in *Table 1* below.

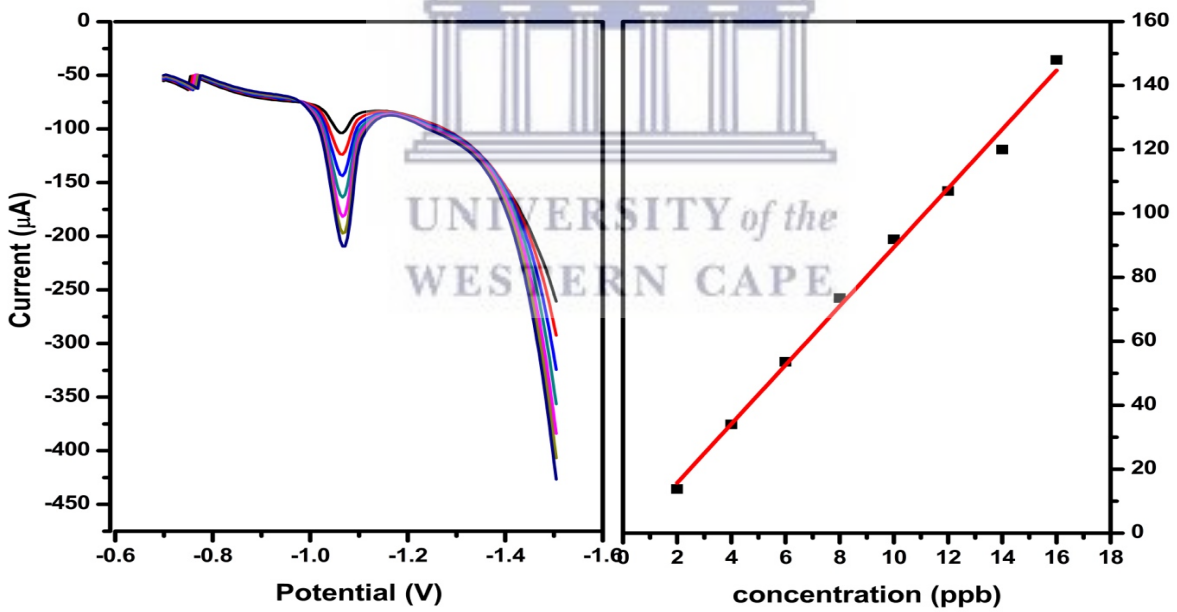

Figure 4.18. SWCSV and a corresponding calibration curve for the individual analysis of Ni^{2+} obtained at the ERGO-PG-MFE, between the concentration of 2 and 16 µg L^{-1}. 0.1 M NH_3-NH_4Cl buffer (pH 9.4) was used as supporting electrolyte. The square-wave voltammetric parameters were a deposition/accumulation time of 210 s, a deposition/accumulation potential of - 0.7 V, a

rotational speed of 800 rpm, a frequency of 50 Hz, an amplitude of + 0.05 V and a sweep rate of 0.2 V s^{-1}.

Table 1.: Calibration data representative individual analysis of Ni^{2+} at ERGO-PG-MFE in 0.1M NH_3-NH_4Cl buffer solution (pH 9.4) under optimized parameters

Analytical Parameter	**Analysis of Ni^{2+} (0 – 16 µgL^{-1})**
Sensitivity (µAL $µg^{-1}$)	9.71 x 10^{-7}
Correlation Coefficient (R^2)	0.997
Detection Limits (µg L^{-1})	0.120 ± 0.002
Limit of Quantification (µg L^{-1})	0.401 ± 0.007

*n = 3, where n is the number of replications.

To evaluate our research results, the accumulation time, calculated linear range, and LOD found in this work was compared with literature reported values for Ni^{2+} detection and illustrated *Table 2*, below. The ERGO-PG-MFE demonstrates comparable results to the reported LODs at similar analysis times. Further, while HMDEs offer the best-reported analysis results and sensitivities at the shortest accumulation times, good and comparable results can still be obtained at the GC and ERGO-PGEs.

Table 2. A selected summary of previously reported detection limits for Ni^{2+} at various Mercury-film electrodes (MFE) and other metal-film electrodes

Electrode substrate	**Measurement technique**	**Deposition time (s)**	**Detection limit (µg L^{-1})**	**Linear range (µg/L)**	**Reference**
GC-HgFE	AdCSV	60	0.1	-	[21]
GCR-HgFE	AdSV	120	0.014	-	[106]
GC-HgFE	DPASV	180	0.000355	-	[107]
GC-PdFE	AdSV	120	0.001	-	[108]

HMDE	DPAdSV	30	0.0087	0.03 - 5.9	[68]
HMDE	AdCSV	70	0.974	0.2 - 100	[109]
HMDE	DPAdCSV	60	0.05	0.1 - 28	[110]
RD-BFE	SWAdSV	300	0.1	0.5 - 5	[111]
MWCNTs paste E	SWASV	60	0.43	0.59 - 59	[24]
ERGO-PG-HgE	AdCSV	120	0.120	0 - 16	This Work

4.3.6. Recoveries Studies of ERGO-PG-MFE

The ERGO-PG-MFE and developed method were used for the analysis of Ni^{2+} in test electrolyte solutions. Known concentrations of Ni^{2+} cations were used to spike 20 mL portions of 0.1 M NH_3-NH_4Cl buffer solutions for recovery determination by a standard addition method. The obtained voltammograms (a) together with their corresponding standard addition curves (b) are shown in *Figure 4.19(a and b)*. Recovery percentages of the Ni^{2+} ions from test solutions spiked with 5 µg L^{-1} Ni^{2+} yielded a recovery of 98.9 % ± 2.4 % for five replications (n = 5).

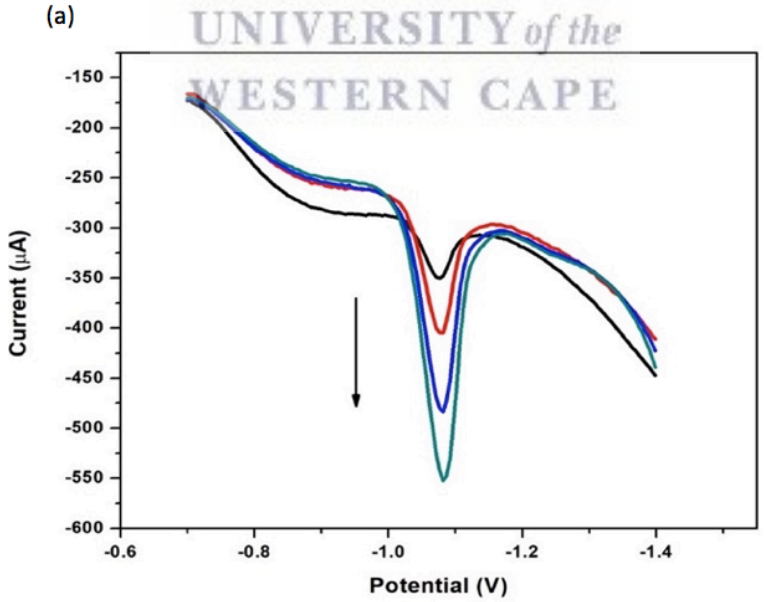

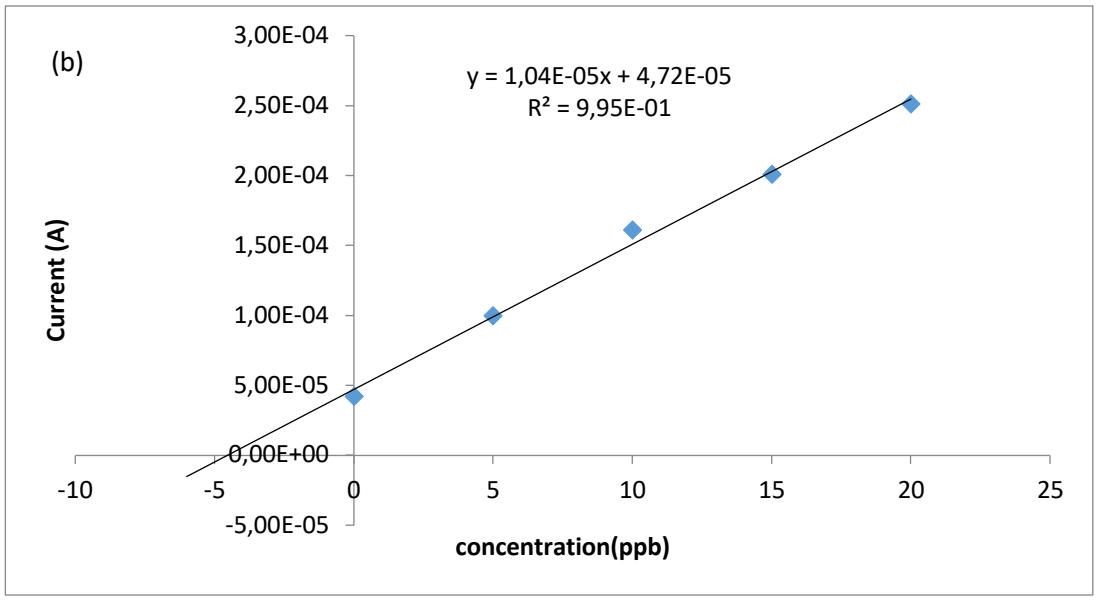

Figure 4.19. (a) Square wave voltammograms (b) Standard addition plots for the determination of Ni^{2+} at ERGO-PG-MFE in test solutions.

4.3.7. Application to tap water samples

The ERGO-PG-MFE was applied to the analysis of Ni^{2+} in tap water samples, as described in **Section 3.9**. SW-AdCSV analysis was performed by *in-situ* deposition of the metal film and target metal under the optimized parameters at a cleaning time of 0 s. Due to the good sensitivity of ERGO-PG-MFE, a peak could be observed due to the nickel ion present in the water sample. The amount of nickel ions present in the tap water sample was determined by the standard additions method as shown in *Figure 4.21*, below. Ni^{2+} was found to be 0.23 ± 0.02 µg L^{-1} in the tap water sample. In addition, tap water samples were spiked with known amounts of target metal ions and then re-determined by applying the method of standards additions for a minimum of 3 times.

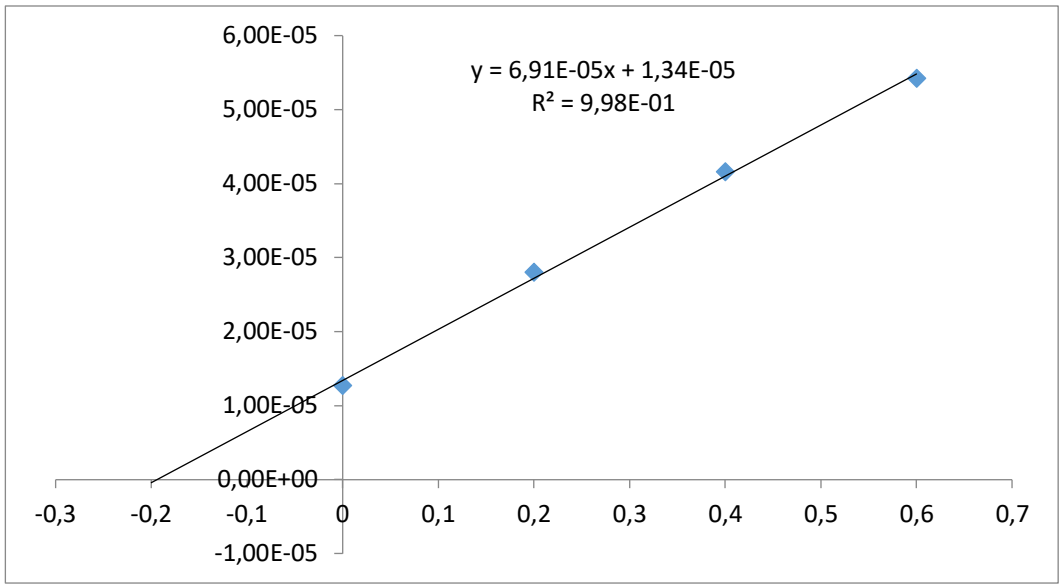

Figure 4.20. Standard addition calibration curve of Ni^{2+} for the analysis of tap water (pH 9.4) spiked with 0.2 µg L^{-1} of Ni^{2+} ions at a deposition/accumulation time of 240 s.

4.3.8. Interferences

The possible Interference of Zn^{2+}, Cd^{2+}, Co^{2+}, Pd^{2+}, Pb^{2+} and Cu^{2+} on the cathodic stripping peak of Ni^{2+} was investigated individually by the addition of the interfering ions between 5 and 40 µg L^{-1} to a solution containing 5 µg L^{-1} of Ni^{2+} under optimized conditions. The intermetallic interference was investigated by a method of standard addition and spiking the solution test with a known concentration of the interfering ions. Metal ions interfere with the stripping peak by complexing competitively with DMG or by producing reduction peaks that overlap with or even completely suppress the Ni peak altogether. Zn^{2+}, Cd^{2+}, Co^{2+}, and Cu^{2+} did not affect the stripping peak of Ni^{2+}. Further, no stripping peak was exhibited within the electrochemical window under investigation. However, at a 5-fold excess of Pd^{2+}, the peak current of Ni^{2+} decreased by ~ 10 %.

Figure 4.21 shows how Co^{2+} does not get reduced on an ERGO-PG-MFE in the presence of DMG complexing agent hence proving how selective ERGO-PG-MFE in the presence of DMG complexing agent is towards the determination of Ni^{2+}. As so, further investigation has been done to look for a ligand which is specific for the reduction of Co^{2+} on an ERGO-PG-MFE, and in **section Part B,** Nioxime was found to be ideal ligand for the individual analysis of Co^{2+}.

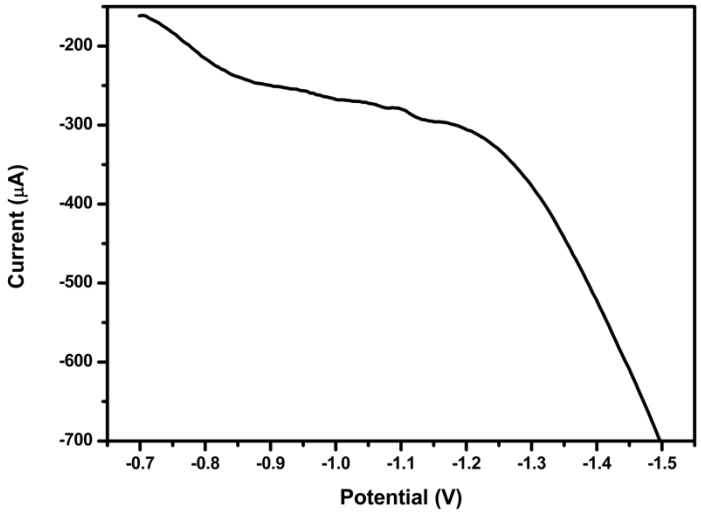

Figure 4.21. The SW-AdCSV representing the characteristic reduction stripping potential of 20 μg L^{-1} Co^{2+} in DMG and 0.1 M NH_3-NH_4Cl buffer solution (pH 9.4) at the ERGO-MF-PGE under the optimized parameters

Figure 4.22 below shows the simultaneous detection of 20 μg L^{-1} Ni^{2+} and Co^{+} at an unmodified-PG-MFE in the presence of 58 mgL^{-1} DMG under the same optimized conditions as of ERGO-PG-MFE in *figure 4.21* below. As shown below, both Ni(II)-$(DMG)_2$ and Co(II)-$(DMG)_2$ are successfully reduced on an unmodified-PG-MFE. This further proves that ERGO on a pencil graphite electrode activate the selectivity of the electrode towards Ni(II)-$(DMG)_2$ as shown on *Figure 4.21*.

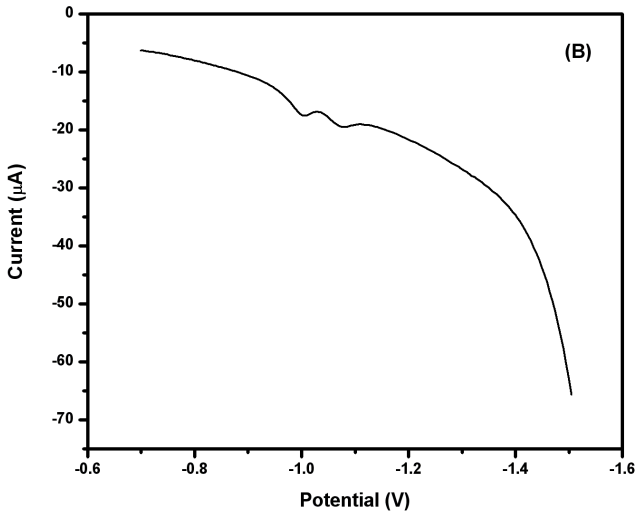

Figure 4.22. The SW-AdCSV representing the simultaneous reduction stripping potential of 20 μg L^{-1} Ni^{2+} and Co^{2+} in DMG and 0.1 M NH_3-NH_4Cl buffer solution (pH 9.4) at the unmodified-MF-PGE under the optimized parameters.

4.3.9. Conclusion

ERGO-PG-MFEs were prepared by immobilizing multilayer graphene-nanosheets directly on a PGE by successive cyclic voltammetric reduction. The as-prepared ERGO-PG-MFE was successfully applied for the accurate and reproducible detection of trace concentrations of Ni^{2+} in electrolyte and water samples by SW-AdCSV. A highly enhanced sensing platform was obtained with improved selectivity, enhanced signal amplification, and antifouling behavior to reduce intermetallic interferences on the disposable and low-cost pencil graphite substrate. The deposited ERGO thin films were found to improve the stripping peak currents 37-times over the unmodified PG-MFE by improving the electron transfer kinetics and surface-area-to-volume ratio. The detection limits (LOD) calculated in water samples using the ERGO-PG-MFE for individual analysis of Ni^{2+} were found to be 0.120 ± 0.002 μg L^{-1} and a sensitivity of 9.71 x 10^{-7} μAL $μg^{-1}$, which is way below the US EPA maximum contaminant level of 0.1 mg L^{-1}. Improved specificity was found in the presence of Zn^{2+}, Cd^{2+}, $Co^{2+,}$ $Pb^{2+,}$ and Cu^{2+} while Pd^{2+} was found to interfere to a small extent. This technique was therefore deemed to be suitable for tap water analysis.

CHAPTER 4: Part B

The determination of Co^{2+} with Nioxime complexes on ERGO-PG-MFE

In this section the stripping voltammetric responses of the Co^{2+} ions, were used to obtain the various optimized instrumental parameters and to determine the analytical parameters for the ERGO-PG-HgE. Nioxime was used as the complexing ligand for the individual analysis of Co^{2+} ions. Here, the selectivity of the ERGO-PG-MFE and Nioxime complexing agent was investigated. Further evidence will be provided that Nioxime is specific on Co^{2+} on an ERGO-PG-MFE under the optimized conditions.

4.4.1. Characteristic reduction potential of Co(II)-(Nioxime)$_2$ complex

Figure 4.23 illustrates the characteristic reduction potential of the cobalt-1,2-cyclohexanedione-dioxime (Co(II)-(Nioxime)$_2$) complex at the ERGO-MF-PGE between – 0.7 and – 1.5 V by SW-AdCSV. A typical well-resolved and symmetrical stripping peak is exemplified at – 1.10 V, corresponding to a reduction of 5 µg L^{-1} of Co^{2+} at the ERGO-MF-PGE in a solution containing 5 mg L^{-1} of Hg^{2+}, 70 mg L^{-1} Nioxime and 0.1 M NH_3-NH_4Cl buffer solution (pH 9.4). A four-step electrochemical reduction mechanism describing the detection of Co^{2+} in the presence of Nioxime complexing agent and *in-situ* plated mercury film can be explained the same way as Ni-(DMG)$_2$, is illustrated below:

$$Co + 2\,Nioxime \rightarrow Co(II)Nioxime_{2(sol)} \quad (1)$$

$$Hg^{2+} + 2\,e^- \rightarrow Hg^o \quad (2)$$

$$Co(II)Nioxime_{2(sol)} + Hg^0 \rightarrow Co(II)Nioxime_{2(ads)}Hg \quad (3)$$

$$Co(II)Nioxime_{2(ads)}Hg + 2\,e^- \rightarrow Co^0 + 2\,Nioxime^{-1}Hg \quad (4)$$

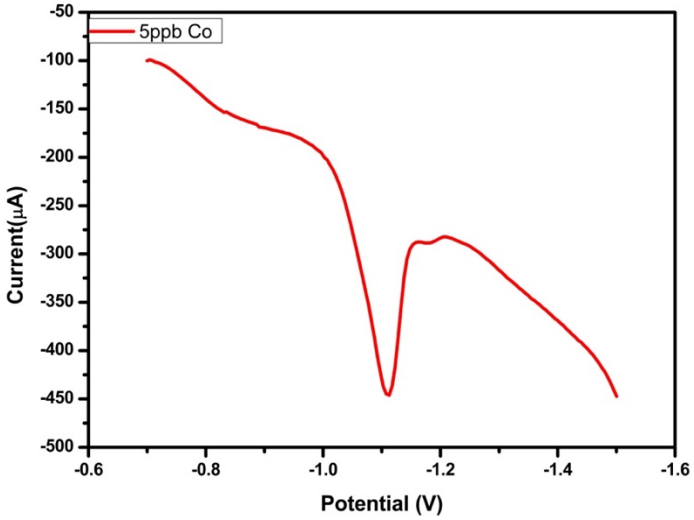

Figure 4.23. Square-wave adsorptive cathodic stripping voltammogram (SW-AdCSV) representing the characteristic reduction stripping potential of 5 μg L^{-1} Co^{2+} in 0.1 M NH_3-NH_4Cl buffer solution (pH 9.4) at the ERGO-MF-PGE under the optimized parameters.

4.4.2. Effects of electrochemically reduced graphene oxide on the stripping peaks currents

The peak current responses of the (a) unmodified-PG-MFE and (b) ERGO-PG-MFE platforms towards Co^{2+} detection in 0.1 M NH_3-NH_4Cl buffer solution (pH 9.4) are compared in *Figure 4.24*. The SW-AdCSVs illustrate the effect of electrode modification with ERGO. The unmodified-PG-MFE shows a small cathodic stripping peak in comparison to the modified-PG-MFE. A considerable increase of ~ 3 times in peak current is observed at the ERGO-PGE in comparison to the unmodified-PG-MFE. The higher surface area-to-volume ratio, enhanced electron-transfer rates and conductivity owing to quantum confinement of ERGO in the nanometre range (1-100 nm) all contribute towards the improvement in stripping peak current.. A single, well-resolved stripping peak is exhibited at – 1.10 V.

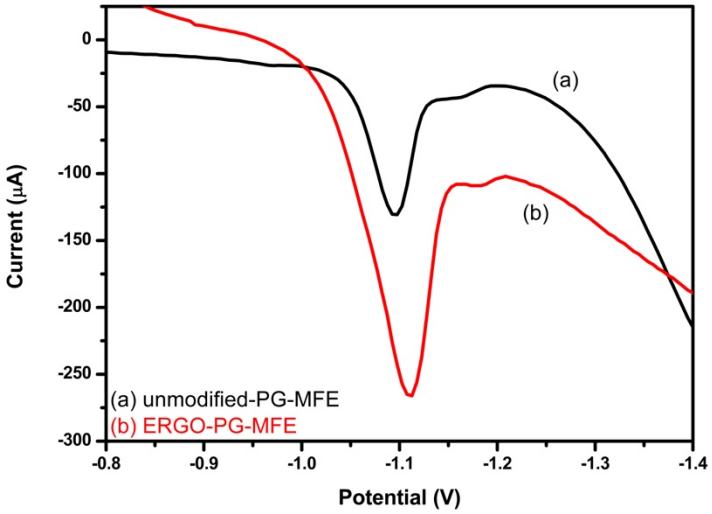

Figure 4.24. SW-AdSV of 5 μg L^{-1} Co^{2+} at (a) unmodified-PG-MFE and (b) ERGO-PG-MFE. Supporting electrolyte (0.1 M NH_3-NH_4Cl buffer solution, pH 9.4), 70 mg L^{-1} Nioxime, deposition potential (- 0.7 V), deposition time (120 s), frequency (60 Hz), amplitude (0.05 V) and voltage step (0.005 V).

4.4.3. Effect of mercury film & Nioxime complexing agent on the stripping peak of Co^{2+}

Figure 4.25. shows the effect of mercury on the stripping current peak of Co^{2+} at an ERGO-PG ,supporting electrolyte (0.1 M NH_3-NH_4Cl buffer solution, pH 9.4) at optimized parameters. In the absence of Hg^{2+} at [(a) ERGO-PGE] the reduction peak current of Co^{2+} could not be observed since the Co(II)-$(Nioxime)_2$ complex was not adsorbed on a thin-mercury film, however in the presence of Hg^{2+} at [(b) ERGO-PG-MFE] a well resolved peak of Co^{2+} is observed confirming the importance of mercury film plated on an electrode. The presence of a mercury film surface area increased the accessibility for the electrochemical adsorption of Co(II)-$(Nioxime)_2$ complex on an electrode surface. Furthermore, a mercury film gives a well resolved background for better observation of the stripping peaks.

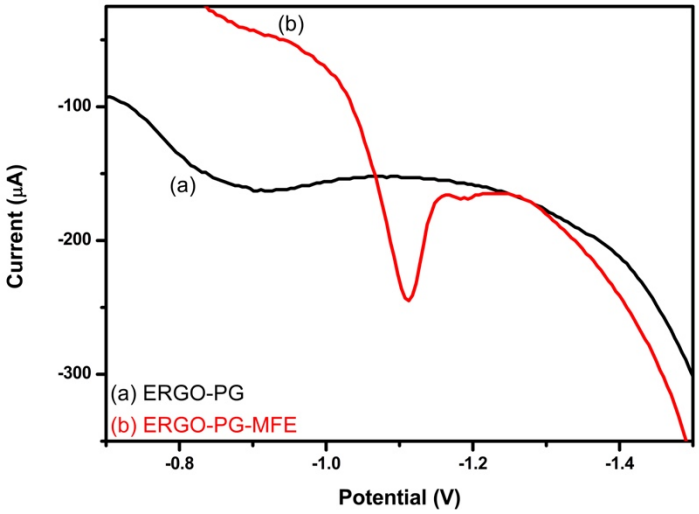

Figure 4.25. SW-AdSV of 5 μgL^{-1} Co^{2+} in the (a) absence of Hg^{2+} ions (ERGO-PG) and (b) presence of 5mg L^{-1} Hg (ERGO-PG-MFE). Supporting electrolyte (0.1 M NH_3-NH_4Cl buffer solution, pH 9.4), 70 mg L^{-1} Nioxime complexing agent, deposition potential (- 0.7 V), deposition time (120 s), frequency (60 Hz), amplitude (0.05 V) and voltage step (0.005 V).

In this section, the Nioxime complexing agent was used to evaluate its sensitivity towards Co^{2+}. *Figure 4.26* below shows that without the Nioxime complexing agent in our solution no Co^{2+} is reduced on our electrode surface as shown by voltammogram (b), however as soon as a known amount of Nioxime is added a well resolved stripping peak of Co^{2+} can be observed as shown by (c) since a complex of Co(II)-(Nioxime)$_2$ could be successfully adsorbed on a thin-mercury film of our electrode. Co^{2+} ions only cannot be adsorbed on the ERGO-PG-MFE. The ERGO-PG-MFE in the absence of both Co^{2+} ions and Nioxime (a), no foreign stripping peaks are observed on our potential window range.

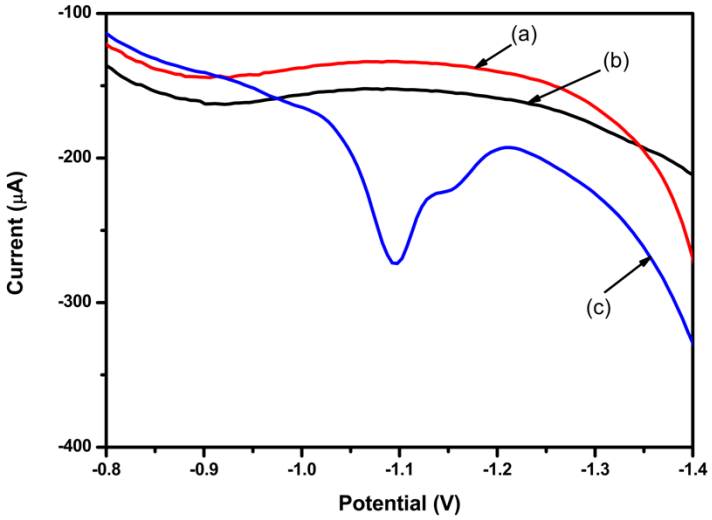

Figure 4.26. SW-AdSV at ERGO-PG-MFE (a) in the absence of both Co^{2+} and Nioxime (b) presence of 5 μgL^{-1} Co^{2+} only (c) presence of both 5 μgL^{-1} Co^{2+} and 70 mgL^{-1} Nioxime. Supporting electrolyte (0.1 M NH_3-NH_4Cl buffer solution, pH 9.4) under the optimized parameters.

Figure 4.27, demonstrates the influence/optimization of Nioxime and Hg on the peak current response of Co^{2+} between 0 to 160 and 0 to 10 mg L^{-1} respectively. The optimal ligand concentration for the maximum sensitivity was investigated after accumulation of 120 s under the optimized parameters. The Co^{2+} stripping peak current increased exponentially with increasing Nioxime up until 120 mg L^{-1} and increasing Hg concentration up until 5 mg L^{-1} and thereafter it increased slowly with the increase concentration in both cases, this is as a result of maximum coverage of the electrode surface. A small and sometimes a shoulder peak to the Co^{2+} peak current is observed as the result of the reduction of the Nioxime ligand on the electrode surface. As a consequence of this behaviour the Nioxime and Mercury ion concentration of 70 and 5 mg L^{-1} respectively were used as optimum concentrations.

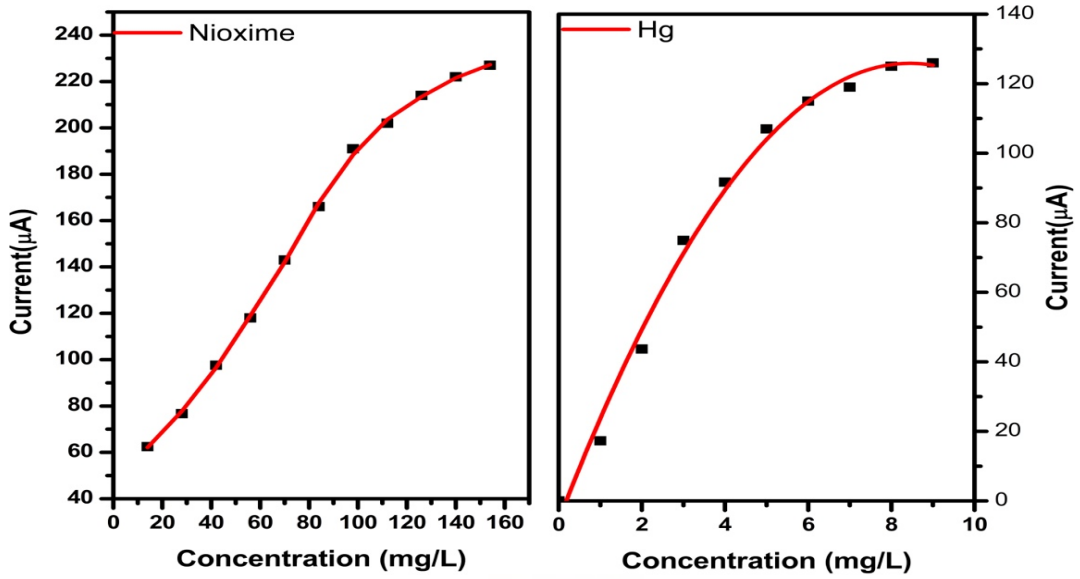

Figure 4.27. The effect of Nioxime and Hg concentration on the stripping peak of Co^{2+} at electrochemically reduced graphene oxide pencil graphite mercury film electrode (ERGO-PG-MFE) in 0.1M ammonium hydroxide ammonium chloride buffer solution (pH 9.4) containing 5 μg L^{-1} of Co^{2+}.

In conclusion both Nioxime complexing agent and thin-mercury film are a necessity for the reduction of Co^{2+} at an ERGO-PGE to take place. Co^{2+} cannot be reduced in the absence of either Nioxime or thin-mercury film.

4.4.4. Film stability and reproducibility

Co^{2+} stripping peak currents were interrogated as a function of square-wave experimental variables; deposition time, deposition potential, cleaning time, frequency, amplitude, and rotation speed at the ERGO-PG-MFE. The performance parameters and analytical response were measured in triplicate (n = 3).

Performance metrics including stability and reproducibility of the ERGO-PG-MFEs were crucially investigated. The reproducibility of Co^{2+} was 6.5 % at lower concentration of 2 μg L^{-1}, however at a much higher concentration of >5 μg L^{-1} the reproducibility was <2.4 %. Good relative standard

deviation (RSD %) < 5 % were obtained when measuring 10 consecutive replicas (n = 10) of 5 μg L^{-1} Co^{2+} cations at the ERGO-PG-MFE in 0.1 M NH_4OH-NH_4C buffer (pH 9.4), at optimum conditions. The low standard deviation provides evidence as to the good reproducibility in preparing the ERGO-PG-MFEs. Moreover, the mechanical stability of the mercury film on the pencil graphite substrate was satisfactory since reproducible and well-defined peaks were obtained even at much higher rotation speeds.

4.4.5. Effect of Supporting Electrolyte and Characteristic oxidation potentials of Co^{2+}

The electrochemical response of ERGO-PG-MFE towards Co^{2+} under the optimized conditions was investigated in different electrolyte solutions of (a) 0.1 M HCl (b) 0.1 M acetate buffer (pH 4.6) (c) 0.1 M ammonium buffer (pH 9.4) and (d) 0.1 M phosphate buffer (pH 7).

Supporting electrolytes regulates cell resistance and mass transport by electrical migration, it is also useful for controlling or buffer the level of hydrogen ion activity in solution. In adsorptive stripping voltammetry the supporting electrolyte plays a role in associating with the electroactive solute, as in the complexing of metal ions by certain ligands and it may impose positive or negative voltage limits because of its redox properties.

In 0.1 M HCl solution, no stripping peak of Co^{2+} were observed as well as in 0,1 M acetate buffer solution. The stripping peak of Co^{2+} could only be observed in ammonium and phosphate buffer solution, however in phosphate buffer the stripping peak of Co^{2+} was more to the positive side with a more distorted shoulder peak while in ammonium buffer a well define reductive stripping peak of Co^{2+} was observed.

Ammonium buffer solution was used further in this investigation as it increases the conductivity of the solution and contributing to elimination of the transport of electro active species by ion migration in the electric field and to maintain the constant ionic strength.

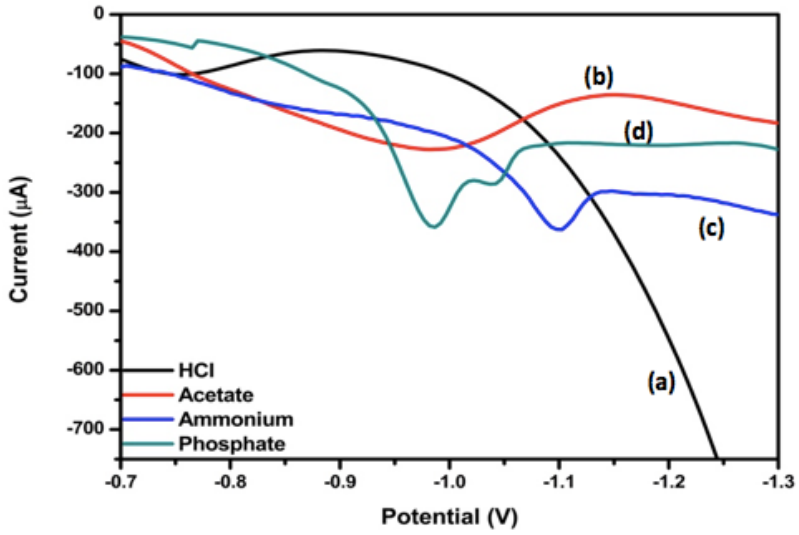

Figure 4.28. SWAdCSV of 5 μg L^{-1} with supporting electrolyte: (a) 0.1 M HCl (b) 0.1 M acetate buffer (pH 4.6) (c) 0.1 M ammonium buffer (pH 9.4) and (d) 0.1 M phosphate buffer (pH 7)

4.4.6. Optimization of instrumental parameters

Co^{2+} stripping peak currents were interrogated as a function of square-wave experimental variables; deposition time, deposition potential, cleaning time, frequency, amplitude, and rotation speed at the ERGO-PG-MFE. The performance parameters and analytical response were measured in triplicate (n = 3). Nioxime and Hg concentration were optimized as well.

The influence of deposition/accumulation potential on the peak currents of Co^{2+} at the ERGO-PG-MFE is demonstrated in *Figure 4.29*. The accumulation potential range from – 0.4 to – 1.2 V was investigated. The deposition potential is applied to the ERGO-PG-MFE to cause the Co^{2+} to be deposited onto the surface of the working electrode. At potentials more negative than the reduction potential of the Co^{2+} cation (- 1.08 V), little or no/inadequate adsorption of the $Co(Nioxime)_2$ complex onto the electrode surface occurred. This resulted in low stripping peak currents being generated. A sharp increase in stripping peak currents between – 0.4 and – 0.8 V can be observed owing to the non-electrolytic accumulation of $Ni(DMG)_2$ in the pre-concentration step. A sharp decrease from -0.8 to more negative potentials can then be seen as demonstrating a dependence on accumulation potential to facilitate the adsorption process. A deposition potential of – 0.8 V was chosen for further experiments.

Figure 4.29b demonstrates the influence of deposition/accumulation time on the peak current response of Co^{2+} between 0 and 300 s. The Co^{2+} stripping peak current increased with increasing accumulation time linearly. Here, more time is allowed for $Co(Nioxime)_2$ to adsorb onto the ERGO-PG-MFE surface during the pre-concentration step. The increase in deposition time increases the degree of preconcentration/deposition making a greater amount of deposited analyte available at the electrode during the stripping step. For all subsequent experiments, a shorter deposition/accumulation time of 120 s was selected in order to enhance the peak current of $Co^{2+}$for shorter and rapid analyses.

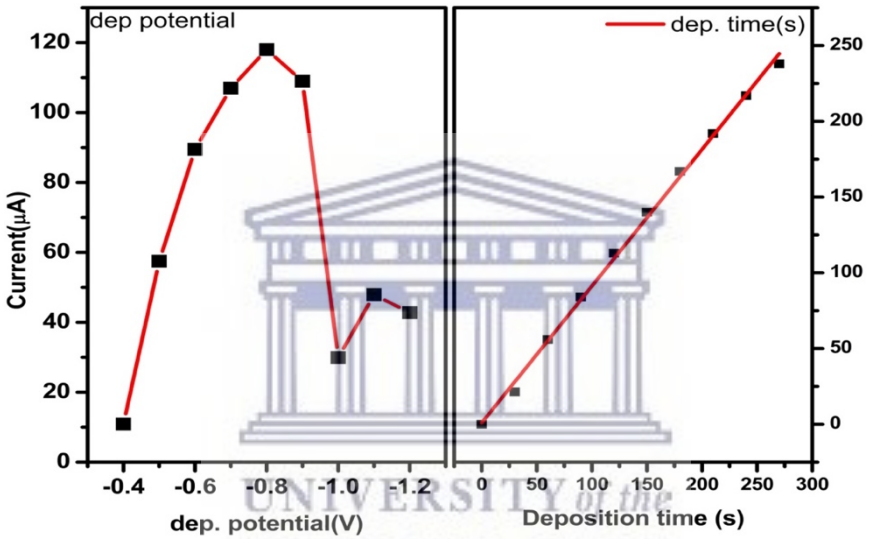

Figure 4.29. The effect of Deposition potential and Deposition potential on the stripping peak of Co^{2+} at electrochemically reduced graphene oxide pencil graphite mercury film electrode (ERGO-PG-MFE) in 0.1M ammonium hydroxide ammonium chloride buffer solution (pH 9.4) containing 5 μg L^{-1} of Co^{2+} and 5 mg L^{-1} of Hg^{2+}.

Amplitude control of the square-wave waveform was varied from 10 to 100 mV and shown in *Figure 4.30a*. An increase in stripping peak current of Ni^{2+} with increasing amplitude was found, however as the amplitude increase, a steady small increase was observed. A 60 mV amplitude of was selected for subsequent experiments.

In *Figure 4.30b,* the change in frequency and its influence on the peak current of the target metal over the range from 0 to 100 Hz was investigated. The peak current of Co^{2+} increased as the frequency was increased. The Co current peak exhibits a linear increase till a frequency of 70 Hz

followed by a steady increase. An increase in the frequency results in an increase of the scan rate. A frequency of 60 Hz was chosen as the optimum frequency for this experiment.

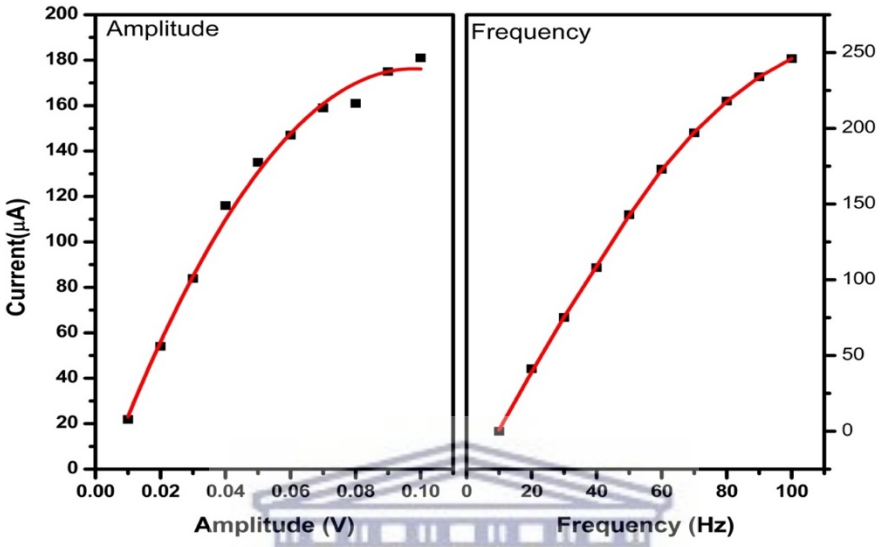

Figure 4.30. The effect of Amplitude and Frequency on the stripping peak of Co^{2+} at electrochemically reduced graphene oxide pencil graphite mercury film electrode (ERGO-PG-MFE) in 0.1M ammonium hydroxide ammonium chloride buffer solution (pH 9.4) containing 5 μg L^{-1} of Co^{2+} and 5 mg L^{-1} of Hg^{2+}.

The effect of the rotational speed on the peak current of Co^{2+} was investigated between 200 and 2,000 rpm. The peak height of the detected target metal was found to increase linearly, to a maximum, between 200 and 1000 rpm. Similar to the trend in accumulation time, a steady and flat peak current is observed above 1,000 rpm. A rotational speed of 1000 rpm was found to deliver adequate amounts of dissolved material to the electrode surface for electrolytic and non-electrolytic accumulation.

4.4.7. Analytical performances of the electrochemically reduced graphene oxide modified pencil graphite mercury film electrode

The analytical performance/calibration of the ERGO-PG-MFE was investigated under optimized conditions by individual analysis of standard Co^{2+} solutions with concentrations that ranged between 0.5 and 5.5 μg L^{-1}. Three replicate SW-AdCSV measurements were performed for each

calibration range. The square wave cathodic stripping voltammograms and its corresponding calibration curve for the analysis of Co^{2+} in 0.1 M NH_3-NH_4Cl electrolyte (pH 9.4), at the ERGO-PG-MFE, is shown in *Figure 4.31,* below. The calibration data was evaluated by linear regression analysis. The limit of detection (LOD) was determined by the $3\sigma_{blank}$/ slope method, where it is 3 times the standard deviation of the blank divided by the slope (sensitivity) of the calibration plot. The limit of quantification (LOQ), described as the lowest concentration at which the performance of a measurement system is acceptable, was calculated as 3.3 times the LOD. The recorded LOD and LOQ are presented in *Table 3* below.

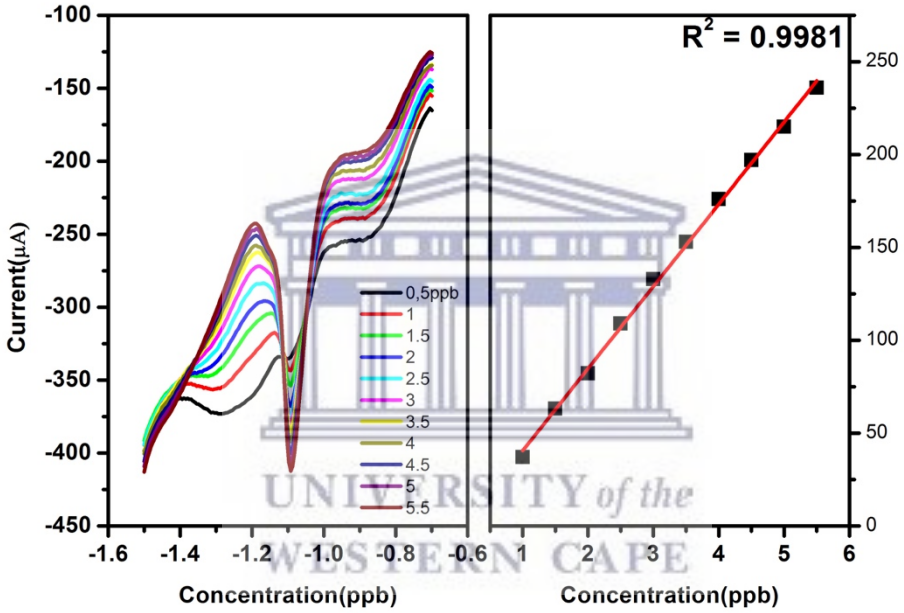

Figure 4.31. SWCSV and a corresponding calibration curve for the individual analysis of Co^{2+} obtained at the ERGO-PG-MFE, between the concentration of 0.5 and 6 µg L^{-1}. 0.1 M NH_3-NH_4Cl buffer (pH 9.4) was used as supporting electrolyte. The square-wave voltammetric parameters were a deposition/accumulation time of 210 s, a deposition/accumulation potential of - 0.7 V, a rotational speed of 800 rpm, a frequency of 50 Hz, an amplitude of + 0.05 V and a sweep rate of 0.2 V s^{-1}.

Table 3: calibration data representation individual analysis of Co^{2+} at ERGO-PG-MFE in 0.1M ammonium buffer solution (pH 9.4) under optimized parameters

Analytical Parameter	Analysis of Co^{2+} (0 – 6 µgL^{-1})
Sensitivity (µAL µg^{-1})	4.43 x 10^{-5}
Correlation Coefficient (R^2)	0.999
Detection Limits (µg L^{-1})	0.219 ± 0.002
Limit of Quantification (µg L^{-1})	0.723 ± 0.007

*n = 3, where n is the number of replications.

To evaluate our research results, the accumulation time, calculated linear range, and LOD found in this work was compared with literature reported values for Co^{2+} detection and illustrated *Table 4*, below. The ERGO-PG-MFE demonstrates comparable results to the reported LODs at similar analysis times. Further, while HMDEs and Bi-AuE offer the best-reported analysis results and sensitivities at the shortest accumulation times, good and comparable results can still be obtained at the ERGO-PGEs.

Table 4. A selected summary of previously reported detection limits for Co^{2+} at various Mercury-film electrodes (HgFE) and other metal-film electrodes

Electrode substrate	Measurement technique	Deposition time (s)	Detection limit (µg L^{-1})	Linear range(µg L^{-1})	Reference
SnBiE	AdCSV	60	0,0026	118 - 11800	[8]
Bi-AuE	AdCSV	120	0.058	10 - 55	[73]
rotating-discBiFE	SWAdSV	300	0.07	1 - 14	[111]
HMDE	AdSV	60	0.02	0 - 40	[67]
CPE	AdSV	25	1.8	3.3 - 187.1	
HMDE	DPASV	110	2.6	10 - 90000	[112]
ERGO-PG-MFE	SWAdSV	120	0.219	0 -5.5	This work

4.4.8. Recoveries Studies of ERGO-PG-MFE

The ERGO-PG-MFE and developed method were used for the analysis of Co^{2+} in test electrolyte solutions. Known concentrations of Co^{2+} cations were used to spike 20 mL portions of 0.1 M NH_3-NH_4Cl buffer solutions for recovery determination by a standard addition method. The obtained standard addition curve is shown in *Figure 4.32*. Recovery percentages of the Co^{2+} ions from test solutions spiked with 1 µg L^{-1} Co^{2+} yielded a recovery of 97 % ± 3.7 % for three replications (n = 3).

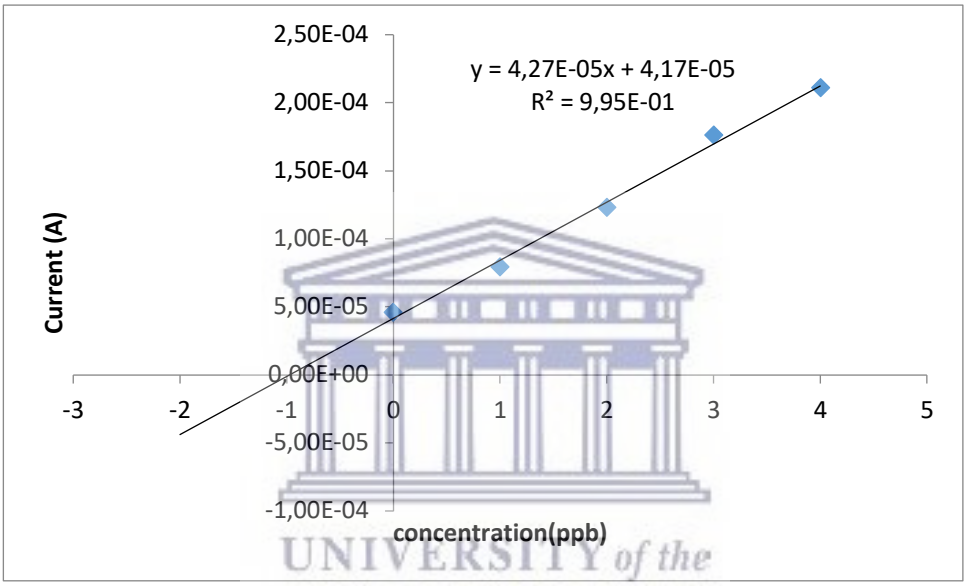

Figure 4.32. Standard addition plots for the determination of Co^{2+} at ERGO-PG-MFE in test solutions.

4.4.9. Application to tap water samples

The accuracy of the method was estimated by using the ERGO-PG-MFE for the analysis of Co^{2+} in tap water samples, as described in **Section 2.9**. SW-AdCSV analysis was performed by *in-situ* deposition of the metal film and target metal under the optimized parameters at a cleaning time of 0 s. Due to the good sensitivity and selectivity of ERGO-PG-MFE, a peak could be observed due to the cobalt ion present in the water sample suggesting that the concentration of the cobalt ion was above its detection limits. The amount of cobalt ions present in the tap water sample was determined by the standard additions method as shown in *Figure 4.33*, below. Co^{2+} was found to be 0.394 ± 0,003 µg L^{-1} in the tap water sample. In addition, four consecutive additions of 1 µg L^{-}

[1] of cobalt ions were added to the tap water samples as shown on the graph below and then re-determined by applying the method of standards additions for a minimum of 3 times.

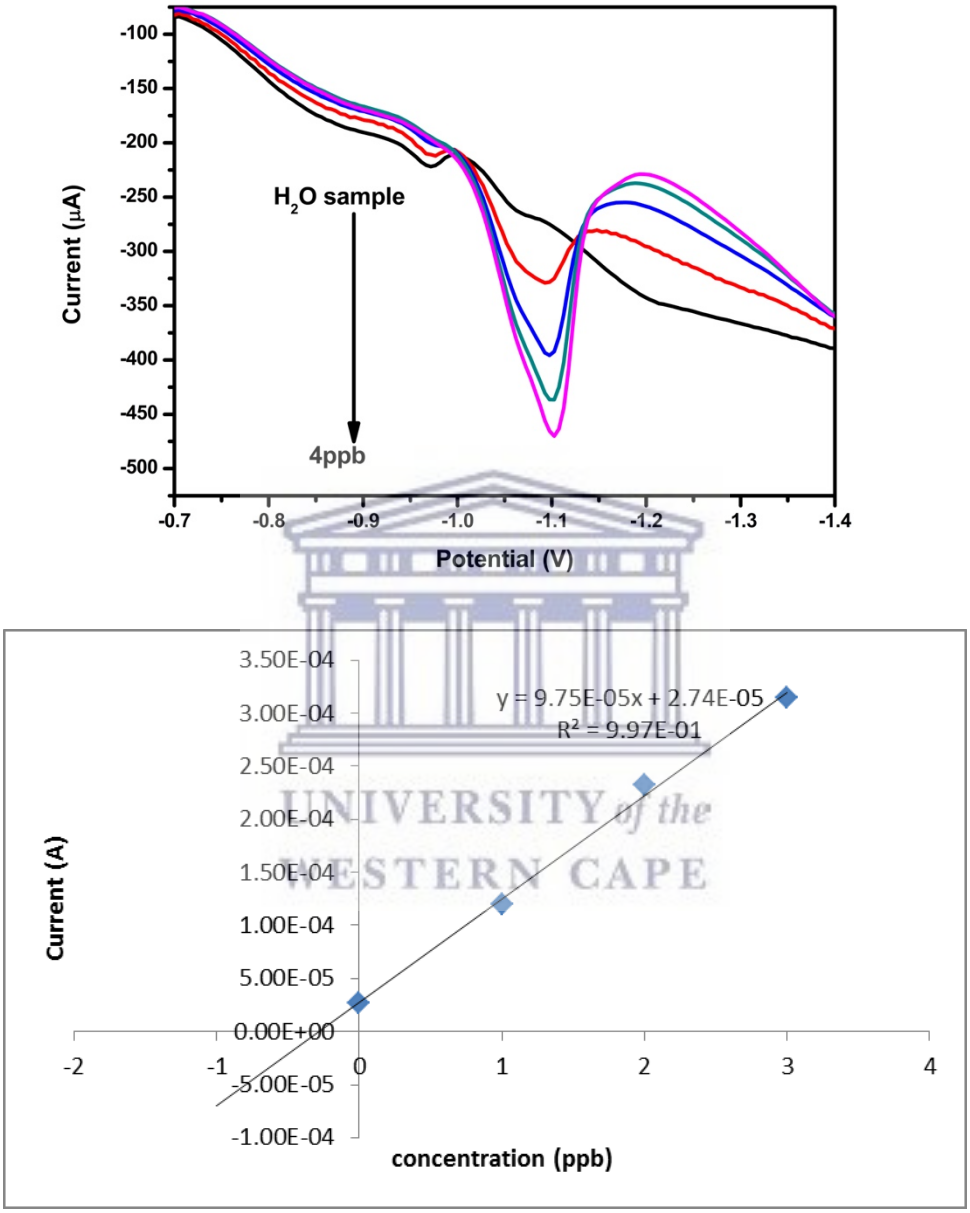

Figure 4.33. (a) Square wave voltammograms and (b) standard addition curve of Co^{2+} for the analysis of tap water (pH 9.4) with 1 µg L^{-1} additions of Co^{2+} ions at a deposition/accumulation time of 240 s.

4.4.10. Interferences

The effect of possible co-existing cationic species such as Zn^{2+}, Cd^{2+}, $Ni^{2+,}$ Pd^{2+}, Pb^{2+} and Cu^{2+} on the AdCSV determination of Co^{2+} was investiged individually by the addition of the interfering ions between 5 and 40 μg L^{-1} to a solution containing 5 μg L^{-1} of Co^{2+} under optimized conditions. The intermetallic interference was investigated by a method of standard addition and spiking the solution test with a known concentration of the interfering ions. Metal ions interfere with the stripping peak by complexing competitively with Nioxime or by producing reduction peaks that overlap with or even completely suppress the Co^{2+} peak altogether. The determination of 5 μg L^{-1} was not influenced by Pd^{2+}, Cd^{2+}, $Ni^{2+,}$ and Cu^{2+}. Further, no stripping peak was exhibited within the electrochemical window under investigation. This shows the selectivity of the Nioxime complexing ligand and also the more negative accumulation potential of (−0.7 V) which avoid effectively the interference of most metal. The use of the standard addition method on real sample successfully eliminated the effect of interferences. However, at a 5-fold excess of Zn^{2+}, the peak current of Co^{2+} decreased by ~ 10 %.

4.4.11. Conclusion

This work describes a successful determination of Co^{2+} in water samples. A highly enhanced sensing platform based on the electrochemically reduction of graphene oxide at pencil graphite electrodes was developed for the determination of Co^{2+} by square-wave adsorptive cathodic stripping voltammetry. The prepared ERGO-PG-MFE was successfully applied for the accurate and reproducible detection of trace concentrations of Co^{2+} in electrolyte and water samples by SW-AdCSV. A highly enhanced sensing platform was obtained with improved selectivity, enhanced signal amplification, and antifouling behavior to reduce intermetallic interferences on the disposable and low-cost pencil graphite substrate. The deposited ERGO thin films were found to improve the stripping peak currents 3-times over the unmodified PG-MFE by improving the electron transfer kinetics and surface-area-to-volume ratio. Nioxime was found to be selective on Co^{2+} over other metals in the potential window. The detection limits (LOD) calculated in water samples using the ERGO-PG-MFE for individual analysis of Co^{2+} were found to be 0.219 μg L^{-1} and a sensitivity of 4.43 x 10^{-5} μAL $μg^{-1}$. Improved specificity was found in the presence of Cd^{2+}, $Ni^{2+,}$ $Pb^{2+,}$ and Cu^{2+}. This technique was therefore deemed to be suitable for tap water analysis.

CHAPTER 4: Part C:

The determination of Ni^{2+} and Co^{2+} with mixed ligands of Dimethylglioxime & Nioxime complexing agents on ERGO-PG-MFE

In this section the stripping voltammetric responses of the Ni and Co ions, were used to obtain the various optimized instrumental parameters and to determine the analytical parameters for the ERGO-PG-MFE simultaneously by a combination of the mixed ligands of DGM (specific for Ni) and Nioxime (specific for Co). Here, a combination of two complexing agents of DMG (as in part A) and Nioxime (as in part B) will be used. Well and resolved stripping peaks of Ni and Co were obtained from mixing the two ligands.

4.5.1. Characteristic reduction potential of Ni^{2+} and Co^{2+} complexes

Figure 4.34. below shows well-resolved, symmetrical characteristic stripping peaks for Ni^{2+} and Co^{2+} at the ERGO-PG-MFE in 0.1M ammonium hydroxide ammonium chloride buffer solution (pH 9.4) containing 5 μg L^{-1} of Ni^{2+}, 1 μg L^{-1} of Co^{2+} and 5 mg L^{-1} of $Hg^{2+}$and a mixture of 23.22 mg L^{-1} and 7.11 mg L^{-1} of DMG and Nioxime respectively. The stripping current peaks of Ni^{2+} and Co^{2+} appears at -0.98 V and -1.1 V respectively. Ni^{2+} and Co^{+} were added individually and simultaneously, yet all yielded the same stripping peaks as shown below. A ration of 1: 3.3 concentration of DMG and Nioxime was used as it yielded better separated and enhanced stripping peaks Ni^{2+} and Co^{2+}.

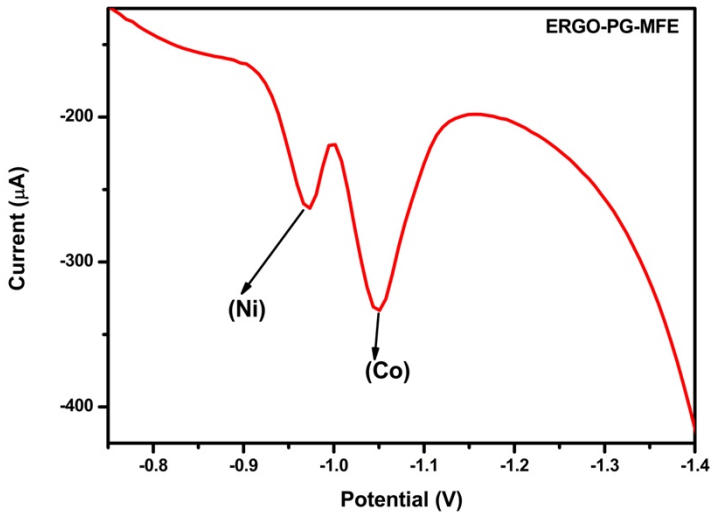

Figure 4.34. Square-wave adsorptive cathodic stripping voltammogram (SW-AdCSV) representing the characteristic reduction stripping potential of 5 μg L^{-1} Ni^{2+} and 1 μg L^{-1} Co^{2+} in 0.1 M NH_3-NH_4Cl buffer solution (pH 9.4) at the ERGO-MF-PGE under the optimized parameters.

4.5.2. Effects of electrochemically reduced graphene oxide on the stripping peaks currents

The peak current response of (a) unmodified-PG-MFE and (b) ERGO-PG-MFE platforms towards 5 μg L^{-1} of both Ni^{2+} and Co^{2+} in 0.1 M ammonium hydroxide ammonium chloride buffer solution (pH 9.4) are compared in *Figure 4.35*. An enhanced current peaks for both Ni^{2+} and Co^{2+} are observed for (b) ERGO-PG-MFE in comparison to unmodified-PG-MFE indicating an improved sensitivity towards the detection of target metals. The ERGO amplify the mass- transport of the target species to the electrode surface as well as enhanced mass-transfer rates. A considerable increase of ~ 4 and 12 times in peak current for Ni^{2+} and Co^{2+} respectively is observed at the ERGO-PGE in comparison to the bare-PG-MFE.

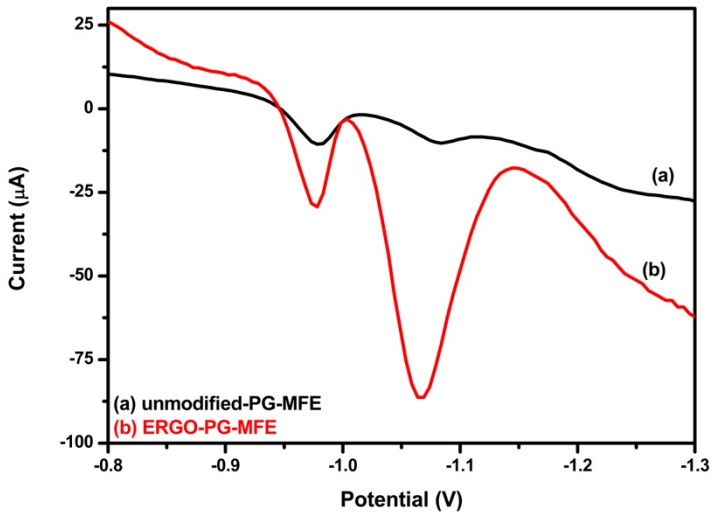

Figure 4.35 SW-AdCSV of 5 μgL^{-1} Ni^{2+} Co^{2+} at (a) unmodified-PG-MFE and (b) ERGO-PG-MFE. Supporting electrolyte (0.1 M NH_3-NH_4Cl buffer solution, pH 9.4), deposition potential (-0.3 V), deposition time (150 s), frequency (60 Hz), amplitude (0.05 V) and voltage step (0.005 V).

4.5.3. The effect of mercury film

The peak current response of (a) ERGO-PG-MFE and (b) ERGO-PG-MFE platforms towards 5 μg L^{-1} of both Ni^{2+} and Co^{2+} in 0.1 M ammonium hydroxide ammonium chloride buffer solution (pH 9.4) are compared in *Figure 4.36*. A well and resolved stripping peak of Co^{2+} is observed in the absents of thin-mercury film, however, as Hg is added, two well separated stripping peak of Ni^{2+} and Co^{2+} are observed which further proves the importance of thin-mercury film on an ERGO-PG indicating the importance of using mercury film as part of the electrochemical platform for heavy metal detection. In the presence of in situ plated Hg film on a ERGO-PG, an enhanced and symmetrical peaks for both Ni^{2+} and Co^{2+} is observed which further proves that enhanced sensitivity and current peak separation is achieved in the presence of in situ plated Hg film.

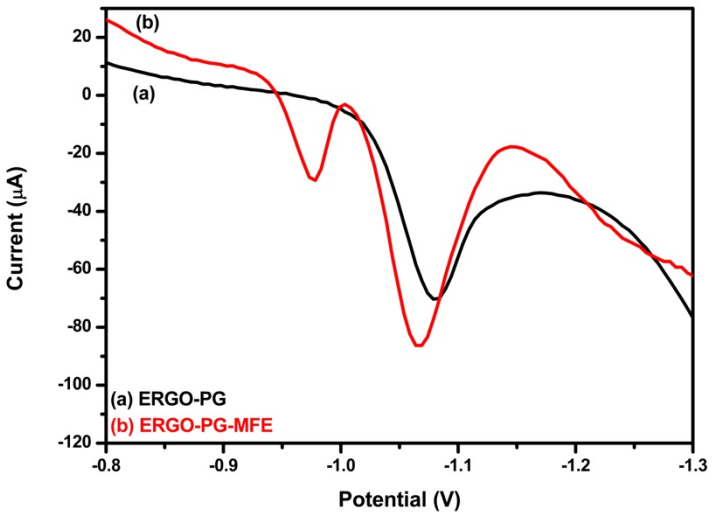

Figure 4.36. SW-AdSV of 5 μg L^{-1} Ni^{2+} and Co^{2+} (a) in the absence of Hg (ERGO-PG) and (b) in the presence of Hg^{2+} (ERGO-PG-MFE). Supporting electrolyte (0.1 M NH_3-NH_4Cl buffer solution, pH 9.4), deposition potential (- 0.3 V), deposition time (150 s), frequency (60 Hz), amplitude (0.07 V) and voltage step (0.007 V).

4.5.4. The effect of Ligands concentration

The effect of the ligands concentration on the Ni and Co peak current was studied in the potential range -0.7 – 1.2 V using a solution containing 5 μg L^{-1} Ni^{2+} and Co^{2+} at ERGO-PG-MFE the results are presented in *figure 4.37* below. In the absence of the mixture of the ligands (a), both Ni and Co could not be adsorbed nor reduced on the electrode surface, however in the presence of both DMG and Nioxime, the target metals could finally be adsorbed and reduced on the electrode surface in the form of Ni(II)-$(DMG)_2$ and Co(II)-$(Nioxime)_2$. *Figure 4.37* shows the importance of ligands in the stripping analysis of both Ni and Co by AdCSV. The ligands were added individually and simultaneously which all yielded the same results. An optimal concentration of 23.22 and 7.11 mg L^{-1} for DMG and Nioxime respectively was further used in this work after a series of investigation. Ligand concentration above the optimal was found to yield interfered peaks of Ni and Co.

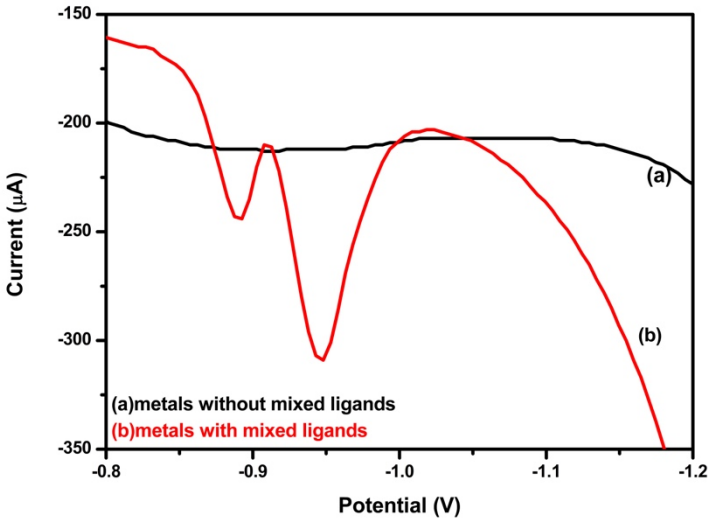

Figure 4.37. SW-AdSV of 5 μg L^{-1} Ni^{2+} and Co^{2+} at ERGO-PG-MFE (a) in the absence of mixed ligands and (b) in the mixture of 23.22 and 7.11 mg L^{-1} of DMG and Nioxime respectively. Supporting electrolyte (0.1 M NH_3-NH_4Cl buffer solution, pH 9.4, under optimized conditions.

4.5.5. Film stability and reproducibility

Performance metrics including stability and reproducibility of the ERGO-PG-MFEs were crucially investigated. Good relative standard deviation (RSD %) < 7 % were obtained when measuring 10 consecutive replicas (n = 10) of 5 μg L^{-1} Ni^{2+} and Co^{2+} cations at the ERGO-PG-MFE in 0.1 M NH_4OH-NH_4C buffer (pH 9.4), at optimum conditions. Furthermore, the stripping peak of both Ni^{2+} and Co^{2+} remained the almost the same for each ERGO-PG-MFE prepared and used to detect 5μg L^{-1} of each target metal under the same conditions. The low standard deviation provides evidence as to the good reproducibility in preparing the ERGO-PG-MFEs. Moreover, the mechanical stability of the mercury film on the pencil graphite substrate was satisfactory since reproducible and well-defined peaks were obtained even at much higher rotation speeds.

4.5.6. Effect of the instrumental parameters on the stripping peaks of Ni^{2+} and Co^{2+} at ERGO-PG-MFE

4.5.6.1. Deposition Potential

Figure 4.38 illustrates the behaviour of deposition time on stripping peak currents of Ni^{2+} and Co^{2+} at ERGO-PG-MFE was investigated in the potential range from 0 V to -0.9 V. A general increase for both peaks is observed with increasing deposition potential peak and decrease gradually from maximum stripping peak potential of -0.3 V for Ni^{2+} while the Co^{2+} increases steadily. Electrode saturation resulted in a decrease of Ni^{2+} stripping current peak from -0.3 V, however the Co^{2+} was not affected much as it continued increasing till a gradual and steady decrease. A potential of -0.3 V was chosen as an optimal deposition potential

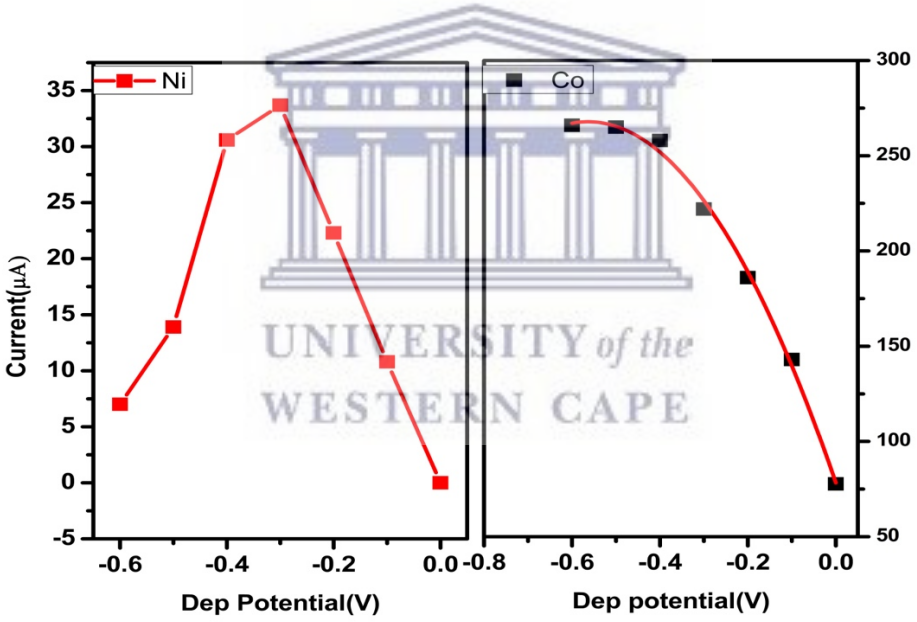

Figure 4.38. The effect of Deposition potential on the stripping peak of $Ni^{2+}$and Co^{2+} at electrochemically reduced graphene oxide pencil graphite mercury film electrode (ERGO-PG-MFE) in 0.1M ammonium hydroxide ammonium chloride buffer solution (pH 9.4) containing 5 μg L^{-1} of Ni^{2+} and 1 μg L^{-1} of Co^{2+} and 5 mg L^{-1} of Hg^{2+}.

4.5.6.2. Frequency

Figure 4.39 shows the dependence of the Ni^{2+} and Co^{2+} stripping peak current over the frequency range of 10 to 100 Hz. The peak current for both metal ions increase with increased frequency which is attributed to the increase in scan rate with increasing frequency, this followed by a steady decrease by a Co^{2+} current peak after a maximum was reach at frequency of 70 Hz while the current peak height of Ni^{2+} started equilibrating from frequency of 70 Hz onwards. A frequency of 70 Hz was chosen as the optimum frequency.

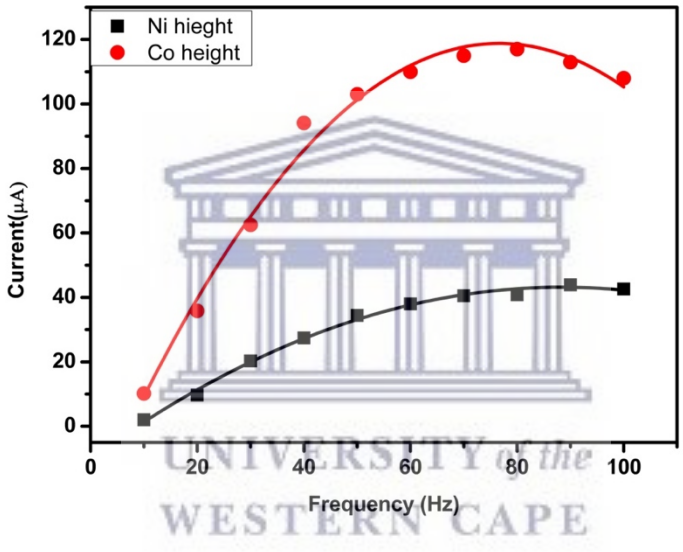

Figure 4.39. The effect of Frequency on the stripping peak of Ni^{2+} and Co^{2+} at electrochemically reduced graphene oxide pencil graphite mercury film electrode (ERGO-PG-MFE) in 0.1M ammonium hydroxide ammonium chloride buffer solution (pH 9.4) containing 5 μg L^{-1} of Ni^{2+} and μg L^{-1} of Co^{2+} and 5 mg L^{-1} of Hg^{2+}.

4.5.6.3. Amplitude

Figure 4.40 shows the effect of amplitude on the stripping peak currents of Ni^{2+} and Co^{2+} which was investigated over the range of 0,01 V to 0,1 V. the peak current of both metal ions increased linearly with increasing amplitude up to a maximum, followed by a steady decrease. An amplitude

of 0.06 V was selected at the optimum amplitude.

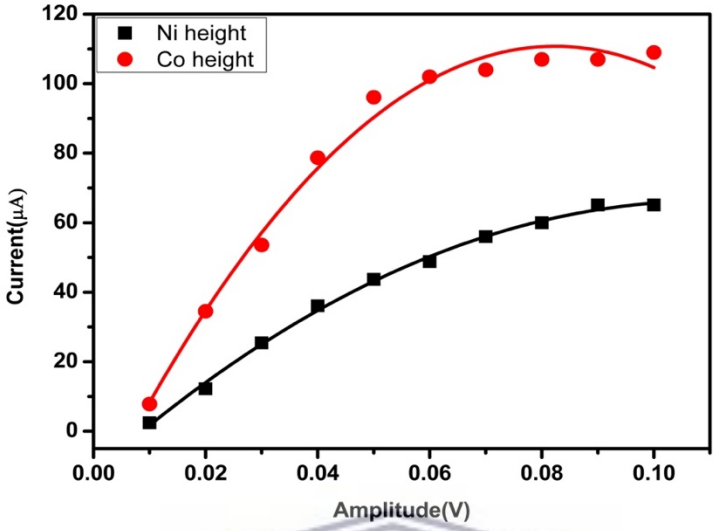

Figure 4.40. The effect of Amplitude on the stripping peak of Ni^{2+} and Co^{2+} at electrochemically reduced graphene oxide pencil graphite mercury film electrode (ERGO-PG-MFE) in 0.1M ammonium hydroxide ammonium chloride buffer solution (pH 9.4) containing 5 µg L^{-1} of Ni^{2+} and Co^{2+} and 5 mg L^{-1} of Hg^{2+}.

4.5.6.4. Voltage step

Figure 4.41 shows the variation of voltage step with the peak currents of Ni^{2+} and Co^{2+} applied over the range of 0,001 V to 0,01V. The peak current for both metals increased with increasing voltage step. A voltage step of 0,007 V was selected as the optimum voltage step.

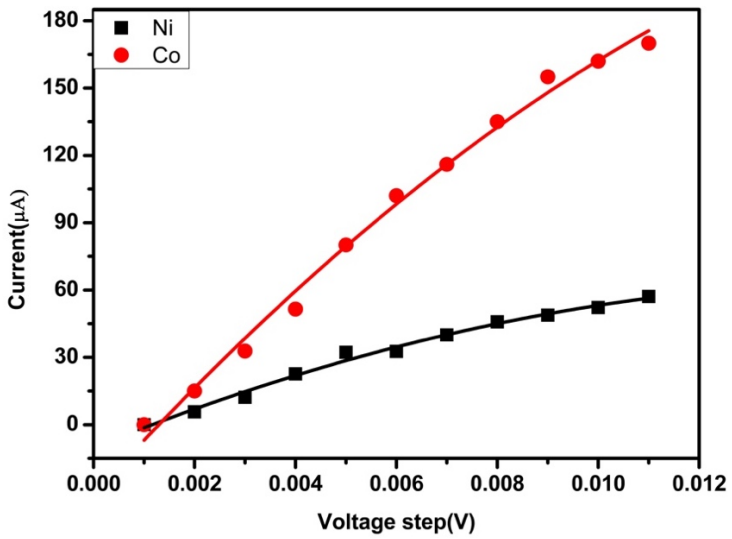

Figure 4.41. The effect of Voltage step on the stripping peak of Ni^{2+} and Co^{2+} at electrochemically reduced graphene oxide pencil graphite mercury film electrode (ERGO-PG-MFE) in 0.1M ammonium hydroxide ammonium chloride buffer solution (pH 9.4) containing 5 μg L^{-1} of Ni^{2+} and Co^{2+} and 5 mg L^{-1} of Hg^{2+}.

4.5.6.5. Deposition time

The deposition time on the peak current of Ni^{2+} and Co^{2+} was investigated over the time interval of 30 to 300 s. As the deposition time increase the peak current for both metals ions increases since more time is allowed for the metal complexes to be deposited on the electrode surface. A slow steady increases and a level off is observed for time above 240s. This is caused by an electrode being over saturated. A deposition time of 150s was further used in this investigation.

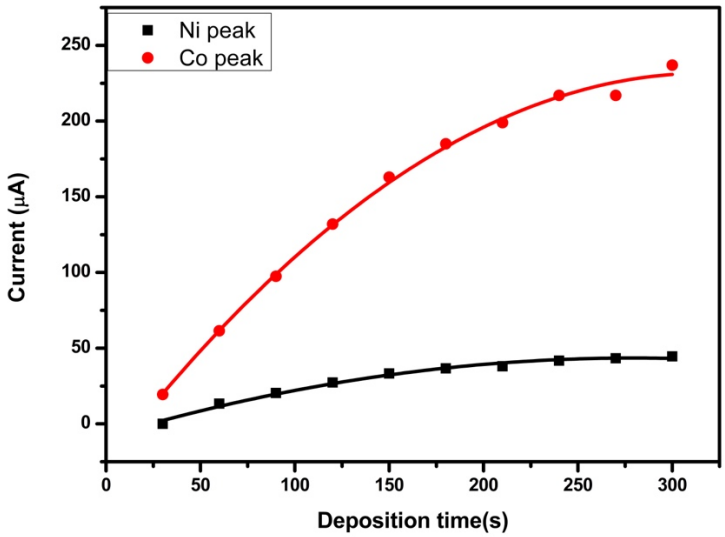

Figure 4.42. The effect of Deposition time on the stripping peak of Ni^{2+} and Co^{2+} at electrochemically reduced graphene oxide pencil graphite mercury film electrode (ERGO-PG-MFE) in 0.1M ammonium hydroxide ammonium chloride buffer solution (pH 9.4) containing 5 μg L^{-1} of Ni^{2+} and 1 μg L^{-1} of Co^{2+} and 5 mg L^{-1} of Hg^{2+}.

4.5.7. Analytical performances of the electrochemically reduced graphene oxide modified pencil graphite mercury film electrode

4.5.7.1. Simultaneous determination of Ni^{2+} and Co^{2+}

In simultaneous analysis all two metal ions are present or mixed together in the same solution and, the signal response (peak current) of each metal ion is obtained by measuring peak height of each. The calibration curve of Ni^{2+} and Co^{2+} determination at the ERGO-PG-MFE by using AdCSV is shown in *figure 4.43*. For a 150 s accumulation/deposition time, a deposition/accumulation potential of - 0.3 V, a rotational speed of 1000 rpm, a frequency of 60 Hz, an amplitude of + 0.07 V and a sweep rate of 0.2 V s^{-1}, a proportional relationship between the reduction peaks current and the concentration of both Ni^{2+} and Co^{2+} was obtained in the range of 0.5 to 5 μg L^{-1}. Three replicate SW-AdCSV measurements were performed for each calibration range.

The sensitivity of the ERGO-PG-MFE to the simultaneous determination of both Ni^{2+} and Co^{2+} is 1.80 x 10^{-5} and 4.80 x 10^{-5} respectively.

The detection limits were determined using the equation below: $3\sigma_{blank}$/ slope

$$LOD = \frac{3\sigma_{blank}}{slope}$$

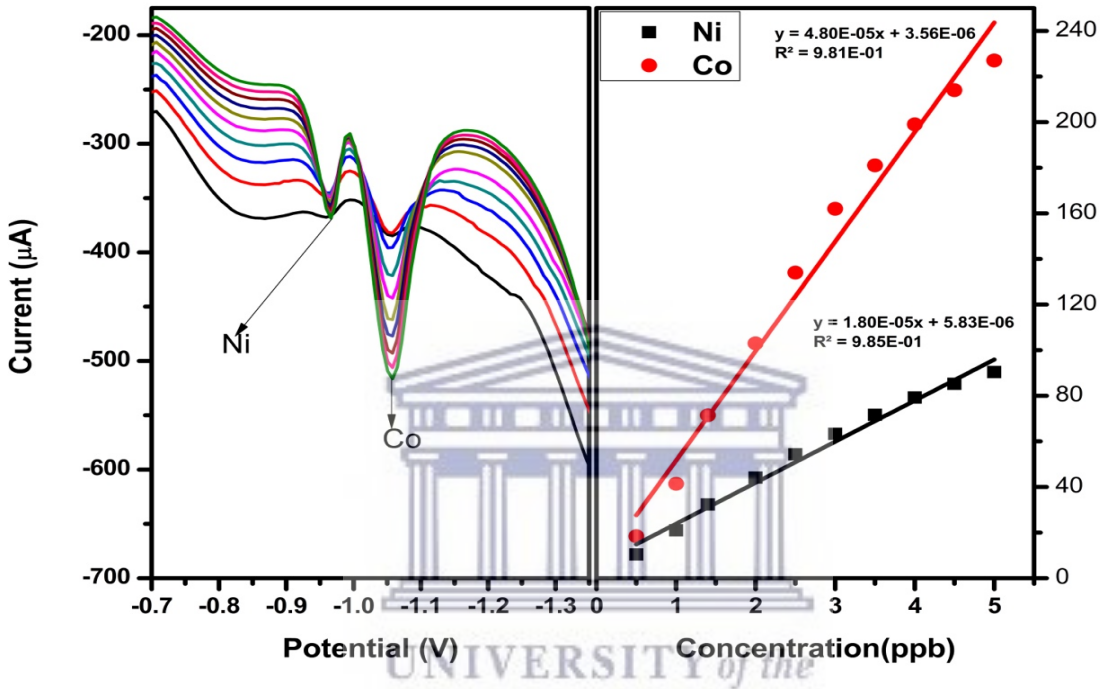

Figure 4.43. SW-AdCSV and a corresponding calibration curve for the simultaneous analysis of Ni^{2+} and Co^{2+} obtained at the ERGO-PG-MFE, between the concentration of 0.5 and 5 µg L^{-1}. 0.1 M NH_3-NH_4Cl buffer (pH 9.4) was used as supporting electrolyte. The square-wave voltammetric parameters were a deposition/accumulation time of 150 s, a deposition/accumulation potential of - 0.3 V, a rotational speed of 1000 rpm, a frequency of 60 Hz, an amplitude of + 0.07 V and a sweep rate of 0.2 V s^{-1}.

Table 5: Calibration data representation of the simultaneous analysis of Ni^{2+} and Co^{2+} at ERGO-PG-MFE in 0.1M ammonium buffer solution (pH 9.4) under optimized parameters.

Analytical Parameter	**Analysis of Ni^{2+} (0.5-5 μgL^{-1})**	**Analysis of Co^{2+} (0.5-5 μgL^{-1})**
Sensitivity ($\mu AL\ \mu g^{-1}$)	$1{,}80 \times 10^{-5}$	$4{,}80 \times 10^{-5}$
Correlation Coefficient (R^2)	0.985	0.981
Detection Limits ($\mu g\ L^{-1}$)	6.1	1.8
Limit of Quantification ($\mu g\ L^{-1}$)	18	6.2

*n = 3, where n is the number of replications.

4.5.7.2. Individual analysis of Ni^{2+} and Co^{2+}

Figure 4.44 below represents the individual analysis of Co^{2+} at an ERGO-PG-MFE in the presents of both DMG and Nioxime in 0.1M ammonium buffer solution (pH 9.4) under optimized parameters. A single, well enhanced and resolved peak of Co^{2+} is observed at -1.12 V, proving that Co^{2+} ions are only complexed by the Nioxime ligand. DMG takes no part in the complexation and stripping of Co^{2+} at ERGO-PG-MFE as the peak size and area is almost the same as the one observed in **Section 4.22** of Part B. The ERGO-PG-MFE is more sensitive towards Co(II)-$(Nioxime)_2$ than it is towards Ni(II)-$(DGM)_2$ as the peak ratio are not the same.

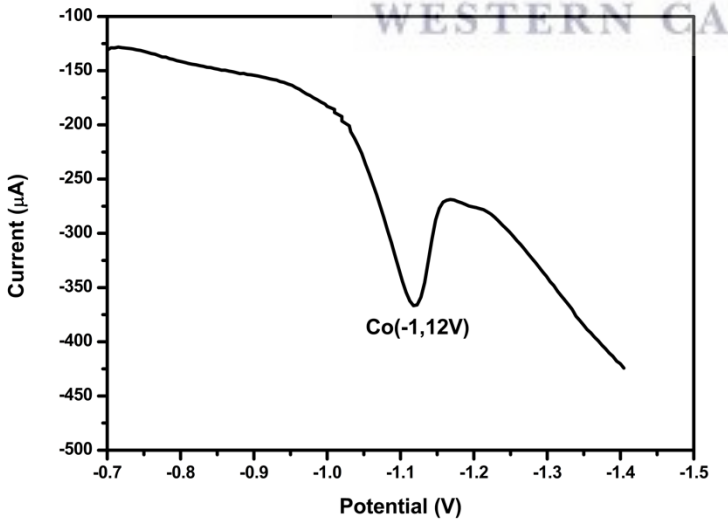

Figure 4.44. The individual analysis of 10 $\mu g\ L^{-1}$ Co^{2+} obtained at the ERGO-PG-MFE after the addition of Nioxime and DMG.

4.5.8. Recoveries Studies of ERGO-PG-MFE

The ERGO-PG-MFE and developed method were used for the simultaneous analysis of both Ni^{2+} and Co^{2+} in test electrolyte solutions. Known concentrations of both Ni^{2+} and Co^{2+} cations were used to spike 20 mL portions of 0.1 M NH_3-NH_4Cl buffer solutions for recovery determination by a standard addition method. The obtained voltammograms together with their corresponding standard addition curves are shown in *Figure 4.45 & 4.46*. Recovery percentages of the Ni^{2+} and Co^{2+} ions from test solutions spiked with 1 µg L^{-1} Ni^{2+} and Co^{2+} yielded a recovery of 109 % ± 3.4 % and 86 ± 5 % respectively for three replications (n = 3). Low recovery yield for Co might be as a result of the interference of Ni at high concentration.

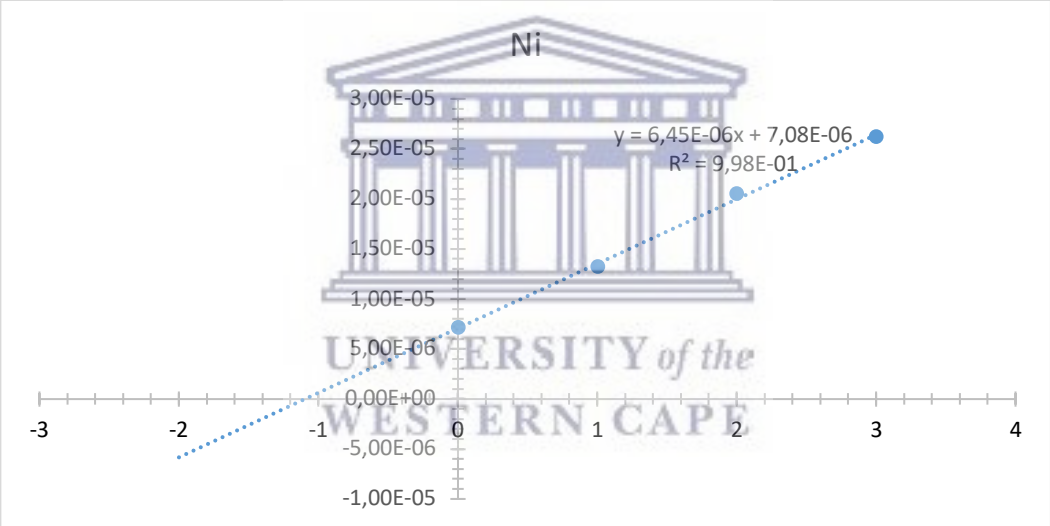

Figure 4.45. Standard addition plots for the determination of Ni^{2+} at ERGO-PG-MFE in test solutions.

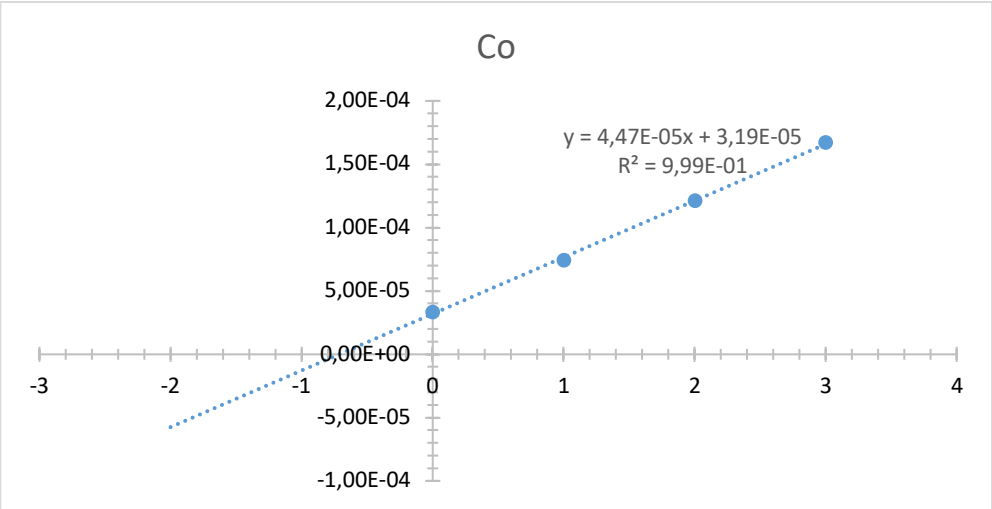

Figure 4.46. Standard addition plots for the determination of Co^{2+} at ERGO-PG-MFE in test solutions.

4.5.9. Application to tap water

The accuracy of the method was assessed by determining nickel and cobalt in real water samples. The ERGO-PG-MFE was applied to the analysis of both Ni^{2+} and Co^{2+} in tap water samples, as described in **Section 2.9**. SW-AdCSV analysis was performed by *in-situ* deposition of the metal film and target metal under the optimized parameters. Due to the good sensitivity of ERGO-PG-MFE, peaks could be observed due to the nickel and cobalt ions present in the water sample. The amount of both nickel and cobalt ions present in the tap water sample was determined by the standard additions method as shown in *Figure 4.47*, below. Ni^{2+} was found to be 0.36 µg L^{-1} and Co^{2+} to be 0.39 µg L^{-1} in the tap water sample. In addition, four consecutive addition of 1 ppb of both nickel and cobalt were added to tap water samples. This method was re-determined/repeated for a minimum of 3 times.

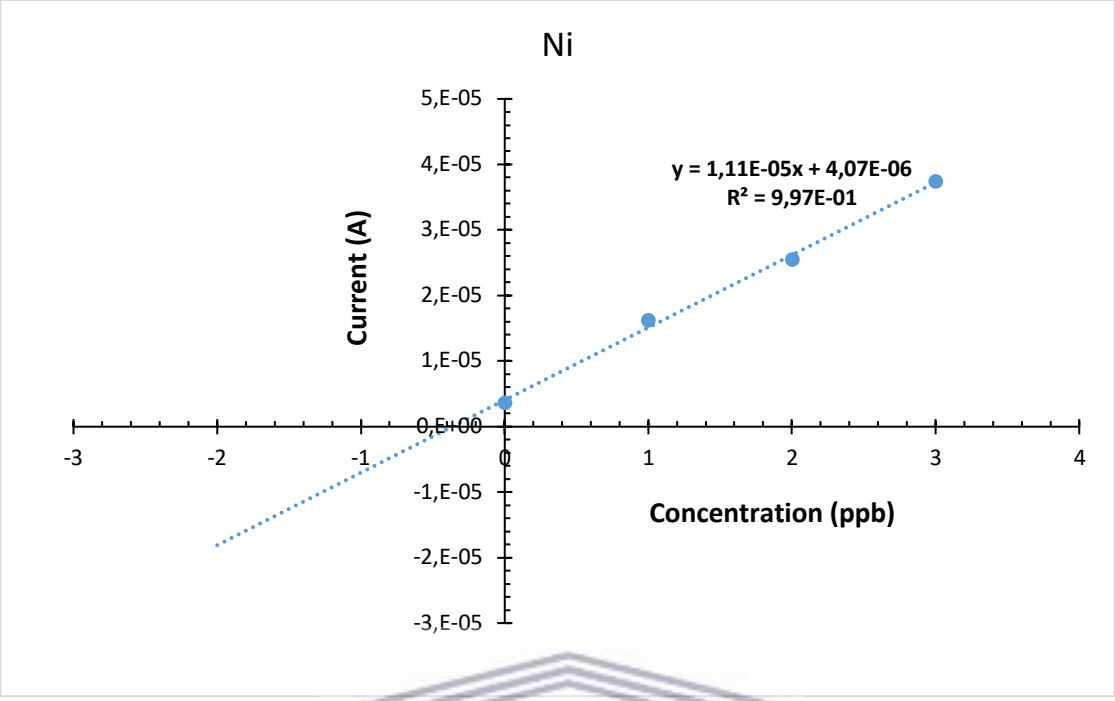

Figure 4.47. Standard addition calibration curve of Ni^{2+} for the analysis of tap water (pH 9.4) spiked with 1 µg L^{-1} of Ni^{2+} ions at a deposition/accumulation time of 150 s.

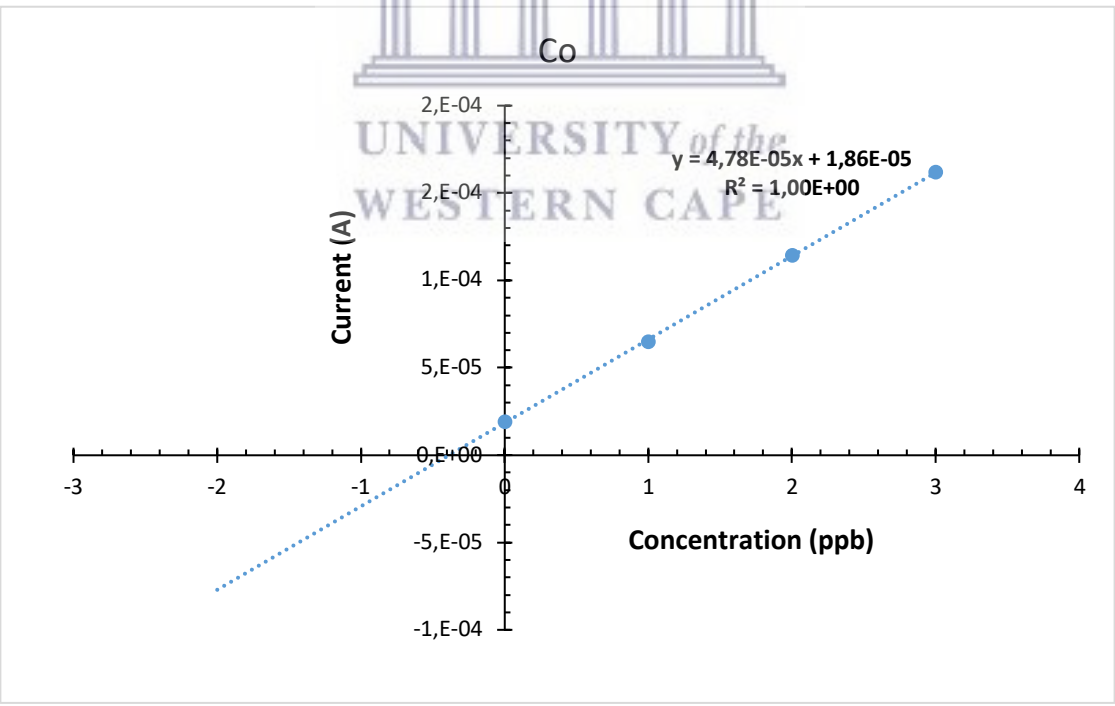

Figure 4.48. Standard addition calibration curve of Co^{2+} for the analysis of tap water (pH 9.4) spiked with 1 µg L^{-1} of Co^{2+} ions at a deposition/accumulation time of 150 s.

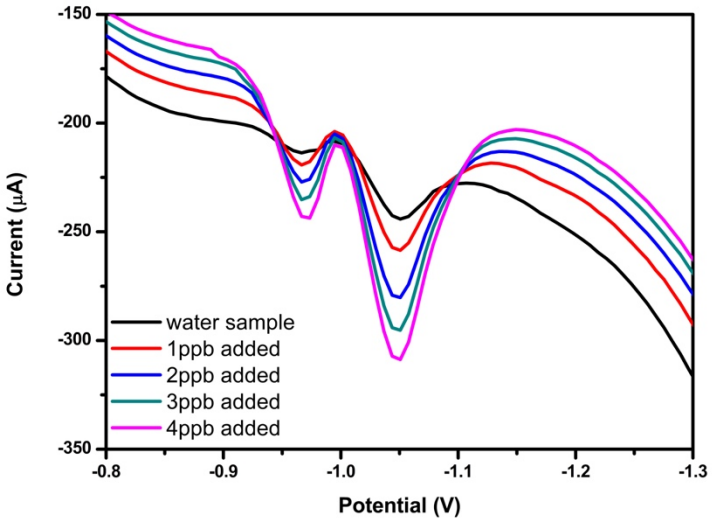

Figure 4.49. Square wave voltammograms for the standard addition of water samples with the addition of 1 ppb of Ni and Co.

4.5.10. Interferences

The possible Interference of Zn^{2+}, Cd^{2+}, Pd^{2+}, Pb^{2+} and Cu^{2+} on the cathodic stripping peak of both Ni^{2+} and Co^{2+} was investigated individually by the addition of the interfering ions between 5 and 40 μg L^{-1} to a solution containing 5 μg L^{-1} of Ni^{2+} and Co^{2+} under optimized conditions. The intermetallic interference was investigated by a method of standard addition and spiking the solution test with a known concentration of the interfering ions. Metal ions interfere with the stripping peak by complexing competitively with either DMG or Nioxime or by producing reduction peaks that overlap with or even completely suppress the Ni and Co peak altogether. Most metals did not interfere with the stripping peak of both Nickel and Co, however, at 5 fold excess of Zn^{2+} both peaks increased ~ 5 %. n.

The possible effect of selected metal ions such as Zn^{2+}, Cd^{2+}, Pd^{2+}, Pb^{2+} and Cu^{2+} in solution containing 5 μg L^{-1} of both Ni^{2+} and Co^{2+} in combination with 150 s accumulation time was studied. The intermetallic interference was investigated by a method of standard addition and spiking the solution test with a known concentration of the interfering ions. Most metals did not

interfere with the stripping peak of both Ni and Co, however, at 6 fold excess of Zn^{2+} both peak increased ~ 11 %.

The interferences by each other was also investigated. The interference of Co on Ni peak was studied in a solution which contained a fix concentration of 5 μg L^{-1} of Ni followed by equal additions of Co from 5 μg L^{-1} to 50 μg L^{-1}. The peak height of Ni had a ~ 4 % change after the addition of 35 μg L^{-1}, however above that the two peaks started overlapping. The same study was done for Ni over Co, however no overlapping was observed for 10-fold excess.

4.5.11. Conclusion

The in situ preparation of ERGO-PG mercury-film electrode allows convenient simultaneous determination of ultra-trace concentration levels of Ni^{2+} and Co^{2+} in combination with adsorptive cathodic stripping voltammetry. After optimization, the developed analytical procedure turned out as a promising method with analytical results characterized by satisfactory accuracy and precision. Mixing the two ligands proves to be effective in terms of being able to complexes and successfully determine the target metals simultaneously. Well define and separate stripping peaks of Ni^{2+} and Co^{2+} were achieved therefore overcoming the challenging of overlapping of the two stripping peaks. The electrochemically reduced graphene oxide pencil-graphite mercury-film electrode (ERGO-PG-MFE) showed improved detection limits compared to some modified mercury-film electrodes reported in literature due to graphene's enhanced electron transfer rate and surface-to-volume ratio. The calculated detection limits for both Ni^{2+} and Co^{2+} were 6.1 and 1.8 μgL^{-1} Furthermore, the ERGO-PG-MFE was successfully used as the electrochemical platform suitable for tap water analysis. The use of mixed ligands was a success as well separated peaks of Ni^{2+} and Co^{2+} were achieved.

CHAPTER 5

Conclusion and Future work

A highly enhanced sensing platform based on the direct electrochemical reduction of graphene oxide on a pencil graphite electrodes was developed for the determination of heavy metals by square-wave adsorptive cathodic stripping voltammetry. The electrochemically reduced graphene oxide pencil graphite mercury-film electrode (EGRO-PG-MFE) showed improved sensitivities and detection limits to mercury-film electrodes due to the combination of enhanced electron transfer rate, surface-to-volume ratio and improved sensitivity due to the graphene and metal-film. Simultaneous determination of Ni^{2+} and Co^{2+} was successfully entailed by the mixing of DMG and Nioxime complexing agents.

The ERGO-PG-MFE *in situ* plated mercury film resulted in an ultra-sensitive sensing platform for the detection of trace amounts of heavy metals by square-wave adsorptive cathodic stripping voltammetry.

Minimizing errors in recoveries of Co^{2+} during the simultaneous analysis of Ni^{2+} and Co^{2+} at MFE is of vital importance hence further investigation in the future of increased pH water samples should also be further interrogated.

Future work will focus on implementing the same principle on a microfluidic paper-based analytical devices (µPADs). Microfluidic paper-based analytical devices introduces an innovative platform technology for fluid handling and analysis, with wide range of applications, prompting high-sensitivity, accuracy and rapid analysis with simplicity, portability and low cost. Being able to replace pencil graphite lead with paper is not only extremely cheap and ubiquity but offers mechanical properties such comprising flexibility, lightness, and low thickness. The successful implementation of µPADs incorporated by ligands such as DMG and Nioxime to the analysis of nickel and cobalt will offer a wide range of applications such as low cost, ease of fabrication/operation and equipment independence. Graphene has proven to be very good in selectivity and sensitivity hence the fabrication of µPADs with graphene oxide will be studied and investigated in the future. The µPADs will not only be limited on cobalt and nickel.

REFERENCES

[1] B. N. Kumar, S. Kanchi, M. I. Sabela, K. Bisetty, and N. V. V. Jyothi, "Spectrophotometric determination of nickel (II) in waters and soils: Novel chelating agents and their biological applications supported by DFT method," *Karbala Int. J. Mod. Sci.*, vol. 2, no. 4, pp. 239–250, 2016.

[2] E. Denkhaus and K. Salnikow, "Nickel essentiality, toxicity, and carcinogenicity," *Crit. Rev. Oncol. Hematol.*, vol. 42, no. 1, pp. 35–56, 2002.

[3] M. Cempel and G. Nikel, "Nickel: A review of its sources and environmental toxicology," *Polish J. Environ. Stud.*, vol. 15, no. 3, pp. 375–382, 2006.

[4] Y. Yao and M. Costa, "Toxicogenomic effect of nickel and beyond," *Arch. Toxicol.*, vol. 88, pp. 1645–1650, 2014.

[5] Ç. Büyükpınar, E. Maltepe, D. S. Chormey, N. San, and S. Bakırdere, "Determination of nickel in water and soil samples at trace levels using photochemical vapor generation-batch type ultrasonication assisted gas liquid separator-atomic absorption spectrometry," *Microchem. J.*, vol. 132, pp. 167–171, 2017.

[6] J. Kristiansen, J. M. Christensen, T. Henriksen, N. H. Nielsen, and T. Menné, "Determination of nickel in fingernails and forearm skin (stratum corneum)," *Anal. Chim. Acta*, vol. 403, no. 1–2, pp. 265–272, 2000.

[7] A. Maher, M. Sadeghi, and A. Moheb, "Heavy metal elimination from drinking water using nanofiltration membrane technology and process optimization using response surface methodology," *Desalination*, vol. 352, pp. 166–173, Nov. 2014.

[8] L. Zhang, D. W. Pan, and Y. S. Liu, "Rapid and sensitive determination of cobalt by adsorptive cathodic stripping voltammetry using tin???bismuth alloy electrode," *Ionics (Kiel).*, vol. 22, no. 5, pp. 721–729, 2016.

[9] R. Galbeiro, S. Garcia, and I. Gaubeur, "A green and efficient procedure for the preconcentration and determination of cadmium, nickel and zinc from freshwater, hemodialysis solutions and tuna fish samples by cloud point extraction and flame atomic absorption spectrometry," *J. Trace Elem. Med. Biol.*, vol. 28, no. 2, pp. 160–165, 2014.

[10] E. Çetinkaya and A. Aydin, "A novel thiocarbohydrazide derivative for preconcentration of copper(II), nickel(II), lead(II), and cadmium(II) in water samples for flame atomic

absorption spectrophotometry," *Desalin. Water Treat.*, vol. 74, pp. 224–236, 2017.

[11] M. Amirkavei, S. Dadfarnia, and A. M. H. Shabani, "Dispersive liquid-liquid microextraction based on solidification of floating organic drop for simultaneous separation/preconcentration of nickel, cobalt and copper prior to determination by electrothermal atomic absorption spectrometry," *Quim. Nova*, vol. 36, no. 1, pp. 63–68, 2013.

[12] W. S. Zhong, T. Ren, and L. J. Zhao, "Determination of Pb (Lead), Cd (Cadmium), Cr (Chromium), Cu (Copper), and Ni (Nickel) in Chinese tea with high-resolution continuum source graphite furnace atomic absorption spectrometry," *J. Food Drug Anal.*, vol. 24, no. 1, pp. 46–55, 2016.

[13] C. Stihi, I. V. Popescu, M. Frontasyeva, C. Radulescu, A. Ene, O. Culicov, I. Zinicovscaia, I. D. Dulama, S. Cucu-Man, R. Todoran, A. I. Gheboianu, A. Bucurica, I. Bancuta, and G. Dima, "Characterization of Heavy Metal Air Pollution in Romania Using Moss Biomonitoring, Neutron Activation Analysis, and Atomic Absorption Spectrometry," *Anal. Lett.*, vol. 2719, no. July, 2017.

[14] A. D. Shinde, R. Acharya, and A. V. R. Reddy, "Analysis of Zirconium and Nickel Based Alloys and Zirconium Oxides by Relative and Internal Monostandard Neutron Activation Analysis Methods," *Nucl. Eng. Technol.*, vol. 49, no. 3, pp. 562–568, 2016.

[15] B. Zawisza, R. Sitko, E. Malicka, E. Talik, Z. Huang, R. Liu, Y. Kuang, X. Wang, R. Wrzalik, R. K. Prud`homme, and I. A. Aksay, "Graphene oxide as a solid sorbent for the preconcentration of cobalt, nickel, copper, zinc and lead prior to determination by energy-dispersive X-ray fluorescence spectrometry," *Anal. Methods*, vol. 5, no. 22, p. 6425, Oct. 2013.

[16] L. Zhao, S. Zhong, K. Fang, Z. Qian, and J. Chen, "Determination of cadmium(II), cobalt(II), nickel(II), lead(II), zinc(II), and copper(II) in water samples using dual-cloud point extraction and inductively coupled plasma emission spectrometry," *J. Hazard. Mater.*, vol. 239–240, pp. 206–212, 2012.

[17] A. Beiraghi, S. Babaee, and M. Roshdi, "Simultaneous preconcentration of cadmium, cobalt and nickel in water samples by cationic micellar precipitation and their determination by inductively coupled plasma-optical emission spectrometry," *Microchem. J.*, vol. 100, no. 1, pp. 66–71, 2012.

[18] K. Pokpas, S. Zbeda, N. Jahed, N. Mohamed, P. G. Baker, and E. I. Iwuoha, "Electrochemically reduced graphene oxide pencil-graphite in situ plated bismuth-film electrode for the determination of trace metals by anodic stripping voltammetry," *Int. J. Electrochem. Sci.*, vol. 9, no. 2, pp. 736–759, 2014.

[19] A. F. Al-Ghamdi, M. M. Hefnawy, A. A. Al-Majed, and F. F. Belal, "Development of square-wave adsorptive stripping voltammetric method for determination of acebutolol in pharmaceutical formulations and biological fluids," *Chem. Cent. J.*, vol. 6, no. 1, p. 15, 2012.

[20] M. Korolczuk, K. Tyszczuk, and M. Grabarczyk, "Adsorptive stripping voltammetry of nickel and cobalt at in situ plated lead film electrode," *Electrochem. commun.*, vol. 7, no. 12, pp. 1185–1189, 2005.

[21] S. B. Adeloju and A. Hadjichari, "Simultaneous Determination of Nickel and Cobalt in Natural Water and Sediment Samples on an in-situ Plated Mercury Film Electrode by Adsorptive Cathodic Stripping Voltammetry.," *Anal. Sci.*, vol. 15, no. 1, pp. 95–100, 1999.

[22] "Trace Nickel Determination with Phenyldithiocarbamate in Sea Water by Adsorptive Stripping Voltammetry.pdf.".

[23] K. Pokpas, N. Jahed, P. G. Baker, and E. I. Iwuoha, "Complexation-Based Detection of Nickel(II) at a Graphene-Chelate Probe in the Presence of Cobalt and Zinc by Adsorptive Stripping Voltammetry," *Sensors*, vol. 17, no. 8, p. 1711, Jul. 2017.

[24] M. I. Saidin, I. M. Isa, M. Ahmad, N. Hashim, and S. Ab Ghani, "Analysis of trace nickel by square wave stripping voltammetry using chloropalladium(II) complex-modified MWCNTs paste electrode," *Sensors Actuators, B Chem.*, vol. 240, pp. 848–856, 2017.

[25] J. Opydo, "Cathodic Adsorptive Stripping Voltammetry for Estimation of the Forest Area Pollution with Nickel and Cobalt," vol. 162, 2001.

[26] N. Gharib Naseri, S. J. Baldock, A. Economou, N. J. Goddard, and P. R. Fielden, "Disposable electrochemical flow cells for catalytic adsorptive stripping voltammetry (CAdSV) at a bismuth film electrode (BiFE)," *Anal. Bioanal. Chem.*, vol. 391, no. 4, pp. 1283–1292, 2008.

[27] P. González, V. A. Cortínez, and C. A. Fontán, "Determination of nickel by anodic adsorptive stripping voltammetry with a cation exchanger-modified carbon paste

electrode," *Talanta*, vol. 58, no. 4, pp. 679–690, 2002.

[28] C. Rojas, V. Arancibia, M. G??mez, and E. Nagles, "Adsorptive stripping voltammetric determination of cobalt in the presence of nickel and zinc using pyrogallol red as chelating agent," *Int. J. Electrochem. Sci.*, vol. 7, no. 2, pp. 979–990, 2012.

[29] J. K. Kiptoo, J. C. Ngila, and G. M. Sawula, "Speciation studies of nickel and chromium in wastewater from an electroplating plant," *Talanta*, vol. 64, no. 1, pp. 54–59, 2004.

[30] P. Kapturski and A. Bobrowski, "The silver amalgam film electrode in catalytic adsorptive stripping voltammetric determination of cobalt and nickel," *J. Electroanal. Chem.*, vol. 617, no. 1, pp. 1–6, 2008.

[31] A. Bobrowski, A. Królicka, M. Maczuga, and J. Zarębski, "A novel screen-printed electrode modified with lead film for adsorptive stripping voltammetric determination of cobalt and nickel," *Sensors Actuators, B Chem.*, vol. 191, no. FEBRUARY, pp. 291–297, 2014.

[32] B. Rezaei and E. Rezaei, "Simultaneous determination of trace amounts of nickel, cobalt, and zinc in the wastewater of a galvanic workshop by using adsorptive cathodic stripping voltammetry," *J. Anal. Chem.*, vol. 61, no. 3, pp. 262–265, 2006.

[33] P. Y. Khashaba, H. R. H. Ali, and M. El-Wekil, "Highly sensitive and selective complexation based voltammetric methods for the analysis of rabeprazole sodium in real samples," *RSC Adv.*, vol. 7, no. 6, pp. 3043–3050, 2017.

[34] J. Li, C. Zheng, L. Qi, M. Yoshio, and H. Wang, "Storage behavior of isomeric quaternary alkyl ammonium cations in graphite electrodes for graphite/activated carbon capacitors," *Electrochim. Acta*, 2017.

[35] L. Baldrianova, I. Svancara, M. Vlcek, a. Economou, and S. Sotiropoulos, "Effect of Bi(III) concentration on the stripping voltammetric response of in situ bismuth-coated carbon paste and gold electrodes," *Electrochim. Acta*, vol. 52, no. 2, pp. 481–490, 2006.

[36] M. Keyvanfard, R. Shakeri, H. Karimi-Maleh, and K. Alizad, "Highly selective and sensitive voltammetric sensor based on modified multiwall carbon nanotube paste electrode for simultaneous determination of ascorbic acid, acetaminophen and tryptophan," *Mater. Sci. Eng. C*, vol. 33, no. 2, pp. 811–816, 2013.

[37] S. Smarzewska, J. Pokora, A. Leniart, N. Festinger, and W. Ciesielski, "Carbon Paste Electrodes Modified with Graphene Oxides - Comparative Electrochemical Studies of

Thioguanine," *Electroanalysis*, p. n/a-n/a, 2016.

[38] D. an Li, T. Okajima, L. Mao, and T. Ohsaka, "Bioelectrocatalytic oxygen reduction reaction by bilirubin oxidase adsorbed on glassy carbon and edge-plane pyrolytic graphite electrodes: Effect of redox mediators," *Int. J. Electrochem. Sci.*, vol. 9, no. 3, pp. 1390–1398, 2014.

[39] K. B. Dönmez, E. Çetinkaya, S. Deveci, S. Karadağ, Y. Şahin, and M. Doğu, "Preparation of electrochemically treated nanoporous pencil-graphite electrodes for the simultaneous determination of Pb and Cd in water samples," *Anal. Bioanal. Chem.*, vol. 409, no. 20, pp. 4827–4837, 2017.

[40] N. Dossi, R. Toniolo, A. Pizzariello, F. Impellizzieri, E. Piccin, and G. Bontempelli, "Pencil-drawn paper supported electrodes as simple electrochemical detectors for paper-based fluidic devices," *Electrophoresis*, vol. 34, no. 14, pp. 2085–2091, 2013.

[41] J. Kariuki, E. Ervin, and C. Olafson, "Development of a novel, low-cost, disposable wooden pencil graphite electrode for use in the determination of antioxidants and other biological compounds," *Sensors (Switzerland)*, vol. 15, no. 8, pp. 18887–18900, 2015.

[42] K. Pokpas, N. Jahed, O. Tovide, P. G. Baker, and E. I. Iwuoha, "Nafion-graphene nanocomposite in situ plated bismuth-film electrodes on pencil graphite substrates for the determination of trace heavy metals by anodic stripping voltammetry," *Int. J. Electrochem. Sci.*, vol. 9, no. 9, pp. 5092–5115, 2014.

[43] M. J. Goldcamp, M. N. Underwood, J. L. Cloud, S. Harshman, and K. Ashley, "An Environmentally Friendly, Cost-Effective Determination of Lead in Environmental Samples Using Anodic Stripping Voltammetry," *J. Chem. Educ.*, vol. 85, no. 7, p. 976, Jul. 2008.

[44] A. Levent, Y. Yardim, and Z. Senturk, "Voltammetric behavior of nicotine at pencil graphite electrode and its enhancement determination in the presence of anionic surfactant," *Electrochim. Acta*, vol. 55, no. 1, pp. 190–195, 2009.

[45] E. Keskin, Y. Yardım, and Z. Şentürk, "Voltammetry of Benzo[a]pyrene in Aqueous and Nonaqueous Media: Adsorptive Stripping Voltammetric Determination at Pencil Graphite Electrode," *Electroanalysis*, vol. 22, no. 11, pp. 1191–1199, 2010.

[46] M. Muti, S. Sharma, A. Erdem, and P. Papakonstantinou, "Electrochemical monitoring of nucleic acid hybridization by single-use graphene oxide-based sensor," *Electroanalysis*,

vol. 23, no. 1, pp. 272–279, 2011.

[47] A. Erdem, H. Karadeniz, and A. Caliskan, “Single-walled carbon nanotubes modified graphite electrodes for electrochemical monitoring of nucleic acids and biomolecular interactions,” *Electroanalysis*, vol. 21, no. 3–5, pp. 464–471, 2009.

[48] S. Alegret and A. (Arben) Merkoçi, *Electrochemical sensor analysis*. Elsevier, 2007.

[49] S. Lee, S. K. Park, E. Choi, and Y. Piao, “Voltammetric determination of trace heavy metals using an electrochemically deposited graphene/bismuth nanocomposite film-modified glassy carbon electrode,” *J. Electroanal. Chem.*, vol. 766, pp. 120–127, 2016.

[50] K. Parvez, Z. Wu, R. Li, X. Liu, and R. Graf, “Exfoliation of Graphite into Graphene in Aqueous Solutions of Inorganic Salts,” 2014.

[51] F. Zhan, F. Gao, X. Wang, L. Xie, F. Gao, and Q. Wang, “Determination of lead(II) by adsorptive stripping voltammetry using a glassy carbon electrode modified with β-cyclodextrin and chemically reduced graphene oxide composite,” *Microchim. Acta*, vol. 183, no. 3, pp. 1169–1176, 2016.

[52] J. Ellis, J. E. Kim, and D. V Nanopoulos, “Voltammetry (Chapter 25) Electrochemistry techniques based on current (i) measurement as function of voltage (E,” *Electrochemistry*, vol. 145, no. Chapter 25, pp. 1–19, 1984.

[53] E. Herrero, V. Arancibia, C. Rojas, and – Romo, “Simultaneous determination of Pb 2+ , Cd 2+ and Zn 2+ by adsorptive stripping voltammetry using Clioquinol as a chelating-adsorbent agent,” *J. Electroanal. Chem.*, vol. 729, pp. 9–14, 2014.

[54] L. M. Cardoso, F. B. Mainier, and J. A. P. Itabirano, “Analysis Voltammetry of Cyanide and Process Electrolytic Removal of Cyanide in Effluents,” *Am. J. Environ. Eng.*, vol. 4, no. 6, pp. 182–188, 2014.

[55] Princeton Applied Research, “Application Note S-6 Subject : Fundamentals of Stripping Voltammetry,” no. 865, 2008.

[56] A. Bott, “Stripping Voltammetry,” *Current Separations*, vol. 12, no. 3. pp. 141–147, 1993.

[57] A. Economou and C. Kokkinos, “Chapter 1. Advances in Stripping Analysis of Metals,” no. 6, pp. 1–18, 2016.

[58] O. A. Farghaly and R. S. A. Hameed, “Analytical Application Using Modern Electrochemical Techniques,” vol. 9, pp. 3287–3318, 2014.

[59] G. March, T. D. Nguyen, and B. Piro, "Modified electrodes used for electrochemical detection of metal ions in environmental analysis," *Biosensors*, vol. 5, no. 2, pp. 241–275, 2015.

[60] "Pdf. Record.pdf." .

[61] M. M. Abdel-Galeil, M. M. Ghoneim, H. S. El-Desoky, T. Hattori, and a. Matsuda, "Anodic Stripping Voltammetry Determination of Lead ions using Highly Sensitive Modified Electrodes Based on Multi-walled Carbon Nanotube," *J. Chem. Biochem.*, vol. 2, no. 2, pp. 25–43, 2014.

[62] L. Zhang, D. Pan, and Y. Liu, "Rapid and sensitive determination of cobalt by adsorptive cathodic stripping voltammetry using tin–bismuth alloy electrode," *Ionics (Kiel).*, vol. 22, no. 5, pp. 721–729, May 2016.

[63] A. M. Beltagi, I. M. Ismail, and M. M. Ghoneim, "Square-Wave Adsorptive Cathodic Stripping Voltammeteric Determination of Manganese (II) Using a Carbon Paste Electrode Modified with Montmorillonite Clay," *Am. J. Anal. Chem.*, vol. 04, no. 04, pp. 197–206, 2013.

[64] S. Mendoza, E. Bustos, J. Manríquez, and L. A. Godínez, "Voltammetric Techniques," *Agric. Food Electroanal.*, pp. 21–48, 2015.

[65] J. Barton, M. B. G. García, D. H. Santos, P. Fanjul-Bolado, A. Ribotti, M. McCaul, D. Diamond, and P. Magni, "Screen-printed electrodes for environmental monitoring of heavy metal ions: a review," *Microchim. Acta*, vol. 183, no. 2, pp. 503–517, 2016.

[66] N. G. V. Gedaminskienė S. Armalis, "Adsorptive stripping voltammetry of cobalt at a hanging mercury drop and mercury film electrodes: a comparative study," *Chem.*, vol. 2, no. 14, pp. 94–98, 2003.

[67] C. Rojas, V. Arancibia, M. Gómez, and E. Nagles, "Adsorptive stripping voltammetric determination of cobalt in the presence of nickel and zinc using pyrogallol red as chelating agent," *Int. J. Electrochem. Sci.*, vol. 7, no. 2, pp. 979–990, 2012.

[68] D. S. Nascimento, M. Insausti, B. S. F. Band, and S. G. Lemos, "Simultaneous determination of Cu, Pb, Cd, Ni, Co and Zn in bioethanol fuel by adsorptive stripping voltammetry and multivariate linear regression," *Fuel*, vol. 137, pp. 172–178, 2014.

[69] S. B. Hocevar, I. Š. Vancara, B. Ogorevc, and K. Vytřas, "Antimony Film Electrode for Electrochemical Stripping Analysis."

[70] F. Paper and S. C. Universitry, “Analytical & Mercury Thin Film at Glassy Carbon Electrode for Captopril in Pharmaceutical Samples,” vol. 7, no. 3, pp. 344–357, 2015.

[71] M. Li, H. Gou, I. Al-Ogaidi, and N. Wu, “Nanostructured Sensors for Detection of Heavy Metals: A Review.”

[72] S. Jadhav, S. Kulkarni, and S. Quadri, “Ultrasound Assisted Synthesis and Physiochemical Investigation of Nickel – Dimethyl Glyoxime Complex,” vol. 5, no. June, pp. 311–316, 2015.

[73] A. Mardegan, S. DalBorgo, P. Scopece, L. M. Moretto, S. B. Hočevar, and P. Ugo, “Simultaneous Adsorptive Cathodic Stripping Voltammetric Determination of Nickel(II) and Cobalt(II) at an In Situ Bismuth-Modified Gold Electrode,” *Electroanalysis*, vol. 25, no. 11, pp. 2471–2479, 2013.

[74] A. Kumar, S. Singh, N. Singh, and S. Arora, “Nanotechnology: a review.,” *J. Pharm. Res.*, vol. 5, no. 7, pp. 3630–3634, 2012.

[75] K. Mikhail I, “Graphene : carbon in Carbon is one of the most intriguing elements in the Periodic Table .,” *Materialstoday*, vol. 10, no. 1, pp. 20–27, 2007.

[76] S. C. Sahu, A. K. Samantara, and J. Mohanta, “Graphene : Synthesis , Properties and Application Graphene : Synthesis , Properties and Application,” no. August, 2015.

[77] Iop, “Single sheets of carbon open up a new field of research,” *Inst. Phys.*, 2011.

[78] S. Li, Q. Zhang, Y. Lu, D. Ji, D. Zhang, J. Wu, X. Chen, and Q. Liu, “One step electrochemical deposition and reduction of graphene oxide on screen printed electrodes for impedance detection of glucose,” *Sensors Actuators, B Chem.*, vol. 244, pp. 290–298, 2017.

[79] T. H. E. Royal, S. Academy, and O. F. Sciences, “Graphene: Scientific background on the Nobel Prize in Physics 2010,” *R. Swedish Acad. Sci.*, vol. 50005, no. October, pp. 0–10, 2010.

[80] Q. Zheng and J.-K. Kim, “Graphene for Transparent Conductors,” 2015.

[81] P. June, A. Eq, and A. Eq, “An Introduction to Graphene Plasmonics Erratum,” pp. 1–2, 2016.

[82] V. Popov, “Graphene : Properties and Application,” 2014.

[83] P. T. Yin, S. Shah, M. Chhowalla, and K.-B. Lee, “Design, Synthesis, and Characterization of Graphene−Nanoparticle Hybrid Materials for Bioapplications.”

[84] K. Pokpas, N. Jahed, P. G. Baker, and E. I. Iwuoha, “Complexation-based detection of nickel(II) at a graphene-chelate probe in the presence of cobalt and zinc by adsorptive stripping voltammetry,” *Sensors (Switzerland)*, vol. 17, no. 8, pp. 1–22, 2017.

[85] C.P., “Experimental and Characterization Techniques,” pp. 21–66, 2009.

[86] M. Joshi, A. Bhattacharyya, and S. W. Ali, “Characterization techniques for nanotechnology applications in textiles,” *Indian J. Fibre Text. Res.*, vol. 33, no. 3, pp. 304–317, 2008.

[87] S. Electron, M. Microscopy, and X. External, “Characterization Techniques,” *Charact. Tech.*, pp. 19–34.

[88] W. S. Hummers and R. E. Offeman, “Preparation of Graphitic Oxide,” *J. Am. Chem. Soc.*, vol. 80, no. 6, pp. 1339–1339, 1958.

[89] M. Fu, Q. Jiao, Y. Zhao, and H. Li, “Vapor diffusion synthesis of CoFe2O4 hollow sphere/graphene composites as absorbing materials,” *J. Mater. Chem. A*, vol. 2, no. 3, pp. 735–744, 2014.

[90] J. S. Park, L. Yu, C. S. Lee, K. Shin, and J. H. Han, “Liquid-phase exfoliation of expanded graphites into graphene nanoplatelets using amphiphilic organic molecules,” *J. Colloid Interface Sci.*, vol. 417, pp. 379–384, 2014.

[91] H. Zhu, Y. Cao, J. Zhang, W. Zhang, Y. Xu, J. Guo, W. Yang, and J. Liu, “One-step preparation of graphene nanosheets via ball milling of graphite and the application in lithium-ion batteries,” *J. Mater. Sci.*, vol. 51, no. 8, pp. 3675–3683, 2016.

[92] V. León, A. M. Rodriguez, P. Prieto, M. Prato, and E. Vázquez, “Exfoliation of Graphite with Triazine Derivatives under Ball-Milling Conditions: Preparation of Few-Layer Graphene *via* Selective Noncovalent Interactions,” *ACS Nano*, vol. 8, no. 1, pp. 563–571, 2014.

[93] B. Ntsendwana, B. B. Mamba, S. Sampath, and O. A. Arotiba, “Electrochemical Detection of Bisphenol A Using Graphene- Modified Glassy Carbon Electrode,” *Int. J. Electrochem. Sci.*, vol. 7, pp. 3501–3512, 2012.

[94] R. Navratil, A. Kotzianova, V. Halouzka, T. Opletal, I. Triskova, L. Trnkova, and J. Hrbac, “Polymer lead pencil graphite as electrode material: Voltammetric, XPS and Raman study,” *J. Electroanal. Chem.*, vol. 783, pp. 152–160, 2016.

[95] F. Ban and S. Majid, “Graphene oxide and its electrochemical performance,” *InterJournal*

Electrochem. ...Journal Electrochem. ..., vol. 7, pp. 4345–4351, 2012.

[96] P. Khanra, T. Kuila, N. H. Kim, S. H. Bae, D. sheng Yu, and J. H. Lee, "Simultaneous bio-functionalization and reduction of graphene oxide by baker's yeast," *Chem. Eng. J.*, vol. 183, no. December 2014, pp. 526–533, 2012.

[97] L. Yang, X. Guan, G. Wang, X. Guan, and B. Jia, "Synthesis of ZnS / CuS nanospheres loaded on reduced graphene oxide as high-performance photocatalysts under simulated sunlight," *New J. Chem.*, 2017.

[98] S. Y. Toh, K. S. Loh, S. K. Kamarudin, and W. R. W. Daud, *Graphene production via electrochemical reduction of graphene oxide: Synthesis and characterisation*, vol. 251. Elsevier B.V., 2014.

[99] Z. Xue, B. Yin, M. Li, H. Rao, H. Wang, X. Zhou, X. Liu, and X. Lu, "Direct electrodeposition of well dispersed electrochemical reduction graphene oxide assembled with nickel oxide nanocomposite and its improved electrocatalytic activity toward 2, 4, 6-Trinitrophenol," *Electrochim. Acta*, vol. 192, pp. 512–520, Feb. 2016.

[100] M. Pandurangachar, B. E. Kumara Swamy, B. N. Chandrashekar, O. Gilbert, S. Reddy, and B. S. Sherigara, "Electrochemical investigations of potassium ferricyanide and dopamine by 1-butyl-4-methylpyridinium tetrafluoro borate modified carbon paste electrode: A cyclic voltammetric study," *Int. J. Electrochem. Sci.*, vol. 5, no. 8, pp. 1187–1202, 2010.

[101] H. M. Elqudaby, H. A. M. Hendawy, E. R. Souaya, G. G. Mohamed, and G. M. G. Eldin, "Utility of Activated Glassy Carbon and Pencil Graphite Electrodes for Voltammetric Determination of Nalbuphine Hydrochloride in Pharmaceutical and Biological Fluids," *Int. J. Electrochem.*, vol. 2016, pp. 1–10, 2016.

[102] H. T. Purushothama and Y. Arthoba Nayaka, "Electrochemical study of hydrochlorothiazide on electrochemically pre-treated pencil graphite electrode as a sensor," *Sens. Bio-Sensing Res.*, vol. 16, no. May, pp. 12–18, 2017.

[103] X. Kang, J. Wang, H. Wu, I. A. Aksay, J. Liu, and Y. Lin, "Glucose Oxidase–graphene–chitosan modified electrode for direct electrochemistry and glucose sensing," *Biosens. Bioelectron.*, vol. 25, no. 4, pp. 901–905, Dec. 2009.

[104] J. Kudr, L. Richtera, L. Nejdl, K. Xhaxhiu, P. Vitek, B. Rutkay-Nedecky, D. Hynek, P. Kopel, V. Adam, and R. Kizek, "Improved electrochemical detection of zinc ions using

electrode modified with electrochemically reduced graphene oxide," *Materials (Basel).*, vol. 9, no. 1, pp. 1–12, 2016.

[105] E. S. S. A, L. Beilby, D. H. Angell, T. Dickinson, M. Avron, N. Shavit, J. Burtxer, A. R. Champion, D.-T. Chin, R. G. Compton, J. S. Foord, F. Marken, B. Devadas, M. Rajkumar, I. Hu, D. H. Karweik, T. Kuwana, R. P. Janek, W. R. Fawcett, A. Ulman, D. Y. Kim, J. J. Y. Wang, J. Yang, H. W. Kim, G. M. Swain, L. T. Kubota, Y. Gushikem, N. S. Lawrence, M. Thompson, C. Prado, L. Jiang, T. G. J. Jones, R. G. Compton, E. A. McGaw, G. M. Swain, R. J. Mortimer, D. R. Rosseinsky, P. M. S. Monk, O. Nekrassova, G. D. Allen, N. S. Lawrence, L. Jiang, T. G. J. Jones, R. G. Compton, M. Noel, P. N. Anantharaman, D. K. Nordstrom, J. E. O'Reilly, S. Petrovic, C. Ponce-De-León, C. T. J. Low, G. Kear, F. C. Walsh, U. De Provence, P. V. Hugo, A. Roig, J. Navarro, R. Tamarit, F. Vicente, M. B. Rooney, D. C. Coomber, A. M. Bond, F. Rourke, J. A. Crayston, E. Scientific, P. Company, W. E. V. A. N. D. E. R. Linden, M. Senthilkumar, J. Mathiyarasu, J. Joseph, K. L. N. Phani, V. Yegnaraman, Y. Shi, C. J. Seliskar, W. R. Heineman, R. J. Taylor, A. a. Humffray, S. Trasatti, O. A. Petrii, R. Trouillon, D. O'Hare, I. Union, O. F. Pure, A. Chemistry, V. S. Vasantha, S. M. Chen, J. J. Y. Wang, C. M. Yu, S. C. Hwang, K. C. Ho, L. C. Chen, C. Yan, M. Zharnikov, A. Gölzhä, M. Grunze, J. K. Zak, J. E. Butler, G. M. Swain, H. E. Zittel, F. J. Miller, I. Zudans, J. R. Paddock, H. Kuramitz, A. T. Maghasi, C. M. Wansapura, S. D. Conklin, N. Kaval, T. Shtoyko, D. J. Monk, S. A. Bryan, T. L. Hubler, J. N. Richardson, C. J. Seliskar, and W. R. Heineman, "Electrochemically Reduced Graphene Oxide/ Neodymium Hexacyanoferrate Modified Electrodes for the Electrochemical Detection of Paracetomol," *Electrochim. Acta*, vol. 37, no. 2, pp. 1835–1841, 1985.

[106] A. Economou, P. R. Fielden, and M. H. Briggs, "Simultaneous determination of nickel(II) and cobalt(II) by square-wave adsorptive stripping voltammetry on a rotating disc mercury film electrode," *Analyst*, vol. 118, no. 1, p. 47, 1993.

[107] O. A. Farghaly, "Direct and simultaneous voltammetric analysis of heavy metals in tap water samples at Assiut city: An approach to improve the analysis time for nickel and cobalt determination at mercury film electrode," *Microchem. J.*, vol. 75, no. 2, pp. 119–131, 2003.

[108] M. Korolczuk and K. Tyszczuk, "Application of lead film electrode for simultaneous

adsorptive stripping voltammetric determination of Ni(II) and Co(II) as their nioxime complexes," *Anal. Chim. Acta*, vol. 580, no. 2, pp. 231–235, 2006.

[109] L. Grogan, "Ournal of," *Education*, vol. 1, no. August, pp. 3978–3982, 2008.

[110] M. K. Amini and M. Kabiri, "Determination of trace amounts of nickel by differential pulse adsorptive cathodic stripping voltammetry using calconcarboxylic acid as a chelating agent," *J. Iran. Chem. Soc.*, vol. 2, no. 1, pp. 32–39, 2005.

[111] M. Morfobos, A. Economou, and A. Voulgaropoulos, "Simultaneous determination of nickel(II) and cobalt(II) by square wave adsorptive stripping voltammetry on a rotating-disc bismuth-film electrode," *Anal. Chim. Acta*, vol. 519, no. 1, pp. 57–64, 2004.

[112] D. G. Krishna, N. Devanna, and B. Chandrasekhar, "International Journal of Analytical and Bioanalytical chemistry," *Anal. Bioanal. Chem.*, vol. 1, no. Ii, pp. 19–24, 2011.